

RADC-TR-89-323
Final Technical Report
January 1990



AD-A219 327

DEVELOPMENT OF NEW METHODS FOR PREDICTING THE BISTATIC ELECTROMAGNETIC SCATTERING FROM ABSORBING SHAPES

Carnegie-Mellon University

Z.J. Cendes, D. Hudak, J.F. Lee, D.Q. Sun



APPROVED FOR PUBLIC RELEASE; DISTRIBUTION UNLIMITED.

Rome Air Development Center
Air Force Systems Command
Griffiss Air Force Base, NY 13441-5700

90 03 16 025

This report has been reviewed by the RADC Public Affairs Division (PA) and is releasable to the National Technical Information Service (NTIS). At NTIS it will be releasable to the general public, including foreign nations.

RADC-TR-89-323 has been reviewed and is approved for publication.

APPROVED: *Robert V. Mc Gahan*

ROBERT V. McGAHAN
Project Engineer

APPROVED: *Richard T. Momberg*

RICHARD T. MOMBERG, Lt Col, USAF
Deputy Director
Directorate of Electromagnetics

FOR THE COMMANDER:

Billy G. Oaks
BILLY G. OAKS
Directorate of Plans & Programs

If your address has changed or if you wish to be removed from the RADC mailing list, or if the addressee is no longer employed by your organization, please notify RADC (EECT) Hanscom AFB MA 01731-5000. This will assist us in maintaining a current mailing list.

Do not return copies of this report unless contractual obligations or notices on a specific document require that it be returned.

UNCLASSIFIED

SECURITY CLASSIFICATION OF THIS PAGE

| REPORT DOCUMENTATION PAGE | | | | Form Approved OMB No. 0704-0188 | | |
|--------------------------------------------------------------------------------------------------------------------------------------------------------------------------------------------------------------------------------------------------------------------------------------------------------------------------------------------------------------------------------------------------------------------------------------------------------------------------------------------------------------------------------------------------------------------------------------------------------------------------------------------------------------------------------------------------------------------------------------------------------------------------------------------------------------------------------------------------------------------------------------------------------------------------------------------------------------------------------------------------------------------------------------------------------------------------------------------------------------------------------------------------------------------------------------------------------------------------------------------------------------------------------------------------------------|-------|----------------------------------------------|---------------------------------------------------------------------------------------------------|-------------------------------------------------------|-----------------------------------|----------------------------|
| 1a. REPORT SECURITY CLASSIFICATION UNCLASSIFIED | | | 1b. RESTRICTIVE MARKINGS N/A | | | |
| 2a. SECURITY CLASSIFICATION AUTHORITY N/A | | | 3. DISTRIBUTION/AVAILABILITY OF REPORT Approved for public release; distribution unlimited. | | | |
| 2b. DECLASSIFICATION/DOWNGRADING SCHEDULE N/A | | | | | | |
| 4. PERFORMING ORGANIZATION REPORT NUMBER(S) N/A | | | 5. MONITORING ORGANIZATION REPORT NUMBER(S) RADC-TR-89-323 | | | |
| 6a. NAME OF PERFORMING ORGANIZATION Carnegie-Mellon University | | 6b. OFFICE SYMBOL (If applicable) | 7a. NAME OF MONITORING ORGANIZATION Rome Air Development Center (EECT) | | | |
| 6c. ADDRESS (City, State, and ZIP Code) Pittsburgh PA 15213 | | | 7b. ADDRESS (City, State, and ZIP Code) Hanscom AFB MA 01731-5000 | | | |
| 8a. NAME OF FUNDING/SPONSORING ORGANIZATION Rome Air Development Center | | 8b. OFFICE SYMBOL (If applicable) EECT | 9. PROCUREMENT INSTRUMENT IDENTIFICATION NUMBER F19628-83-C-0079 | | | |
| 8c. ADDRESS (City, State, and ZIP Code) Hanscom AFB MA 01731-5000 | | | 10. SOURCE OF FUNDING NUMBERS | | | |
| | | | PROGRAM ELEMENT NO. | PROJECT NO. | TASK NO. | WORK UNIT ACCESSION NO. |
| | | | 61102F | 2305 | J4 | 52 |
| 11. TITLE (Include Security Classification) DEVELOPMENT OF NEW METHODS FOR PREDICTING THE BISTATIC ELECTROMAGNETIC SCATTERING FROM ABSORBING SHAPES | | | | | | |
| 12. PERSONAL AUTHOR(S) Z. J. Cendes, D. Hudak, J. F. Lee, D. Q. Sun | | | | | | |
| 13a. TYPE OF REPORT Final | | 13b. TIME COVERED FROM Sep 83 TO Apr 86 | | 14. DATE OF REPORT (Year, Month, Day) January 1990 | | |
| | | | | 15. PAGE COUNT 192 | | |
| 16. SUPPLEMENTARY NOTATION N/A | | | | | | |
| 17. COSATI CODES | | | 18. SUBJECT TERMS (Continue on reverse if necessary and identify by block number) | | | |
| FIELD | GROUP | SUB-GROUP | | | | |
| 17 | 09 | | Bistatic scattering | | | |
| 20 | 03 | | Finite elements | | | |
| | | | Cloning | | | |
| | | | Measurements | | | |
| 19. ABSTRACT (Continue on reverse if necessary and identify by block number) More accurate, more reliable and more efficient methods to calculate the bistatic scattering of electromagnetic fields from absorbing dielectric objects have been developed. While the solution of three dimensional scattering problems has not been achieved, the methods developed here provide for the first time, finite element solutions of closed three-dimensional electromagnetic fields free of the spurious solutions that have plagued previous procedures. These stable finite elements are defined in three varieties: 1) mixed-order rectangular parallelepiped elements, 2) edge-based tangential vector finite elements, and 3) derivative continuous C^1 elements. Each are shown to give only physically correct solutions. In addition, a new procedure called the transfinite element method is presented for the solution of open or unbounded electromagnetic scattering problems. This method provides a one step procedure to compute scattered fields in electromagnetics. Prior to the transfinite element method, scattering problems required that many time steps or many modes be used to produce each field solution. The transfinite element method is applied --(Continued on reverse) | | | | | | |
| 20. DISTRIBUTION/AVAILABILITY OF ABSTRACT <input type="checkbox"/> UNCLASSIFIED/UNLIMITED <input checked="" type="checkbox"/> SAME AS RPT. <input type="checkbox"/> DTIC USERS | | | 21. ABSTRACT SECURITY CLASSIFICATION UNCLASSIFIED | | | |
| 22a. NAME OF RESPONSIBLE INDIVIDUAL Robert V. McGahan | | | 22b. TELEPHONE (Include Area Code) (617) 377-4237 | | 22c. OFFICE SYMBOL RADC (EECT) | |

DD Form 1473, JUN 86

Previous editions are obsolete.

SECURITY CLASSIFICATION OF THIS PAGE
UNCLASSIFIED

UNCLASSIFIED

Block 17 Continued:

20 14

Block 19 Continued:

here only in two dimensions. Finally, a new high efficiency algorithm is proposed to compute electromagnetic scattering over a specified frequency range. In this algorithm, frequencies are selected adaptively to ensure a given accuracy in minimum computation time for the specified frequency range. The individual procedures are illustrated with a variety of examples. Thus, a great deal of progress in the solution of electromagnetic scattering problems has been achieved, although the major program goal of solving for the electromagnetic fields scattered by large three dimensional objects has not been accomplished.

UNCLASSIFIED

Table of Contents

| | | <u>Page</u> |
|-------------|------------------------------------------------------------------------------------------------------------|-------------|
| SECTION 1 | INTRODUCTION | 2 |
| SECTION 2 | FINITE ELEMENT FORMULATIONS | 10 |
| SECTION 3 | THE FINITE SOLUTION REGION | 14 |
| SECTION 4 | SPECTRAL METHODS | 19 |
| SECTION 5 | CONCLUSIONS | 20 |
| APPENDIX A | MIXED-ORDER RECTANGULAR FINITE ELEMENTS FOR THE SOLUTION OF THREE-DIMENSIONAL ELECTROMAGNETIC FIELDS | 24 |
| APPENDIX AA | RECTANGULAR BASIS FUNCTIONS | 33 |
| APPENDIX B | EDGE-BASED VECTOR FINITE ELEMENTS FOR SOLVING THE ELECTROMAGNETIC WAVE EQUATIONS | 40 |
| APPENDIX C | C^1 QUADRATIC INTERPOLATION FOR DERIVATIVE CONTINUOUS FINITE ELEMENT APPROXIMATIONS | 60 |
| APPENDIX D | ELIMINATING SPURIOUS SOLUTIONS IN ELECTROMAGNETIC WAVE PROBLEMS BY USING C^1 FINITE ELEMENTS | 81 |
| APPENDIX E | MODELING THE OPEN BOUNDARY CONDITION IN THE FINITE ELEMENT SOLUTION OF ELECTROMAGNETIC SCATTERING PROBLEMS | 92 |
| APPENDIX F | AN ADAPTIVE SPECTRAL RESPONSE MODELING PROCEDURE FOR ELECTROMAGNETIC SCATTERING | 170 |

| | |
|--------------------|-------------------------------------|
| Accession For | |
| NTIS | <input checked="" type="checkbox"/> |
| DTIC TAB | <input type="checkbox"/> |
| Unannounced | <input type="checkbox"/> |
| Justification | |
| By | |
| Distribution/ | |
| Availability Codes | |
| Dist | Avail and/or Special |
| A-1 | |



ABSTRACT

More accurate, more reliable and more efficient methods to calculate the bistatic scattering of electromagnetic fields from absorbing dielectric objects have been developed. While the solution of three dimensional scattering problems has not been achieved, the methods developed here provide for the first time finite element solutions of closed three-dimensional electromagnetic fields free of the spurious solutions that have plagued previous procedures. These stable finite elements are defined in three varieties: (1) mixed-order rectangular parallelepiped elements, (2) edge-based tangential vector finite elements, and (3) derivative continuous C^1 elements. Each are shown to give only physically correct solutions. In addition, a new procedure called the transfinite element method is presented for the solution of open or unbounded electromagnetic scattering problems. This method provides a one step procedure to compute scattered fields in electromagnetics. Prior to the transfinite element method, scattering problems required that many time steps or many modes be used to produce each field solution. The transfinite element method is applied here only in two dimensions. Finally, a new high efficiency algorithm is proposed to compute electromagnetic scattering over a specified frequency range. In this algorithm, frequencies are selected adaptively to ensure a given accuracy in minimum computation time for the specified frequency range. The individual procedures are illustrated with a variety of examples. Thus, a great deal of progress in the solution of electromagnetic scattering problems has been achieved, although the major program goal of solving for the electromagnetic fields scattered by large three dimensional objects has not been accomplished.

SECTION 1 INTRODUCTION

A program of work has been completed to develop more accurate, more reliable and more efficient numerical procedures for the computation of electromagnetic fields scattered by absorbing dielectric objects. This work has focused on the application of the finite element method to this problem since the finite element method is well suited to modeling problems involving complex shapes and material properties. It involved the solution of two separate fundamental problems in electromagnetics: (1) How does one approximate electromagnetic fields over finite element domains such that stable solutions are produced? and (2) How does one interface the open boundary condition encountered in scattering problems to the finite element solution in an accurate and efficient manner?

The first application of the finite element method in electromagnetics was published by Silvester in 1969[1]. In this application, the finite element method was used to solve for the resonant electromagnetic fields in homogeneous waveguides. Subsequently, Silvester and his coworkers published a series of papers [2-6] extending the realm of application of the finite element method in high frequency electromagnetics. However, it soon became apparent that the category of problem with which the finite element method was stable was quite limited: the finite element method only gave good answers to problems in which a single scalar variable was the unknown. Three-dimensional problems or two-dimensional problems that required the solution of *vector* field quantities gave spurious solutions[3-6]. In fact, the subject of spurious modes in finite element solutions of electromagnetics problems has generated considerable literature in recent years[7-11].

Parallel to the work of Silvester and others on the application of the finite element method to closed high-frequency electromagnetics problems, Mei and his coworkers developed a procedure called the unimoment method for solving scalar variable unbounded electromagnetic field problems using the finite element method[12-13]. This procedure makes it possible to solve complicated scattering problems by placing the scatterer inside a circular boundary, discretizing the region inside the circle with finite elements, and coupling the finite element solution to the analytical solution outside the circle through interface conditions. Unfortunately, however, this coupling requires that a full set of modal finite element solutions be evaluated such that each finite element solution and its derivative match the corresponding free space solution on the circular interface. This process is relatively time consuming because many finite element problems need to be solved to obtain a single scattered field solution and it is relatively inaccurate because numerical derivatives are employed in the formulation.

The goal in this work is to develop numerical procedures by which relatively large three dimensional dielectric scatterers can be modeled. To achieve this goal, two new developments were required: First, it was essential to develop numerical procedures for modeling three dimensional electromagnetic field problems in a stable way. Second, more efficient numerical procedures for setting up and solving open electromagnetic field problems were needed.

This report documents progress we have made towards achieving these goals. With respect to the problem of spurious solutions in three dimensional electromagnetic field calculations, we have developed three new finite element procedures by which the problem of spurious solutions in electromagnetics is eliminated. These procedures are: (1) mixed-order finite elements over rectangular parallelepipeds, (2) tangentially continuous vector finite elements over tetrahedrons, and (3) C^1 derivative continuous finite elements over tetrahedrons. With respect to the problem of more efficient modeling of open electromagnetics problems, we have developed a new procedure called the transfinite element method that is orders of magnitude more efficient and more accurate than the unimoment method. We have also developed an adaptive spectral modeling procedure that speeds up the solution of scattering problems over a range of frequencies by at least an order of magnitude. Although time did not permit us to put everything together to solve three dimensional scattering problems, we have developed the major theoretical components required for this purpose.

1.1 MOTIVATION

1.1.1 INTEGRAL VERSUS DIFFERENTIAL METHODS

Most common methods for solving electromagnetic scattering problems are based on integral equation formulations. In general, these equations are discretized by using pulse or linear piecewise polynomial basis functions and are solved by using Galerkin's method. Originated by Roger F. Harrington, and dubbed the method of moments, such procedures for solving the electromagnetic field equations have been applied in both two and three dimensional scattering. Although these procedures have been successful in solving two dimensional scattering problems, their success in modeling three dimensional scattering has been more limited.

An alternative to solving electromagnetic field problems using integral equation methods is to solve these problems by using methods based on differential formulations of the electromagnetic field. The two best known methods to solve differential equations are the finite difference and the finite element method. Although there are some advantages to differential methods - such as much simpler expressions of the field equations - these methods have been seldom used to solve electromagnetic scattering problems. Indeed, until recently, in the United States there were only two research groups working on modeling electromagnetic scattering using differential methods: (K. K. Mei at the University of California at Berkeley and Alan Taflove at Northwestern University). There are two obvious reasons for this: (1) the number of data points required by differential methods appears at first glance to be daunting, and (2) representing open, unbounded field problems is difficult with differential methods. With integral methods these issues are less important: only the surfaces of objects need to be discretized with integral methods so that relatively few data points are required. Further, the far field boundary conditions are embedded in the Green's functions used in integral formulations so that open problems are easily addressed.

While it thus appears that integral methods have the advantage in solving electromagnetic scattering problems, this is in fact not the case. As described in more detail below, a large number of methods to solve open field problems by truncating the finite difference or finite element mesh have been developed. And, surprisingly, the advantage of less computer storage requirements and of less computer time requirements is actually on the side of differential methods. This is surprising because differential methods require many more node points than integral methods. However, all of the interactions in a differential method are local in the sense that all information in a differential model is passed directly from one element to the next. The differential system is tied together by these local interactions, and the response of individual elements is obtained by solving a matrix equation. With integral methods, information may pass directly from one side of the structure to the other. The entire integral structure is tied together analytically from the very beginning by evaluating the interaction that occurs directly between any two points. This process is not only analytically challenging, it is also computationally intensive.

Thus, although differential methods are at a disadvantage because the full space must be modeled and not just the object surfaces, they do have the advantage that global interactions are obtained numerically by means of the matrix solution process rather than by using analytical expressions. Since computing the interactions between different surface elements with integral methods is expensive, integral methods are at a disadvantage in this respect compared to differential methods. Further, each element in an integral method interacts with many other elements so that the matrix equation to be solved to compute scattering is full. In contrast, the matrices arising in differential methods are sparse since each element interacts only with its immediate neighbors.

The efficiency of numerical methods in solving electromagnetic scattering problems is determined by several factors: (1) the efficiency of the mesh used to represent the objects and the solution variables, (2) the difficulty and cost of mesh generation, (3) the cost of generating the solution matrix, (4) the matrix storage and solution time requirements of the algorithm, and (5) the robustness of computer implementations with respect to geometric and material complexity. These factors are examined next:

1. **Mesh efficiency.** An important consideration in evaluating the efficiency of both differential and integral solution methods is the type of mesh required for its operation. The application of some numerical methods is restricted to regular or rectangular meshes while other methods allow irregular meshes with arbitrary orientations and sizes. Except in special cases, a mesh that conforms to the boundaries of the objects that are modeled and that is refined locally in regions of rapid field variation is much more efficient in modeling electromagnetic field problems than is a regular, rectangular mesh. The gain in efficiency depends on a number of factors such as the problem geometry and the method used to construct the mesh and is therefore difficult to quantify. Fortunately, however, methods for constructing *optimal* triangular meshes in two dimensions and optimal tetrahedral meshes in three dimensions have been developed [29-33]. These methods are based on the concept of Delaunay tessellation that guarantees that the mesh employed is optimal with respect to the element angles regardless of the point spacing. Furthermore, with irregular meshes, it is possible to construct the mesh adaptively [29-32]. In adaptive mesh generation, elements are refined iteratively in the areas having the largest error until all elements in the mesh

have approximately the same error. In terms of accuracy for a given mesh size, adaptive Delaunay mesh generation is the most efficient procedure, followed by non-adaptive Delaunay mesh generation, other irregular mesh generation algorithms, and, last, regular mesh generation. The advantage of regular mesh generation is, of course, that it is very easy and inexpensive to compute. We believe, however, that the modeling efficiency obtained by using irregular meshes outweighs the increased algorithmic complexity of these procedures in most cases.

2. **Difficulty and cost of mesh generation.** Since only the surfaces of objects need to be discretized with integral methods while the entire volume must be discretized with differential methods, it appears at first that it is easier to create a mesh with integral methods. However, it turns out that this is not true if the goal is to obtain irregular meshes for arbitrary objects having complicated shapes. (Creating regular meshes corresponding to simple shapes is easy with both differential and integral methods). The reason for this is that the Delaunay approach to mesh generation is well known and can be automated in both two and three dimensions. No direct, automatic, optimal procedure to generate the surface mesh of arbitrary objects is known. At this time, the only known way to create an optimal surface mesh for an arbitrary object is to first create the three dimensional volume Delaunay mesh for the object and then to extract the corresponding surface mesh. Thus, the difficulty and cost of mesh generation is roughly the same for both differential and integral methods.
3. **Matrix set up cost.** Differential methods have a very great advantage over integral methods with respect to matrix evaluation cost. When they are available, the formulas to compute matrix entries with differential methods are simple and just involve arithmetic expressions. In comparison, relatively complicated analytic expressions are required to set up matrices with integral methods. The net result is that matrix evaluation cost is negligible with differential methods, but is often substantial with integral methods.
4. **Matrix storage and solution time requirements.** The analysis of matrix storage and solution time requirements is complicated because several different solution procedures exist. In the past decade, the use of the preconditioned conjugate gradient algorithm has had a profound effect on both differential and integral methods. The advantage of the preconditioned conjugate gradient algorithm is that with differential methods matrix solution time increases linearly with matrix size, compared to order N^3 solution times for solving full matrix equations. In practice with non-adaptive differential meshing procedures, solution time grows as $N^{1.2}$ with both two and three dimensional geometries [28]. However, if adaptive finite element mesh generation procedures are employed, the theoretical ideal limit $N^{1.0}$ is achieved [29]. Thus, in the finite element discretization of a three dimensional problem with an $n \times n \times n$ mesh, the matrix size N grows as $N = n^3$ and storage and solution time for these sparse matrices increases linearly. The net result is that computer storage requirements and solution times grow as $N = n^3$ with differential methods. This value can be achieved in practice by using adaptive or multigrid methods. (The primary difference between multigrid and adaptive methods are that multigrid methods employ rectangular meshes while adaptive methods allow irregular meshes; they are similar in that several levels of meshes are

required). If non-adaptive mesh generation procedures are employed, then the performance of the algorithm with respect to solution time deteriorates to approximately $N^{3.6}$.

With boundary element methods, only the elements on the surface of three dimensional objects need to be modeled and the corresponding mesh grows as $N = n^2$. The straightforward application of direct solvers to the corresponding full matrices results in storage and solution times growing as N^3 . Thus, with integral methods and full matrix solution algorithms, computer requirements grow as n^6 . The application of the conjugate gradient algorithm to these matrices lowers the solution time requirement to n^4 and recent work by Catedra, Gago and Nuno [34] shows that combining the conjugate gradient method and the fast Fourier transform reduces this further to $n^{2.667} \log n$. This last result however only applies to problems having a uniform mesh and hence applies only to problems having simple shapes. As stated earlier, with complicated geometries it is very inefficient to use a uniform mesh and hence the fast Fourier transform conjugate gradient method is not competitive in these cases.

5. **Robustness.** An important consideration in evaluating numerical algorithms for modeling electromagnetic scattering is robustness with respect to the complexity of the geometry and of the material properties of the scatterers. Here differential methods have a clear advantage: provided that the same mesh is used in both cases, with differential methods it makes relatively little difference whether the material characteristic of the entire problem domain is homogeneous or whether the material characteristic of every single element in the mesh is different. Thus, although differential methods solution requirements grow as the size of an object grows, they are relatively insensitive to the complexity of the boundaries and to the number of material types that make up the object. Further, differential methods can model extreme changes of material characteristics with ease and can handle material nonlinearity efficiently. The performance of integral methods, on the other hand, deteriorates not only as the size of a scatterer grows but also as its structure becomes more complicated. Unlike the case with differential methods, the size of integral solution matrices increases with the addition of each new boundary in a structure of given size and modeling nonlinear material characteristics with integral methods is difficult.

In the final analysis, the efficiency of any method for solving electromagnetic scattering problems must be judged by running actual computer programs. The performance of any algorithm is affected by the implementation and sometimes synergisms exist in implementations that are difficult to quantify. However, the above analysis shows that differential methods are clearly favored as scattering problems become larger and more complicated. In the five categories examined above, where there is a difference, differential methods prove to be superior to integral methods. In particular, in terms of matrix set up time, matrix solution time, and robustness the better choice is the differential approach.

1.1.2 TIME DOMAIN VERSUS FREQUENCY DOMAIN

A second issue in modeling electromagnetic scattering from dielectric scatterers is the choice of analysis in the time or the frequency domain. With continuous wave (CW) signals, the logical choice is to solve for the electromagnetic wave in the frequency domain since that is where the CW signals reside; with pulsed signals, time domain methods appear to be the most appropriate choice since the signal is in fact a transient in time. However, as discussed more fully below, time domain solutions are expensive since they require many time steps to produce acceptable results. For large problems it is more efficient to decompose the transient into a few Fourier components, solve the problem in the frequency domain at these few frequencies and then reassemble the solution in the time domain. In addition to efficiency, this procedure has the advantage that the dielectric constant of many materials is given as a function of frequency; with time domain solutions, correct material property values are difficult to determine since they are usually given as frequency dependent functions.

Nevertheless, all published work for modeling three dimensional scattering using differential methods is in the time domain. Taflov and his coworkers [14,15] have employed the finite difference method in the time domain, while Mei and his coworkers [12,13] have employed the finite element method in the time domain. Common with both approaches is the time integration formula of Yee [16] that provides a stable time integration procedure for Maxwell's equations. The Yee integration algorithm is the key to time domain solution procedures: it is stable and does not require the solution of matrix equations. As we will see below, stable solution procedures for three dimensional problems in the frequency domain have not appeared in the literature previously.

The major advantages of the finite difference time domain (FDTD) method is that it is extremely simple and that it is unnecessary to store matrix entries. Its disadvantages are that it is a low order method and that it employs rectangular meshes with minor variations in element size and shape. With the finite element method in the frequency domain (FEFD), although a matrix equation needs to be solved, the accuracy of the solution can be improved by using higher order approximation functions and by employing irregular meshes.

To compare the relative efficiency of the FDTD and the FEFD methods, we will make an order of magnitude comparison. As is the case in comparing differential and integral methods, this comparison will neglect all factors except the highest order trends and thus will serve to indicate only theoretical limits as the problem size grows. To begin, the number elements N to achieve a given accuracy in three dimensional problems goes as: $N \approx h^{-3}$ where h is the mesh size used. Since the FDTD algorithm is based on linear field interpolation, the order of accuracy of the FDTD algorithm is h^2 . It has been shown [12-15] that, to obtain accurate solutions, the time step Δt should be of the same order as the mesh size: $\Delta t \approx h$. Thus, the number of time steps to obtain the solution goes as h^{-1} . The total complexity to obtain a FDTD solution goes in the limit of increasing problem size as $N/h \approx N^{1.333}$.

The order of accuracy of the finite element method depends on the order of polynomial interpolation used. As a reasonable value and one that makes the calculation relatively easy, we will use cubic order finite elements in the following. The order of accuracy of cubics is s^4 , where s is the largest edge length in the mesh. Assuming a uniform mesh (which greatly lowers the efficiency of finite element methods), we see that,

to achieve the same accuracy, the FDTD mesh size h and the FEFD mesh size s are related by: $h = s^2$. Thus the number of finite elements M required to achieve the same accuracy as a FDTD mesh of N elements is $M \approx \sqrt{N}$ or in terms of mesh size $M \approx s^{-3} \approx h^{-1.5}$. In the FEFD method, one must solve a sparse matrix equation. As discussed before, the order of magnitude work required to do this increases linearly with the number of elements if the preconditioned conjugate gradient algorithm is used with a multigrid mesh and goes as $M^{1.2}$ if a single level mesh is employed. The net result is that the total complexity if the FEFD method goes either as $M \approx N^{0.5}$ or as $N^{0.6}$ depending on the number of mesh levels employed. In either case, the FEFD method is far more efficient than the FDTD method.

It must be emphasized that the above analysis ignores the algorithmic details of computing solutions on relatively small meshes and only examines global trends as the problem size grows. Since the FDTD method is very simple while the FEFD is relatively complicated, it may be that for small, fixed-sized problems the FDTD method is actually faster. The above analysis shows, however, that, as the problem size gets larger, eventually the FEFD method will be the most efficient. Also, the FEFD method allows the use of irregular meshes that are clearly superior for modeling problems having complicated geometries.

1.1.3 FINITE DIFFERENCES VERSUS FINITE ELEMENTS

It thus appears that the most efficient procedure to model three dimensional electromagnetic scattering is to use differential methods in the frequency domain. There remains, however, the question of which differential method to employ: the finite difference method or the finite element method. We note here that the differences between these methods is often just semantics: different people will sometimes call the same method finite elements or finite differences depending on their viewpoint. For example, the methods developed by Taflov and by Mei are identical except that Taflov uses a rectangular mesh and calls it finite differences while Mei allows the mesh to be distorted and calls it finite elements. Here we take a finite difference method to be one that is derived by considering the difference equations formed by point values of the differential equation without reference to variational calculus. A finite element method, on the other hand, is taken to be a method that employs basis functions to approximate the field in a variational procedure - either a Galerkin method or the Rayleigh-Ritz method.

From the point of view of accuracy and efficiency, finite element methods have four advantages over finite difference methods. The first of these advantages is the fact that one can show [17] that the errors in finite element methods are minimized in a least squares sense and hence, in general, will be more accurate than finite difference methods. Second, since the finite elements may be of any shape, the meshes formed in finite element methods are often more flexible geometrically than the meshes formed in finite difference methods. Third, it is relatively easy with finite element methods to construct elements having a high order of interpolation; high order formula are hard to construct with finite difference methods. And fourth, finite element methods satisfy certain boundary conditions automatically - called the natural boundary conditions - that are lacking in finite difference methods.

1.1.4 SCOPE OF THIS PROJECT

For the above reasons, the direction of research pursued in this project was to develop finite element methods in the frequency domain for the solution of open three dimensional electromagnetic scattering problems. This was an ambitious goal: prior to the work in this project, no stable finite element method in the frequency domain for solving even closed cavity three dimensional electromagnetic fields was known. Further, methods of coupling the finite element solution region to the exterior field were grossly inefficient. Unfortunately, due to budgetary constraints the manpower available to work on this project was limited and it was not possible to develop a three dimensional scattering program during the course of this project. However, a great deal of useful work was accomplished. In particular, we solved the two bottleneck issues in applying finite element analysis to this area: in this project we developed and tested for the first time stable finite element methods for the steady-state three dimensional analysis of electromagnetic fields, and we developed the transfinite element method for the analysis of unbounded problems in electromagnetics and tested this method in two dimensions. Thus, although we did not accomplish the original project goal of solving the electromagnetic scattering from large three dimensional dielectric objects, we are proud to have developed three important new concepts - tangential finite elements, C^1 quadratic finite elements, the transfinite element method, as well as the lesser but useful adaptive spectral response modeling procedure - during the course of this project. It should be noted that work reported here has been invited for presentation at two conferences, one to be given at the IEEE APS/URSI Symposium to be held in Syracuse, NY in June, 1988 and the second invited paper to be given at the IEEE Intermag Conference to be held in Vancouver, BC in July, 1988.

SECTION 2 FINITE ELEMENT FORMULATIONS

2.1 THE ZERO DIVERGENCE CONDITION

Although the application of the finite element method to three dimensional electromagnetic field problems appears at first glance to be straightforward, this in fact is not the case. As described more fully in Appendix A, the application of the standard finite element method to three dimensional electromagnetics results in "spurious modes". These spurious modes make the solution procedure worthless. It should be noted that the problem of spurious modes is not limited to closed cavity problems; finite element solutions of any electromagnetics problem - open or closed - will be spurious if the basic approximation procedure is incorrect.

Although we now know that it is not true, the common view published in the literature [3-11] is that spurious modes are a result of not enforcing the zero divergence of the electric or of the magnetic field rigorously. This view was created by the fact that spurious modes do exhibit a non-zero divergence. To solve for the electromagnetic field, the finite element method is applied to the vector wave equation. While the zero divergence of the field is a consequence of this equation, zero divergence is not enforced explicitly in the usual finite element procedure. Several published papers [9-11] attempt to eliminate spurious modes by attempting to enforce the zero divergence condition on the vector field. In the published work, this is achieved only in a least-squares sense by adding a penalty term proportional to the square of the divergence to the variational principle

At the start of this project, we also believed that the way to eliminate spurious modes was to enforce the zero divergence condition on the electromagnetic field. In fact, at the time that we wrote the proposal for this project, we had just developed a numerical procedure by which the zero divergence condition could be imposed explicitly in the finite element method. This procedure is published in reference [18]. This procedure did exactly what we believed was required to eliminate spurious modes: it enforced the zero divergence of the field exactly. Consequently, we stated in our proposal that we would employ this procedure to generate stable solutions for three dimensional electromagnetics problems; we began work on this project believing that this approach would solve the instability problem.

Unfortunately, however, we discovered later that the zero divergence condition is in fact unrelated to the problem of spurious modes. Enforcing the the zero divergence condition by the method of reference [18] does not alter the fundamental characteristic of standard finite element methods: the solution is unstable at certain unpredictable frequencies. The idea that we had worked towards - namely to enforce the zero divergence condition exactly on the vector field - did not accomplish the desired result. The failure of this approach to produce stable three dimensional field solutions was both disappointing and perplexing.

2.2 THE ORIGIN OF SPURIOUS MODES

Fortunately, a publication in the IEEE Transactions on Microwave Theory and Techniques set us on the path that would lead to the eventual solution of the spurious mode problem. A paper by Hano [19] showed that spurious modes do not appear in two dimensional finite element solutions if rectangular mixed constant-linear elements are used as the basis functions in the approximation. While rectangular elements are not ideal for modeling complicated shapes, Hano's paper did allow us to derive the key principle required for stable solutions of the electromagnetic field: *It must be possible to express the basis functions used in the finite element method as the gradient of a scalar for this method to provide stable solutions of the vector wave equation.* As will be described below, we have used this principle to derive several different methods for computing stable solutions to electromagnetic field problems.

To understand above principle, notice that the curl of the gradient of any scalar function is zero. Thus, these functions are nullvectors of the curl operator. Since the operator in the vector wave equation is the curl operator twice over, the gradient of any scalar is an eigenvector of the vector wave equation with eigenvalue zero. Provided that the finite element approximation functions can be expressed as the gradient of a scalar, the approximation functions themselves provide a basis for the nullspace of the curl operator. The eigenvalues of the approximation functions will thus be zero. However, if the approximation functions cannot be expressed in the required form then their eigenvalues will not be zero. Hence, the eigenvalues of the nullspace, which should all be zero, will be shifted to non-zero values. This is the source of spurious modes: spurious modes are approximations to the nullvectors of the vector wave equation that are shifted in frequency so much that they interfere with the real physical modes.

2.3 STABLE FINITE ELEMENTS

We are thus able to explain the cause and the origin of spurious modes. The next step is to develop finite elements with the required properties to avoid them. The first way to accomplish this is to extend Hano's element to three dimensions and to higher order polynomials. This is relatively straightforward; the mathematical details are presented in Appendix A. As shown by the example problems in this Appendix, these elements work exactly as predicted: no spurious modes occur when solving three dimensional field problems using these new elements. There are zero eigenvalues but these zero eigenvalues do not interfere with the physical solutions. Furthermore, the number of zero eigenvalues equals exactly the dimension of the nullspace of the curl operator.

While the success of the rectangular elements in Appendix A in eliminating spurious modes is encouraging, it is not sufficient. Rectangular elements are just as crude for approximating complex shapes as are finite difference methods. Clearly, triangular finite element methods that satisfy the above property are required if we are to achieve the efficiencies hoped for at the start of this project.

Finding triangular finite elements that represent the gradients of scalars is not an easy task. Suppose that we choose the scalar to be an ordinary triangular finite element complete in polynomials of order n . It is easily seen that the derivative of a complete n 'th order polynomial is a complete polynomial of order $(n - 1)$. However, since $(n - 1)$ 'st order finite elements are basically the same as n 'th order elements, we are lead to the false conclusion that the components of the gradient can be expressed in terms of ordinary triangular finite elements. We know that this conclusion is false: ordinary finite elements generate spurious modes in general!

To resolve the above paradox, we need to consider not only the effect of the gradient on the inside of the element but also its effect along the element edges. Ordinary triangular finite elements are said to be C^0 continuous. This means that the functions in these approximation are continuous but that their derivatives are not continuous. The gradient of a C^0 finite element will therefore be a vector that has continuous tangential components but discontinuous normal components. Thus, stable triangular finite elements are obtained by creating elements that impose continuity of the tangential component of the vector field but allow the normal component to be discontinuous. Such finite elements are indeed possible; Appendix B presents details of the mathematical derivation. It should be noted that although it is possible to create these tangential vector approximation functions, this does not guarantee that they will provide correct solutions to the electromagnetic field; the fact that they do is a consequence of the natural boundary conditions in the variational procedure. The full details of the synergism between tangential elements and the natural boundary conditions of the variational procedure are given in Appendix B.

There is, however, a second solution to the above paradox. Let us repeat the above discussion, but replace the C^0 scalar with a C^1 scalar. With a C^1 scalar, both the function and its first derivative are continuous so that both the tangential and normal components of its gradient are continuous. The components of the gradient are thus ordinary C^0 finite elements; this time, however, they must be compatible with a C^1 scalar as its parent.

The lowest order polynomials that allow C^1 continuity are quadratics. Surprisingly, no one had developed an explicit form for these polynomials prior to the work reported here. The basic idea with C^1 quadratics is that it is impossible to generate derivative continuous polynomials one element at a time; rather, one must subdivide each triangular element in a certain way into six subtriangles in order to achieve C^1 continuity. The full details of this process are given in Appendix C.

Thus the C^1 elements developed in Appendix C provide a fascinating irony. It turns out that ordinary finite elements work correctly after all, but only if they are placed in a special pattern. If an arbitrary pattern of finite elements is used to approximate the components of electric or magnetic field vector, then in general the nullspace of the curl operator will be improperly modeled and spurious modes will result. If, however, the pattern of finite elements that approximate the vector field is such that a C^1 scalar is possible, then no spurious modes will result. Note that it is not required in this process to form the C^1 scalar explicitly; the *possibility* of these C^1 scalars is sufficient to ensure stability of the electromagnetic solution.

Finally, the C^1 elements may themselves be used directly to generate stable finite element solutions of electromagnetic field problems. Since the electric and magnetic fields are nondivergent, one may

define a vector potential that provides these fields. The divergence of this potential function is arbitrary; all that is required is that its curl equal the field variable. Substituting this vector potential into the vector wave equation gives a new equation that requires continuity of the potential and of its derivative. The C^1 finite elements of Appendix C have exactly the required properties. Consequently, if we use these C^1 elements to approximate each component of the vector potential function, stable finite element solutions result. Details of this procedure are presented in Appendix D.

Since we have now developed not one but three different stable procedures for solving three dimensional electromagnetic field problems using triangular finite elements, it is appropriate to ask: Which is the best? From the point of view of simplicity of formulation and ease of use, the answer is clear: The tangential finite elements of Appendix B are simpler to understand and to program than the C^1 elements of Appendix C or the potential formulation of Appendix D. Fortunately, this simplicity also translates into a computational advantage: since the matrices produced by tangential elements are very sparse, while the matrices produced by the C^1 elements are relatively full, tangential elements are not only simpler to use than the C^1 elements, they are faster.

3. THE INFINITE SOLUTION REGION

3.1 EXTERIOR FIELD MODELS

A basic characteristic of scattering problems is that the solution region is infinite. A plane wave originates at infinity and travels through free space, impinging on an object that scatters the wave in various directions back towards infinity. In order to solve this problem with finite elements, the problem region must be divided into two parts: (1) an interior region surrounded by a boundary called a "picture frame" that completely encloses the scatterer, and (2) an exterior region that extends from the picture frame to infinity.

The problem of modeling the exterior field region is difficult because the solution region encompasses an infinite number of wavelengths. Furthermore, while the energy in the scattered wave is finite, the energy in the incident plane wave is infinite; this fact complicates the use of energy-based solution methods. Despite these difficulties, however, a variety of methods have been developed to solve scattering problems by finite element methods. Exterior field formulations may be divided into three groups: those based on integral methods, those based on differential methods, and those based on modal analysis. In the following, we list the essential characteristics of each approach.

3.1.1 BOUNDARY INTEGRAL AND BOUNDARY ELEMENT METHODS

The oldest way to model open boundary problems with finite element methods is simply to resort to integral methods to handle the infinite exterior region. Such solution procedures are usually called boundary integral methods. A common variant of boundary integral methods is the boundary element method in which the boundary integral is discretized by using the piecewise polynomials first employed in the finite element method [20]. With these methods, one has to compute the values of an integral that is singular on the boundary. A way to circumvent this difficulty is to employ two picture frames, one for the equivalent boundary integral sources, another for the observation points. This procedure was employed early in the history of numerical methods by Silvester [21] and by Wexler [22]. The separate source-observation approach has been converted into a pure integral equation form by Ludwig recently [23].

The advantage of boundary integral and boundary element methods is that they are very well known. Their disadvantage is that they are relatively expensive because it is necessary to compute the required integrals of the Green's functions and because the boundary elements produce a full matrix on the picture frame boundary.

3.1.2 BALLOONING, CLONING AND INFINITESIMAL SCALING

Ballooning is an entirely different approach to modeling the exterior field region. It was invented by Silvester [24] in 1974 and has the advantage of being a pure differential approach. The idea is the following: A single layer of finite elements is created outside the picture frame boundary. This layer has elements placed such that the radial edges all converge to a single point called the star point. By "blowing" this layer of elements up so that the inner boundary of the new layer coincides with the outer boundary of the original layer, a second layer of elements is formed that is similar in a geometrical hence to the original layer. These two layers are then joined and the nodes on the common boundary are eliminated. The resulting double layer has the same number of unknowns as the original single layer but is more than twice as large. It is then also blown up, the two double layers joined and the in between common nodes eliminated. This process is repeated until it approximates the infinite region as closely as desired. (In practice, seven or eight iterations are usually sufficient). The exterior field approximation is then combined with the interior field approximation and the problem solved.

The original approach of Silvester could only be used to model Laplacean regions. This is because in two and three dimensions the size of the finite elements in each layer grows larger and larger. In a Laplacean region this is desirable because the solution becomes smoother with increasing distance from the object, but this is inappropriate with wave problems where the distance between waves is invariant with distance from the scatterer. The ballooning approach was extended to wave propagation by Das Gupta and renamed cloning [25]. In cloning, only a single layer of finite elements are required, but the property of geometric similarity is used to create an eigenvalue equation that represents the entire exterior field region.

A third variant of ballooning was developed by Hurowitz [26]. In this approach, called infinitesimal scaling, the single layer of finite elements is made infinitely thin. In this limit, the exterior field problem is converted into an ordinary differential equation. Unfortunately, this differential equation is nonlinear and expensive to solve.

3.1.3 MODAL ANALYSIS METHODS

The third procedure for solving open scattering problems is semi-analytical. In this case, the electromagnetic field in the exterior region is expressed as a linear combination of orthogonal modes and the field in the interior region is expressed as a linear combination of finite elements. The entire solution region is solved by tying these two approximations together with continuity conditions along the picture frame boundary.

The modal approximation method for electromagnetic scattering was once again first proposed by Silvester for one dimensional propagation to infinity [27]. Electromagnetic scattering in one dimension

assumes that the scattered field is confined to waveguides that are connected to a two dimensional waveguide junction. In Silvester's approach, the electromagnetic field in the waveguides are expressed in terms of normal modes and the normal modes in the waveguide junction are solved by using the finite element method. Continuity of the field between the two sets of modes is then used to determine the total field.

The modal approach to two dimensional scattering was developed by Mei [12,13] and called the unimoment method. In Mei's approach, the electromagnetic field in the exterior region is expressed in terms of the normal modes for this open region. Each mode is then used to set up a finite element problem that is solved for the interior field. The total field is given by a linear combination of these finite element solutions. An unfortunate aspect of this approach is that continuity must be imposed on both the field and its derivative along the picture frame boundary.

While both of these modal solution procedures work, they are both expensive. Silvester's approach requires that the normal modes of the finite element region be computed; finding these eigenfunctions is a very costly process. Mei's approach requires that n finite element problems be solved where n is the number of modes used in the exterior region. Further, Mei's method results in non-symmetric matrices with which the standard preconditioned conjugate gradient algorithm doesn't work.

3.2 PRELIMINARY INVESTIGATIONS

At the start of this project, we planned to use the cloning algorithm to model the field in the exterior region. It promised to be fast and accurate, and was simple to program. As stated above, in cloning a single layer of finite elements is created on the surface of a picture frame boundary. The entire exterior field description is extracted from this single layer in cloning, while in ballooning layer after layer of similar, larger elements are added to the first. The idea is that since all of the field information is in the single layer - after all it is just replicated in ballooning to form the other layers - it should be possible to obtain the essential characteristics of the exterior field from this one layer. The way this was accomplished by Das Gupta is to assume that the field falls off as $1/R$ from the inside to the outside of this layer: imposing this condition on the single layer finite element model results in an eigenvalue equation for the field in the single layer and hence for the full problem. However, in using the algorithm to solve some test problems, we were unable to get the correct answers. We believe now that decay rate of $1/R$ is correct only far from the scatterer and does not apply to a layer of elements that are close to the scattering object. To make the procedure valid, we must move the picture frame far enough from the scatterer to make the $1/R$ decay rate valid; however, at that distance there is no need to compute the exterior field any further - one has already obtained the far field pattern. Consequently, we abandoned the idea of using the cloning algorithm of Das Gupta to compute the exterior field.

The next approach we used to solve the exterior field problem was to modify the ballooning algorithm in such a way that the size of the elements in the replicated layers stays constant. The purpose of this, of course, is to ensure that if the first layer of finite elements is small enough to approximate the wave

correctly, then all other layers of elements are small enough as well. To accomplish this objective, we had to abandon the idea of using a radial star point to generate the elements; instead, we devised various rectangular patterns of elements with the desired property. However, it became apparent in working with these patterns in two dimensions that this approach was quite unwieldy; it would be impossible to use in three dimensions. Thus, we were forced to abandon the ballooning approach as well.

Fortunately, we next turned to the modal approach to model the exterior field. After a few false starts, we discovered an excellent way to model the exterior field in scattering problems. We call the new approach the transfinite element method, and it is described next.

3.3 THE TRANSFINITE ELEMENT METHOD

The basic idea of the transfinite element method is to use the modal expansion functions that represent the exterior field as approximation functions in the variation procedure. In effect, the modes form semi-infinite finite element basis functions for the semi-infinite region. Full details of the transfinite element method along with some examples of solutions of two dimensional scattering problems are given in Appendix E.

There are many advantages of the transfinite element method compared with other procedures:

1. **It is a direct method.** Since the modal functions in the transfinite element method are used in exactly the same way as finite element functions, this method gives the solution of scattering problems directly in one step. In the unimoment method, modal functions are used to match the exterior and interior field solutions but are not used directly in the variational procedure. Consequently, many finite element solutions must be computed to obtain a single field solution with the unimoment method, while only one finite element solution is required for each frequency with the transfinite element method.
2. **It is a symmetric method.** The transfinite element method produces symmetric matrix equations that are easily solved by the preconditioned conjugate gradient algorithm. With large problems, this is orders of magnitude faster than solving non-symmetric matrix equations by other sparse matrix techniques.
3. **It is a simple method.** Only one solution is required and only continuity of the field is required in the transfinite element method. Methods that require multiple solutions and continuity of both the field and its derivative are more difficult to program and are less accurate as well.
4. **It is an efficient method.** With almost all exterior boundary models, the number of variables corresponding to the exterior field is equal to the number of nodes on the picture frame boundary. This is very costly: there are many picture frame boundary nodes and all of these nodes are

interconnected so that the corresponding matrix elements are full. In the transfinite element method, the number of variables corresponding to the exterior field is equal to the number of modes - not nodes - used to approximate the exterior field. This is a relatively small number - usually on the order of ten or twenty - compared to the hundreds or even thousands of nodes on the boundary. Thus, the transfinite element method provides a relatively efficient procedure for approximating the exterior field.

In every respect, the transfinite element method is better than the existing alternatives. By making the exterior field model simple and efficient, the solution of large scattering problems becomes possible. In fact, the transfinite element method is so good and so simple that one is tempted to ask: Why wasn't the transfinite element method invented years ago? The answer seems to be that very few people have ever worked on differential methods to model scattering problems, and the few that have worked in this area have pursued other directions of research.

4. SPECTRAL METHODS

As noted in the Introduction, frequency domain methods are more efficient for continuous wave modeling than are time domain methods. However, many problems require that the response to electromagnetic scattering be computed over a wide frequency range. If done by brute force, this still may require considerable computer time. Often, a hundred or more frequency points are required implying that a hundred or more finite element problems must be solved.

In an effort to decrease the computational requirements, we have pursued the following idea: Suppose that we compute the field problem at just a few frequencies and then use these frequencies to give the solution everywhere within the band of interest. This linear combination of solutions will provide a good approximation to the field at other frequencies provided that the solution frequencies account for all of the significant events in the scattering. The question is thus: How can one determine the proper subset of frequencies in a frequency range that gives the correct overall solution?

To answer this question we have developed an adaptive frequency response modeling procedure. Essentially, the idea is a simple one: First solve the problem twice - once at a low frequency and a second time at a high frequency - and then evaluate the residual of the linear combination solution at one hundred points in between. Then solve the problem again at the frequency that gives the highest residual, form the linear combination solution with all three solutions, compute the residuals, and repeat the process over and over. After six or seven iterations, the residuals at all one hundred points are usually within acceptable limits so that the procedure stops; instead of computing a hundred finite element solutions, we have obtained the same accuracy over the full frequency range with only six or seven finite element solution. Details of the adaptive spectral response modeling procedure are given in Appendix F. Although the application in this Appendix is for modeling one dimensional electromagnetic scattering, no change is required to use this procedure in modeling two and three dimensional scattering.

5. CONCLUSIONS

This report provides several breakthroughs in the computation of electromagnetic fields. For the first time stable finite element solutions of three dimensional electromagnetics problems have been obtained. Further, a new method of solving two dimensional scattering problems called the transfinite element method has been developed that is much more efficient than the existing alternatives.

With regard to the issue of stability, until now, no one could be certain with a finite element solution whether the computed solution corresponded to a real physical field or was nonsense. We have, however, explained in this report the root cause of these spurious solutions. We have also developed three different procedures to eliminate them: (1) use mixed-order rectangular elements, (2) use edge-based tangential continuity elements, or (3) use derivative continuous C^1 elements. Although the mixed-order rectangular elements were the first to be developed, they are perhaps the least useful because of the inflexibility of rectangles in modeling complex shapes. The edge-based and the C^1 elements are both tetrahedral and do not suffer from this geometric limitation. Of these two elements, the edge-based element is the most useful since it is simpler and more efficient than the C^1 element.

With regard to the problem of efficiency, two major developments are reported: First, for the first time finite element solutions of open electromagnetic scattering problems have been obtained by using a *one-step* process that we have called the transfinite element method. Prior to the transfinite element method, scattering problems required that many time steps or many modes be used to produce each finite element solution. The one step transfinite element method is many orders of magnitude more efficient for solving scattering problems than the existing alternatives. In addition, it is more accurate since it does not require that derivatives of the solution be computed numerically but relies on variational principles to set derivative values.

The second major efficiency improvement reported here is the creation of an adaptive algorithm to compute the scattered fields over a range of frequencies. Heretofore, the computation of electromagnetic scattering over a frequency range required that it be performed perhaps a hundred different times; we have shown that, by adaptively selecting the solution frequencies, the same accuracy throughout the frequency range of interest can be obtained by using only six or seven properly chosen frequencies. Thus, for scattering problems in which the response over a range of frequencies is desired, the adaptive algorithm provides an order of magnitude improvement in the efficiency of the solution process. The algorithm was applied in this report to the solution of the one-dimensional scattering problems encountered in waveguide junctions; extension to two and three-dimensional scatterers is straightforward.

Unfortunately, while considerable progress has been reported, there was insufficient time to put all of the pieces together and develop a working computer code to solve three-dimensional scattering problems. Although we pursued this research in a logical, methodical manner, one graduate student working for thirty months could not complete the desired three dimensional scattering computer program. In fact, the nominal 'one' graduate student supported by this project turned out to be three different students in succession since, due to various circumstances, two students left this project and had to be replaced. However, several major difficult theoretical problems have been solved. The fact that we did not succeed in solving bistatic scattering problems from large three dimensional absorbing bodies does not mean that the approach taken here is not a good one.

REFERENCES

1. P. Silvester, "A General High-Order Finite-Element Waveguide Analysis Program," *IEEE Trans.*, Vol MTT-17, pp. 204-210, April 1969.
2. Z.J. Cendes and P.J. Silvester, "Numerical Solution of Dielectric Loaded Waveguides: I - Finite-Element Analysis," *IEEE Trans. Microwave Theory Tech.*, Vol. MTT-18, pp. 1124-1131, Dec. 1970.
3. S. Ahmed and P.J. Daly, "Finite-Element Methods for Inhomogeneous Waveguides," *Proc. Inst. Elec. Eng.*, Vol. 116, pp. 1661-1664, Oct. 1969.
4. N. Mabaya, P.E. Lagasse and P. Vandenbulke, "Finite Element Analysis of Optical Waveguides," *IEEE Trans.*, Vol. MTT-29, pp. 600-605, June 1981.
5. J.B. Davies, F.A. Fernandez and G.Y. Philippori, "Finite Element Analysis of All Modes in Cavities with Circular Symmetry," *IEEE Trans.*, Vol. MTT-30, pp. 1975-1980, 1982.
6. B.M.A. Rahman and J.B. Davies, "Finite-Element Analysis of Optical and Microwave Waveguide Problems," *IEEE Trans.*, Vol MTT-32, pp. 20-28, 1984.
7. A. Konrad, "Vector Variational Formulation of Electromagnetic Fields in Anisotropic Media," *IEEE Trans.*, Vol MTT-24, pp. 553-559, September 1976.
8. M. Koshiba, K. Hayota and M. Suzuki, "Improved Finite-Element Formulation in Terms of the Magnetic Field Vector for Dielectric Waveguides," *IEEE Trans.*, Vol. MTT-33, pp. 227-233, March 1985.
9. J.R. Winkler and J.B. Davies, "Elimination of Spurious Modes in Finite Element Analysis," *J. Computational Physics*, Vol. 56, pp. 1-14, 1984.
10. M. Hara, T. Wada, T. Fukasawa and F. Kikuchi, "Three-Dimensional Analysis of RF Electromagnetic Field by the Finite Element Method," *IEEE Trans.*, Vol. MAG-19, pp. 2417-2420, November 1983.
11. A. Konrad, "On the Reduction of the Number of Spurious Modes in the Vectorial Finite Element Solution of Three-Dimensional Cavities and Waveguides," General Electric Company, Technical Information Series, Report No. 84 CRD275, October 1984.
12. S.-K. Chang and K.K. Mei, "Application of the Unimoment Method to Electromagnetic Scattering of Dielectric Cylinders," *IEEE Trans.*, pp. 35-42, January 1976.
13. A.C. Cangellaris, C.C. Lin and K.K. Mei, "Point Matching Time Domain Finite Element Methods for Electromagnetic Radiation and Scattering," *IEEE Trans on Antennas and Propagation*, Vol. AP-35, pp. 1160-1173, 1987.
14. A. Taflov and M.E. Brodwin, "Numerical Solution of Steady-State Electromagnetics Equations Using Time-Dependent Maxwell's Equations," *IEEE Trans. on Microwave Theory & Techniques*, Vol. MTT-23, pp. 623-630, 1975.

15. A. Taflov, "Application of the Finite-Difference Time-Domain Method to Sinusoidal Steady-State Electromagnetic-Penetration Problems," *IEEE Trans on Electromag. Compat.*, Vol. EMC-22, pp. 191-203, 1980.
16. K.S. Yee, "Numerical Solution of Initial Boundary Value Problems Involving Maxwell's Equations in Isotropic Media," *IEEE Trans. Antennas & Prop.*, Vol. AP-14, pp. 302-307, 1966.
17. G. Strang and G.J. Fix, *An Analysis of the Finite Element Method*, Prentice-Hall, NJ., 1973.
18. S.R.H. Hoole and Z.J. Cendes, "Projective Methods for Laplacian Fields," *COMPEL*, Vol. 4, pp. 195-207, 1985.
19. M. Hano, "Finite-Element Analysis of Dielectric-Loaded Waveguides," *IEEE Trans.*, Vol. MTT-32, pp. 1275-1279, 1984.
20. P. Silvester and M.S. Hsieh, "Finite-Element Solution of 2-Dimensional Exterior Field Problems," *Proc. Inst. Elec. Eng.*, pp. 1743-1747, December 1971.
21. I.A. Cermak and P. Silvester, "Solution of 2-Dimensional Field Problems by Boundary Relaxation," *Proc. IEE*, Vol. 115, pp. 1341-1348, 1968.
22. B.H. McDonald and A. Wexler, "Finite-Element Solution of Unbounded Field Problems," *IEEE Trans.*, pp. 841-847, December 1972.
23. A.C. Ludwig, "A Comparison of Spherical Wave Boundary Value Matching Versus Integral Equation Scattering Solutions for a Perfectly Conducting Body," *IEEE Trans. on Antennas & Prop.*, Vol. AP-34, pp. 857-865, 1986.
24. P.P. Silvester, D.A. Lowther, C.J. Carpenter, "Exterior Finite Elements for Two-Dimensional Field Problems with Open Boundaries," *Proc. IEE*, pp. 1267-1270, 1977.
25. G. Dasgupta, "Computation of Exterior Potential Fields by Infinite Substructuring," *Computer Methods in Applied Mechanics and Engineering*, pp. 295-305, 1984.
26. H. Hurwitz, Jr., "Tests of a Nonlinear Matrix Equation Formulation of Infinitesimal Scaling," General Electric Corporate Research and Development Report 83CRD084, May 1983.
27. P. Silvester, "Finite Element Analysis of Planar Microwave Networks," *IEEE Trans. Microwave Theory Tech.*, Vol. MTT-221, pp. 104-108, February 1973.
28. Cendes, Z.J., D.N. Shenton and H. Shahnasser, "Magnetic Field Computation Using Delaunay Triangulation and Complementary Finite Element Methods", *IEEE Transactions on Magnetics*, Vol. MAG-19, No. 6, November 1983, pp. 2551-2554.
29. Cendes, Z.J. and D.N. Shenton, "Complementary Error Bounds for Foolproof Finite Element Mesh Generation", *Mathematics and Computers in Simulation*, Vol. 27, 1985, pp. 295-305.
30. Cendes, Z.J. and D.N. Shenton, "Adaptive Mesh Refinement in the Finite Element Computation of Magnetic Fields", *IEEE Transactions on Magnetics*, Vol. MAG-21, No. 5, September 1985, pp. 1811-1816.
31. Shenton, D.N. and Z.J. Cendes, "MAX - An Expert System for Automatic Adaptive Magnetics Modeling", *IEEE Transactions on Magnetics*, Vol. MAG-22, pp. 805-807, 1986.

32. Shenton, D.N. and Z.J. Cendes, "Three-Dimensional Finite Element Mesh Generation Using Delaunay Tessellation", *IEEE Transactions on Magnetics*, Vol. MAG-21, No. 6, November 1985, pp. 2535-2538.
33. Barton, M.L. and Z.J. Cendes, "New Vector Finite Elements for Three-Dimensional Magnetic Field Computation", *Journal of Applied Physics*, Vol. 61 (8), 1987, pp. 3919-3921.
34. M.F. Catedra, E. Gago and L. Nuno, "A Numerical Scheme to Obtain the RCS of Three-Dimensional Bodies of Resonant Size Using the Conjugate Gradient Method and the Fast Fourier Transform", *IEEE Trans. Antennas & Prop.*, Vol. 37, pp. 528-537, 1989.

APPENDIX A - MIXED-ORDER RECTANGULAR FINITE ELEMENTS FOR THE SOLUTION OF THREE-DIMENSIONAL ELECTROMAGNETIC FIELDS

ABSTRACT

A new method for modeling electromagnetic waves by the finite element method is presented in this appendix. In this formulation, different orders of polynomials are used to approximate the three different components of either the electric or the magnetic field vectors. We show that this procedure eliminates the problem of spurious nodes that has plagued previous three-dimensional finite element solutions. The method is applied to find the electromagnetic fields in homogeneous and dielectric-loaded cavities.

INTRODUCTION

The finite element method is often advanced as a useful numerical procedure for modeling high-frequency electromagnetic wave phenomena. Applied at an early date to solve homogeneous waveguide problems,¹ the method has proved to be extremely accurate and reliable for these problems. However, when the finite element method was applied to the study of inhomogeneous waveguides, to three-dimensional resonant cavities and to scattering problems, difficulties in the form of "spurious" modes were encountered. In the context of numerical modeling, a spurious mode is defined to be a non-physical solution of the electromagnetic field equations that is computed simultaneously with the correct physical solutions.

Since the presence of a spurious mode in a numerical solution can destroy the validity of the solution, much effort has been directed at reducing or eliminating the unwanted behavior. The first approach, originally suggested by Konrad,² is to enforce the electromagnetic field boundary conditions exactly on the finite element approximation space. This procedure has been used by Mabaya, Lagasse and Vandenbulke³ in an $E_z - H_z$ formulation and by Davies, Fernandez and Philippon⁴ and by Rahman and Davies⁵ in the 3-component H formulation; all three papers report only limited success in eliminating spurious modes by this technique. Recently, Koshiba, Hayata, and Suzuki⁶ have shown that rigorous enforcement of boundary conditions does indeed eliminate spurious modes above the "air line" (i.e. the line $\beta/k_0 = 1$ in a β/k_0 plot) but does not work in general below the air line.

The second approach to eliminating spurious modes is to modify the functional in the variational principle used to approximate the fields. Working independently, Winkler and Davies⁷ and Hara, Wada, Fukasawa and Kikuchi⁸ have recognized that the spurious modes do not satisfy the zero divergence condition on the electric or magnetic field. Both references suggest adding a penalty term proportional to the norm of the divergence of the field to the functional. Unfortunately, this procedure does not eliminate the spurious modes completely. However, as demonstrated in reference 8, the spurious modes are not stable with respect to the amount of penalty, and can be distinguished from correct solutions by plotting

the finite element eigenvalue spectra with respect to the penalty parameter. Of course, this procedure is highly inefficient and cumbersome: each new field problem must be solved repeatedly and all of the eigenvalues plotted in order to identify the correct solution.

The related procedure to reducing the number of spurious modes was proposed recently by Konrad.⁹ References 7 and 8 are based on minimizing a functional derived from the vector wave equation with the addition of a zero-divergence penalty term. Konrad suggests using the vector Helmholtz equation instead and finds that "... a great number, though not all of the spurious solutions are indeed eliminated." This result is not surprising since the variational expressions derived for the vector Helmholtz equation and for the vector wave equation with the addition of a unit penalty term are identical in the case of homogeneous media.

The third approach to eliminating spurious modes in finite element solutions is to restrict the finite element approximation functions to lie in a reduced vector space. In this view, spurious modes are the result of using improper functions in the variational procedure. To ensure that only correct solutions are generated, one must employ only admissible functions in the finite element approximation. This is the approach taken in this report.

The use of a restricted function space to eliminate spurious modes in finite element analysis was first suggested by Hano.¹⁰ Hano showed that, in two dimensional problems, spurious modes are completely eliminated by using combination constant-linear finite element approximation functions. These functions have two interesting properties: (1) their divergence is identically zero, and (2) they are discontinuous at element boundaries.

In this paper, we derive a set of restricted finite element basis functions for the solution of three dimensional electromagnetic field problems and show that only correct, physical solutions are obtained with the new elements. As in the case in reference 10, the functions reported here employ different orders of polynomial approximation in different directions in each element. However, in addition to being three dimensional, the approximation functions presented here are high-order, are continuous across element boundaries and are not necessarily non-divergent.

FORMULATION OF THE EM FIELD EQUATIONS

Electromagnetic wave propagation is governed by the vector wave equations.

$$\nabla \times \frac{1}{\mu_r} \nabla \times \mathbf{E} = \epsilon_r k_o^2 \mathbf{E} \quad (1)$$

$$\nabla \times \frac{1}{\epsilon_r} \nabla \times \mathbf{H} = \mu_r k_o^2 \mathbf{H} \quad (2)$$

where μ_r and ϵ_r are the relative permeability and relative permittivity of the material, respectively, and $k_o^2 = \omega^2 \mu_o \epsilon_o$. At the interface between two dielectrics, the tangential components of the electric and magnetic fields must be continuous

$$\mathbf{1}_n \times (\mathbf{E}^{(1)} - \mathbf{E}^{(2)}) = 0 \quad (3)$$

$$\mathbf{1}_n \times (\mathbf{H}^{(1)} - \mathbf{H}^{(2)}) = 0 \quad (4)$$

while the normal components are discontinuous as follows

$$\mathbf{1}_n \cdot (\epsilon_1 \mathbf{E}^{(1)} - \epsilon_2 \mathbf{E}^{(2)}) = 0 \quad (5)$$

$$\mathbf{1}_n \cdot (\mu_1 \mathbf{H}^{(1)} - \mu_2 \mathbf{H}^{(2)}) = 0 \quad (6)$$

In these equations, superscripts (1) and (2) refer to media 1 and media 2, respectively, and $\mathbf{1}_n$ represents the unit normal to the boundary.

In the remainder of this paper, we shall use the electric field \mathbf{E} as the unknown. Obviously, a similar treatment holds for \mathbf{H} . In terms of \mathbf{E} , equation (4) and (6) become

$$\mathbf{1}_n \times \left(\frac{1}{\mu_1} \nabla \times \mathbf{E}^{(1)} - \frac{1}{\mu_2} \nabla \times \mathbf{E}^{(2)} \right) = 0 \quad (7)$$

$$\mathbf{1}_n \cdot (\nabla \times \mathbf{E}^{(1)} - \nabla \times \mathbf{E}^{(2)}) = 0 \quad (8)$$

We must therefore solve equation (1) subject to the interface conditions (3), (5), (7) and (8).

Konrad¹ has shown that the Euler equation of the functional

$$F = \frac{1}{2} \int \left\{ \frac{1}{\mu_r} |\nabla \times \mathbf{E}|^2 - \epsilon_r k_o^2 |\mathbf{E}|^2 \right\} d\Omega \quad (9)$$

is equation (1) and that the corresponding natural boundary equation (7) is the natural boundary condition for this functional. If one wants to compute the electric field inside a cavity containing variable-permeability materials, one needs to minimize (9) in an appropriate function space.

While the solution process described above has been widely reported in the literature^{2,4-7,10-13}, as noted in the introduction, there are serious problems. To eliminate these problems, we need to define the approximation functions for \mathbf{E} carefully.

A BASIS FOR CURL

To solve for E via equation (9), we must find a legitimate approximation for the curl operator. An operator has a domain, a nullspace and a range; it is not enough — as had been done in the past — to approximate only the domain of the curl operation.

The nullspace of an operator is defined to be the set of functions that produce zero when the operator acts on it

$$N(A) = \{x: Ax = 0 \text{ for all } x\} \quad (10)$$

It is well known that the nullspace of the curl operator is provided by the gradient operator

$$N(\text{curl}) = \nabla \phi \quad (11)$$

where ϕ is an arbitrary scalar.

Let us approximate ϕ by finite element basis functions $\tilde{\alpha}(x,y,z)$ over a rectangular parallelepiped

$$\phi(x,y,z) = \tilde{\alpha}^{(m,n,p)}(x,y,z)\phi \quad (12)$$

The polynomial $\tilde{\alpha}^{(m,n,p)}(x,y,z)$ is m 'th order in the x -direction, n 'th in y , and p 'th in z . Using the Kronecker matrix product, three-dimensional interpolation polynomials for brick-shaped elements are given by

$$\tilde{\alpha}^{(m,n,p)}(x,y,z) = \tilde{\alpha}^{(m)}(x) \otimes \tilde{\alpha}^{(n)}(y) \otimes \tilde{\alpha}^{(p)}(z) \quad (13)$$

where $\alpha^{(m)}$ is a one-dimensional m 'th order interpolation polynomial and the symbol \otimes denotes the Kronecker product defined in Appendix AA.

Since the derivative of an n 'th order polynomial is $(n-1)$ 'st order, it follows that the nullvectors of the curl operator must have the form

$$\begin{aligned} E_x(x,y,z) &= \tilde{\alpha}^{(m-1,n,p)} E_x \\ E_y(x,y,z) &= \tilde{\alpha}^{(m,n-1,p)} E_y \\ E_z(x,y,z) &= \tilde{\alpha}^{(m,n,p-1)} E_z \end{aligned} \quad (14)$$

We may write this in the compact form

$$E = \gamma \tilde{E} \quad (15)$$

where

$$\gamma = \begin{bmatrix} \tilde{\alpha}^{(m-1,n,p)} & 0 & 0 \\ 0 & \tilde{\alpha}^{(m,n-1,p)} & 0 \\ 0 & 0 & \tilde{\alpha}^{(m,n,p-1)} \end{bmatrix} \quad (16)$$

$$\underline{E} = \begin{bmatrix} E_x \\ E_y \\ E_z \end{bmatrix} \quad (17)$$

The curl of \underline{E} is evaluated as

$$\nabla \times \underline{E} = \begin{bmatrix} 0 & -\partial/\partial z & \partial/\partial y \\ \partial/\partial z & 0 & -\partial/\partial x \\ -\partial/\partial y & \partial/\partial x & 0 \end{bmatrix} \begin{bmatrix} E_x \\ E_y \\ E_z \end{bmatrix} \quad (18)$$

Substituting (13) into (19) gives

$$\nabla \times \underline{E} = \beta \underline{C} \underline{E} \quad (19)$$

where

$$\beta = \begin{bmatrix} \tilde{\alpha}^{(m,n-1,p-1)} & 0 & 0 \\ 0 & \tilde{\alpha}^{(m-1,n,p-1)} & 0 \\ 0 & 0 & \tilde{\alpha}^{(m-1,n-1,p)} \end{bmatrix} \quad (20)$$

$$\underline{C} = \begin{bmatrix} 0 & -D_z & D_y \\ D_z & 0 & -D_x \\ -D_y & D_x & 0 \end{bmatrix}$$

where the matrices D_i are called differentiation matrices and are defined in the Appendix.

We note that the factorization in equation (19) is not possible if the same order of polynomial is used to approximate E_i in all three directions.

COMPUTING THE MATRIX ELEMENTS

Substituting equations (15) and (19) into equation (9) and minimizing with respect to the coefficients \underline{E} results in the matrix equation

$$\mathbf{C}^T \mathbf{K} \mathbf{C} \underline{E} = k_0^2 \mathbf{M} \underline{E} \quad (21)$$

where \mathbf{K} and \mathbf{M} are the matrices

$$\mathbf{K} = \int \frac{1}{\mu_r} \beta^T \beta \, d\Omega \quad (22)$$

$$\mathbf{M} = \int \epsilon_r \gamma^T \gamma \, d\Omega \quad (23)$$

To evaluate the matrix elements in \mathbf{K} and \mathbf{M} , it is sufficient to evaluate the integral

$$G^{(r,s)} = \int \tilde{\alpha}^{(r,s)} T \tilde{\alpha}^{(r,s)} \, d\Omega \quad (24)$$

Substituting equation (13) into (25) gives

$$\mathbf{G} = (1/L_x L_y L_z) \int (\tilde{\alpha}^r(\zeta) \otimes \tilde{\alpha}^s(\xi) \otimes \tilde{\alpha}^t(\lambda))^T (\tilde{\alpha}^r(\zeta) \otimes \tilde{\alpha}^s(\xi) \otimes \tilde{\alpha}^t(\lambda)) \, d\zeta d\xi d\lambda \quad (25)$$

where L_x , L_y and L_z are the dimensions of the brick element, and ζ , ξ and λ are homogeneous coordinates in the brick. This can be converted into

$$\mathbf{G} = (1/L_x L_y L_z) T^{(r)} \otimes T^{(s)} \otimes T^{(t)} \quad (26)$$

where

$$T^{(1)} = \int \tilde{\alpha}^{(1)}(\zeta) \tilde{\alpha}^{(1)}(\zeta) \, d\zeta \quad (27)$$

$$T^{(2)} = \frac{1}{6} \begin{bmatrix} 2 & 1 \\ 1 & 2 \end{bmatrix} \quad (28)$$

$$T^{(3)} = \frac{1}{30} \begin{bmatrix} 4 & 2 & -1 \\ 2 & 16 & 2 \\ -1 & 2 & 4 \end{bmatrix} \quad (29)$$

To evaluate the finite element coefficient matrix for one element, one therefore needs to form the matrices \mathbf{K} and \mathbf{M} using equations (27) and (28), evaluate \mathbf{C} by using the values in the Appendix, and pre- and post-multiply \mathbf{K} by \mathbf{C}^T and \mathbf{C} , respectively. The contribution from each element is combined with the other elements in the grid to form a large, sparse matrix eigenvalue problem. This eigenvalue problem is solved by using established techniques for the eigenvalues k_0^2 and eigenvectors \underline{E} .

COMPUTATIONAL RESULTS

A computer program has been developed based on the above formulation to solve for the electromagnetic fields in resonant cavities. The program allows finite elements of mixed orders to be assembled and solved for complex three-dimensional geometries.

EMPTY CUBIC BOX

The solution provided by the present method is first tested with the analytical solution of an empty cubic cavity of 1 m^3 . The cubic box is divided into $2 \times 2 \times 2$ elements. The results obtained by using constant-bilinear ($m = n = p = 1$), linear-biquadratic ($m = n = p = 2$) and quadratic-bicubic ($m = n = p = 3$) elements are shown in Tables 1-3. A one-to-one correspondence exists between the approximate eigenvalues and the exact ones. Since no spurious modes are produced, the approximate eigenvalues are easily identified. The results also show that the dominant eigenvalue is approximated reasonably well even with a small number of elements.

Solutions obtained by using high-order elements are seen to be much more precise than is the case with constant-bilinear element solutions. The reason for the increased accuracy is twofold: (1) Higher-order polynomials are more accurate than low-order ones, and (2) higher-order elements are continuous across element boundaries while constant-bilinear elements are not.

DIELECTRIC-LOADED BOX

Our computational procedure has also been applied to solve the dielectric-loaded cavities shown in Figure 1 and the results compared with those obtained by other methods. In this case, the magnetic field is solved subject to natural boundary conditions $1_n \times (\nabla \times H) = 0$ on perfectly conducting walls and Dirichlet conditions $1_n \times H = 0$ on symmetry planes. Comparison of our results with previous solutions is shown in Table 4, where the cavities are divided into $2 \times 2 \times 2$ linear-biquadratic elements. Again, the dominant eigenvalue is approximated well, despite the fact that only 8 elements are employed.

NUMBER OF ZERO EIGENVALUES

The number of the unknowns and the number of zero eigenvalues computed depends not only on the number of elements employed but also on the type of boundary conditions imposed. There are two kinds of vector Dirichlet boundary conditions: One is a tangential boundary where the tangential components of the field vector are set to zero; the other is normal boundary where the normal component of the field vector is set to zero. Empirically, we find that the number of zero eigenvalues for a box divided into $a \times b \times c$ elements is given by

$$\text{number zero} = (ta + s - na)(tb + s - nb)(tc + s - nc) - 1 \quad (30)$$

+ number of disjointed tangential boundaries

where $t = 1$ and $s = 1$ for constant bilinear elements, $t = 1$ and $s = 2$ for linear biquadratic elements, $t = 2$ and $s = 2$ for quadratic-bicubic elements, and na , nb and nc are numbers of Dirichlet boundary

conditions imposed on the walls normal to the x , y and z directions, respectively. Enforcing boundary conditions exactly does reduce the size of global matrix and, consequently, the number of zero eigenvalues. We have not yet been able to explain the empirical formula in equation (30) by theoretical means.

CONCLUSIONS

Three-dimensional electromagnetic field problems may be solved by using mixed order finite elements to approximate the vector field. In this approach, a consistent numerical approximation is made for the domain, range, and null spaces of the curl operator. Such a consistent approximation in the solution of the vector wave equation eliminates the problem of spurious modes that had plagued previous solution procedures.

A limitation of the present formulation is the restriction of the element shapes to be rectangular parallelepipeds. For problems involving complicated shapes, tetrahedral or isoparametric elements would be preferred. The use of such elements with mixed-order polynomial basis functions is presently under investigation.

REFERENCES

1. P. Silvester, "A General High-Order Finite-Element Waveguide Analysis Program," IEEE Trans., Vol. MTT-17, pp. 204-210, April 1969.
2. A. Konrad, "Vector Variational Formulation of electromagnetic Fields In Anisotropic Media", IEEE Trans., Vol. MTT-24, pp. 553-559, September 1976.
3. N. Mabaya, P.E. Lagasse and P. Vandenbulke, "Finite Element Analysis of Optical Waveguides," IEEE Trans., Vol. MTT-29, pp. 600-605, June 1981.
4. J.B. Davies, F.A. Fernandes and G.Y. Philippori, "Finite Element Analysis of All Modes in Cavities with Circular Symmetry," IEEE Trans., Vol. MTT-30, pp. 1975-1980, 1982.
5. B.M.A. Rahman and J.B. Davies, "Finite-Element Analysis of Optical and Microwave Waveguide Problems," IEEE Trans., Vol. MTT-32, pp. 20-28, 1984.
6. M. Koshiha, K. Hayota, and M. Suzuki, "Improved Finite-Element Formulation in Terms of the Magnetic Field Vector for Dielectric Waveguides", IEEE Trans., Vol. MTT-33, pp. 227-233, March 1985.
7. J.R. Winkler and J.B. Davies, "Elimination of Spurious Modes in Finite Element Analysis", J. Computational Physics, Vol. 56, pp. 1-14, 1984.
8. M. Hara, T. Wada, T. Fukasawa, and F. Kikuchi, "Three Dimensional Analysis of RF Electromagnetic Field by the Finite Element Method", IEEE Trans., Vol. MAG-19, pp. 2417-2420, Nov. 1983.
9. A. Konrad, "On the Reduction of the Number of Spurious Modes in the Vectorial Finite Element Solution of Three-Dimensional Cavities and Waveguides", General Electric Company, Technical Information Series, Report No. 84 CRD275, October, 1984.

10. M. Hano, "Finite-Element Analysis of Dielectric-Loaded Waveguides," IEEE Trans., Vol. MTT-32, pp. 1275-1279, 1984.
11. R.L. Ferrari and G.L. Maile, "Three-Dimensional Finite Element Method for Solving Electromagnetic Problems", Electronics Letters, Vol. 14, pp. 467-468, 1978.
12. J.P. Webb, G. L. Maile, and R.L. Ferrari, "Finite Element Solution of Three-Dimensional Electromagnetic Problems," IEE Proc. H, Microwaves, Optics and Antennas, Vol. 130, pp. 153-159, 1983.
13. M. de Pourcq, "Field and Power-Density Calculations by Three-Dimensional Finite Elements", IEE Proc. H, Vol. 130, pp. 377-384, 1983.
14. Z. Cendes, "A Finite Element Method for the General Solution of Ordinary Differential Equations", Int. J. Num. Meth. Engn., Vol. 9, pp. 551-561, 1975.

APPENDIX AA - RECTANGULAR BASIS FUNCTIONS

To see how approximation functions are formed for bricks, first consider the two-dimensional case. An arbitrary rectangular reference element is mapped onto the unit square by the transformation

$$\zeta = (x - x_R)/L_x \quad (A1)$$

$$\xi = (y - y_R)/L_y \quad (A2)$$

Two-dimensional basis functions may be obtained from one-dimensional functions by using the Kronecker matrix product.

Definition:

If A is an nxm matrix and B is a pxq matrix, then the Kronecker matrix product of A and B is denoted by $A \otimes B$ and is the npxmq matrix

$$A \otimes B = \begin{bmatrix} a_{11}B & a_{12}B & \dots & a_{1m}B \\ \vdots & \vdots & & \vdots \\ \vdots & \vdots & & \vdots \\ a_{n1}B & a_{n2}B & \dots & a_{nm}B \end{bmatrix} \quad (A3)$$

Kronecker matrix products satisfy the following useful identities¹⁴

$$(i) \quad A \otimes (B+C) = A \otimes B + A \otimes C$$

$$(ii) \quad \alpha A \otimes \beta B = \alpha\beta(A \otimes B)$$

$$(iii) \quad AB \otimes CD = (A \otimes C)(B \otimes D)$$

$$(iv) \quad (A \otimes B)^{-1} = A^{-1} \otimes B^{-1}$$

$$(v) \quad (A \otimes B)^T = A^T \otimes B^T$$

In general, one-dimensional n'th order interpolation polynomials are defined as

$$\alpha^{(n)}_k(\zeta) = \prod_{i=1}^{n+1} \frac{(\zeta - \zeta_i)}{(\zeta_k - \zeta_i)} \quad (A4)$$

where the ζ_i are the interpolation nodes. Using the Kronecker matrix product, two-dimensional interpolation polynomials are given by

$$\tilde{\alpha}^{(n,m)}(\zeta, \xi) = \tilde{\alpha}^{(n)}(\zeta) \otimes \tilde{\alpha}^{(m)}(\xi) \quad (A5)$$

Now consider approximating an arbitrary function $\phi(\zeta, \xi)$ in terms of the finite element approximation functions. We may write this as

$$\phi(\zeta, \xi) = \tilde{\alpha}^{(m)}(\xi) \phi_{\mathcal{Q}}^{(n)}(\zeta) \quad (A6)$$

where Φ is an m by n matrix of values at the interpolation nodes. Equation (A7) is converted into the standard matrix form

$$\Phi(s, \xi) = \tilde{\alpha}(s, \xi) \underline{\phi} \quad (A7)$$

by defining a vector operation called *vec* in the following manner:

$$\text{Vec} A = \begin{bmatrix} \underline{A}_1 \\ \underline{A}_2 \\ \vdots \\ \underline{A}_n \end{bmatrix} \quad (A8)$$

where \underline{A}_i is the i 'th column of the matrix A . The operator *vec* and the Kronecker product are related by the identity

$$\text{vec } ABC = (C^T \otimes A) \text{vec} B \quad (A9)$$

The *vec* of a scalar is simply itself; therefore, taking *vec* of both sides of equation (A8) yields

$$\Phi(s, \xi) = (\tilde{\alpha}^{(n)}(s) \otimes \tilde{\alpha}^{(m)}(\xi)) \underline{\phi} \quad (A10)$$

where

$$\underline{\phi} = \text{vec} \Phi \quad (A11)$$

Three-dimensional finite elements are generated by an analogous procedure to that used in two-dimensions. Approximation functions for brick-shaped elements are given by the equation

$$\tilde{\alpha}^{(n,m,p)} = \tilde{\alpha}^{(n)}(s) \otimes \tilde{\alpha}^{(m)}(\xi) \otimes \alpha^{(p)}(\lambda) \quad (A12)$$

where (s, ξ, λ) are homogeneous coordinates in the brick.

DIFFERENTIAL MATRICES

One-dimensional differentiation matrices are defined by the equation¹⁴

$$\frac{d\alpha^{(n)}(\zeta)}{d\zeta} = \tilde{\alpha}^{(n-1)}(\zeta) D^{(n)} \quad (B1)$$

where $D^{(n)}$ is the n by $n+1$ differentiation matrix. The polynomials $\tilde{\alpha}^{(n-1)}(\zeta)$ in equation (B1) are of one order less than that of $\alpha^{(n)}(\zeta)$ because the derivative of an n 'th order polynomial is $(n-1)$ 'st order. Evaluating both sides of equation (B1) at the $(n-1)$ 'st order interpolation nodes $a_i^{(n-1)}, i = 1, \dots, n$ provides the elements of the differentiation matrix as

$$D_{ij}^{(n)} = D_{ij}^{(n)} = \left. \frac{d\alpha^{(n)}(\zeta)}{d\zeta} \right|_{\zeta = a_i^{(n-1)}}$$

Performing the indicated operations with the equispaced node interpolation polynomials gives the numerical values

$$\begin{aligned} D^{(1)} &= \begin{bmatrix} -1. & 1. \end{bmatrix} \\ D^{(2)} &= \begin{bmatrix} -3. & 4. & -1. \\ 1. & -4. & 3. \end{bmatrix} \\ D^{(3)} &= \begin{bmatrix} 05.5 & 9. & -4.5 & 1. \\ .125 & -3.375 & 3.375 & -.125 \\ -1. & 4.5 & -9. & -5.5 \end{bmatrix} \end{aligned} \quad (B3)$$

Note that the matrix D has the following anti-symmetry property

$$D_{ij}^{(n)} = -D_{n-i+1, n-j+2}^{(n)} \quad (B4)$$

To extend the above result to two-dimensions, we need to evaluate

$$\begin{aligned} \frac{\partial}{\partial \zeta} \tilde{\alpha}^{(m,n)}(\zeta, \xi) &= \frac{\partial}{\partial \zeta} \tilde{\alpha}^{(m)}(\zeta) \otimes \tilde{\alpha}^{(n)}(\xi) \\ &= \tilde{\alpha}^{(m-1)}(\zeta) D^{(m)} \otimes \tilde{\alpha}^{(n)}(\xi) \\ &= (\tilde{\alpha}^{(m-1)}(\zeta) \otimes \tilde{\alpha}^{(n)}(\xi)) (D^{(m)} \otimes I) \end{aligned} \quad (B5)$$

Thus we find that

$$\frac{\partial}{\partial \zeta} \tilde{\alpha}^{(m,n)}(\zeta, \xi) = \tilde{\alpha}^{(m-1,n)}(\zeta, \xi) D_{\zeta} \quad (\text{B6})$$

where

$$D_{\zeta} = D^{(m)} \otimes I \quad (\text{B7})$$

Similar results hold for derivatives in the ξ -direction and for three-dimensional elements.

Table 1. Eigenvalues of a homogeneous cubic cavity obtained by using constant-bilinear elements.

| | approx-eigenvalue | modes | exact-eigenvalue |
|---|-------------------|---------|------------------|
| 0 | 8.881784e-16 | | |
| 1 | 2.400000e+01 | (1,1,0) | 19.7392 |
| 2 | 2.400000e+01 | (1,0,1) | 19.7392 |
| 3 | 2.400000e+01 | (0,1,1) | 19.7392 |
| 4 | 3.600000e+01 | (1,1,1) | 29.6088 |
| 5 | 3.600000e+01 | (1,1,1) | 29.6088 |

Table 2. Eigenvalues obtained by using linear-biquadratic elements.

| | approx-eigenvalue | modes | exact-eigenvalue |
|----|-------------------|---------|------------------|
| 0 | -1.114664e-13 | | |
| 1 | -9.570122e-14 | | |
| 2 | -7.971401e-14 | | |
| 3 | -6.372680e-14 | | |
| 4 | -4.773959e-14 | | |
| 5 | -3.175238e-14 | | |
| 6 | -1.576517e-14 | | |
| 7 | 2.220446e-16 | | |
| 8 | 1.988769e+01 | (1,1,0) | 19.7392 |
| 9 | 1.988769e+01 | (1,0,1) | 19.7392 |
| 10 | 1.988769e+01 | (0,1,1) | 19.7392 |
| 11 | 2.961547e+01 | (1,1,1) | 29.6088 |
| 12 | 2.961547e+01 | (1,1,1) | 29.6088 |
| 13 | 4.994385e+01 | (2,1,0) | 49.3480 |
| 14 | 4.994385e+01 | (2,0,1) | 49.3480 |
| 15 | 4.994385e+01 | (1,2,0) | 49.3480 |
| 16 | 4.994385e+01 | (1,0,2) | 49.3480 |
| 17 | 4.994385e+01 | (0,2,1) | 49.3480 |
| 18 | 4.994385e+01 | (0,1,2) | 49.3480 |
| 19 | 5.926624e+01 | (2,1,1) | 59.2176 |
| 20 | 5.926624e+01 | (1,2,1) | 59.2176 |
| 21 | 5.926624e+01 | (1,1,2) | 59.2176 |
| 22 | 5.947009e+01 | (2,1,1) | 59.2176 |
| 23 | 5.947009e+01 | (1,2,1) | 59.2176 |
| 24 | 5.947009e+01 | (1,1,2) | 59.2176 |
| 25 | 8.000000e+01 | (2,2,0) | 73.9568 |
| 25 | 8.000000e+01 | (2,0,2) | 73.9568 |
| 26 | 8.000000e+01 | (0,2,2) | 73.9568 |

Table 3. Eigenvalues obtained by using quadratic-bicubic elements. The number of zero eigenvalues is equal to 64.

| approx-eigenvalue | modes | exact-eigenvalue |
|-------------------|---------|------------------|
| 64 1.974191e+01 | (1,1,0) | 19.7392 |
| 65 1.974191e+01 | (1,0,1) | 19.7392 |
| 66 1.974191e+01 | (0,1,1) | 19.7392 |
| 67 2.960891e+01 | (1,1,1) | 29.6088 |
| 68 2.960891e+01 | (1,1,1) | 29.6088 |
| 69 4.987095e+01 | (2,1,0) | 49.3480 |
| 70 4.987095e+01 | (2,0,1) | 49.3480 |
| 71 4.987095e+01 | (1,2,0) | 49.3480 |
| 72 4.987095e+01 | (1,0,2) | 49.3480 |
| 73 4.987095e+01 | (0,2,1) | 49.3480 |
| 74 4.987095e+01 | (0,1,2) | 49.3480 |
| 75 5.973327e+01 | (2,1,1) | 59.2176 |
| 76 5.973327e+01 | (1,2,1) | 59.2176 |
| 77 5.973327e+01 | (1,1,2) | 59.2176 |
| 78 5.973613e+01 | (2,1,1) | 59.2176 |
| 79 5.973613e+01 | (1,2,1) | 59.2176 |
| 80 5.973613e+01 | (1,1,2) | 59.2176 |
| 81 8.000000e+01 | (2,2,0) | 78.9568 |
| 82 8.000000e+01 | (2,0,2) | 78.9568 |
| 83 8.000000e+01 | (0,2,2) | 78.9568 |

Table 4. Dominant resonant frequency $K_0 a$ in Figure 1.

| Cavity | Analytical | Ref. 15 | Ref. 16 | This method |
|---------|------------|---------|---------|-------------|
| Fig. 1a | 2.5829 | 2.4292 | 2.5761 | 2.5565 |
| Fig. 1b | | 3.447 | 3.5387 | 3.5763 |
| Fig. 1c | | 4.907 | 5.5290 | 5.4811 |

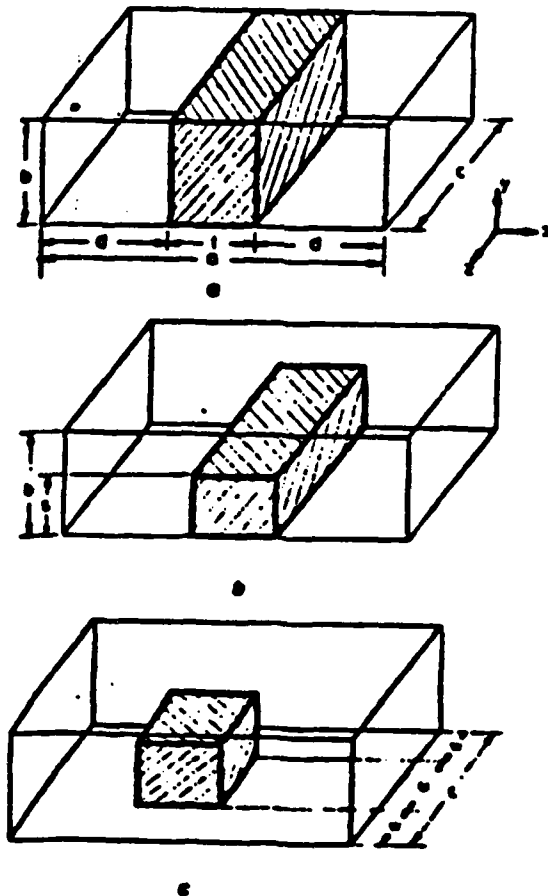


Figure 1. Dielectric loaded box.

$$\epsilon_r = 16, b/a = 3/10, c/a = 4/10, t/a = 1/4, s/b = 7/12, u/c = 3/8$$

APPENDIX B - EDGE-BASED VECTOR FINITE ELEMENTS FOR SOLVING THE ELECTROMAGNETIC WAVE EQUATIONS

ABSTRACT

This appendix examines the requirements on finite element approximation functions that must be satisfied to provide consistent solutions of electromagnetic wave problems. We show that continuity of the tangential component of the electric or of the magnetic field is required in the variational procedure but that the normal component of the field need not be continuous. We present a new triangular finite element that provides for only continuity of the tangential component of the field. In this element, the tangential components of the field represent the unknowns to be determined and are evaluated separately on each side of the element. The finite element analysis based on this new element leads to the complete elimination of the spurious modes. Wave propagation in dielectric-loaded waveguides is examined to test the validity of the new vector element. Extension to three-dimensionals is made by requiring that the tangential components of the field interpolate at the edges of tetrahedra. This 3-D vector element is shown to model three-dimensional cavity problems correctly without the presence of spurious modes.

INTRODUCTION

While the finite element method is known to be a powerful tool in the analysis of many physical systems, its application in electromagnetics has been limited by the presence of spurious or non-physical solutions in the computation of electromagnetic wave problems. Several investigators have attempted to eliminate these spurious nodes by either employing a penalty method or by strongly imposing boundary conditions. However, all of these attempts have only reduced the appearance of the spurious modes to a lesser degree. Recently, a rectangular mixed-order element has been developed based on the consistency of the orders of the polynomials used among the three components of the field vector in the three independent directions^{1,2}. With these elements, the problem of spurious modes is eliminated. However, the elements reported are rectangles in 2-D or rectangular parallelepipeds in 3-D and hence provide only a limited degree of geometrical flexibility. An extension of this concept to triangular or tetrahedral finite elements is required to model many problems efficiently.

The approach reported in reference [2] can be traced to the mathematicians Raviart and Thomas³ and to Nedelec⁴ who were the first to seek vector solutions in the range space of the operator. These researchers have presented a vector finite element that approximates either the normal or the tangential components of a vector field and have established also the convergence of the new elements. However, the elements reported in [3] and [4] are not interpolatory and hence are difficult to apply.

In this paper, we take a different point of view: We examine the variational principle corresponding to the Maxwell equations and show that electromagnetic field problems are best solved not by using three separate scalar approximations for the three components of the field, but by using new vector elements that require only the continuity of the tangential component of the field. With this new element, the normal component of the field is allowed to jump across the material interfaces. Further, we improve Nedelec's tangential elements by writing the field vector explicitly in terms of point values. This interpolation property makes the process of imposing the necessary continuity conditions between vector elements easy to program and provides a practical and extremely reliable approach for solving electromagnetic field problems.

VARIATIONAL FORMULATION ELEMENT MATRICES S AND T THE ASSEMBLY OF GLOBAL MATRICES

Variational procedures for solving electromagnetic field problems by the finite element method were originally proposed by Konrad¹² and used subsequently by others¹³⁻¹⁵. While the essence of Konrad's derivation is correct, the interface between elements were not examined in detail. This oversight has led to the appearance of spurious modes in finite element solutions. In the following we examine these equations in detail, paying particularly close attention to the interface requirements on the approximation subspace.

The basic equations that govern electromagnetic fields in source-free, time-harmonic regions are the Maxwell equations

$$\nabla \times \vec{E} = -j\omega\mu\vec{H} \quad (1)$$

$$\nabla \times \vec{H} = j\omega\epsilon\vec{E} \quad (2)$$

We note that since the divergence of the curl of anything is zero, Equations (1) and (2) imply that

$$\nabla \cdot \mu \bar{H} = 0 \quad (3)$$

$$\nabla \cdot \epsilon \bar{E} = 0 \quad (4)$$

The substitution of \bar{E} from Equation (2) into (1) and of \bar{H} from (1) into (2) yields the vector wave equations

$$\nabla \times \frac{1}{\mu} \nabla \times \bar{E} = \frac{k^2}{\mu} \bar{H} \quad (5)$$

$$\nabla \times \frac{1}{\epsilon} \nabla \times \bar{H} = \frac{k^2}{\epsilon} \bar{H} \quad (6)$$

where $k^2 = \omega^2 \mu \epsilon$. In view of the similarity between Equations (5) and (6), the following analysis will be presented in terms of the vector \bar{E} ; the parallel development for the vector \bar{H} is obtained by making the substitutions $\bar{E} \rightarrow \bar{H}$ and $\mu \rightarrow \epsilon$.

INTERFACE CONDITIONS

The interface conditions that must be satisfied by the electric field \bar{E} are that its tangential component is continuous

$$\bar{I}_n \times \bar{E}_1 = \bar{I}_n \times \bar{E}_2 \quad (7)$$

and that the normal component of the flux $\bar{D} = \epsilon \bar{E}$ is continuous

$$\bar{I}_n \cdot \epsilon_1 \bar{E}_1 = \bar{I}_n \cdot \epsilon_2 \bar{E}_2 \quad (8)$$

For the magnetic field \bar{H} , the corresponding interface conditions are

$$\bar{I}_n \times \bar{H}_1 = \bar{I}_n \times \bar{H}_2 \quad (9)$$

$$\bar{I}_n \cdot \mu_1 \bar{H} = \bar{I}_n \cdot \mu_2 \bar{H}_2 \quad (10)$$

Equation (10) may be expressed in terms of the electric field by using Equation (1). The result is

$$\bar{\Gamma}_n \cdot \nabla \times \bar{E}_1 = \bar{\Gamma}_n \cdot \nabla \times \bar{E}_2 \quad (11)$$

Adopting an (n, r, λ) coordinate system, where $\bar{\Gamma}_n$ is normal to the interface and $\bar{\Gamma}_r$ and $\bar{\Gamma}_\lambda$ are parallel to it, Equation (11) becomes

$$\left(\frac{\partial E_\lambda}{\partial r} - \frac{\partial E_r}{\partial \lambda} \right)_1 = \left(\frac{\partial E_\lambda}{\partial r} - \frac{\partial E_r}{\partial \lambda} \right)_2 \quad (12)$$

Notice that Equation (12) only involves the tangential components and the tangential derivatives of \bar{E} . We therefore arrive at the important result:

Continuity of the normal component of magnetic flux $\bar{B} = \mu \bar{H}$ is ensured by setting the tangential component of the electric field \bar{E} to be continuous.

There is of course the corollary:

Continuity of the normal component of electric flux $\bar{D} = \epsilon \bar{E}$ is ensured by setting the tangential component of the magnetic field \bar{H} to be continuous.

It follows from the above that if we impose the continuity of the tangential components of \bar{E} and \bar{H} , Equations (7) and (9), directly then continuity of the normal components of the fluxes, Equations (8) and (10), are automatically ensured.

In an \bar{E} -field solution procedure, we must express the tangential component of the magnetic field in terms of the electric field. Using Equation (1), the result is

$$\bar{\Gamma}_n \times \frac{1}{\mu_1} (\nabla \times \bar{E}_1) = \bar{\Gamma}_n \times \frac{1}{\mu_2} (\nabla \times \bar{E}_2) \quad (13)$$

Evaluating this by components yields the two equations

$$\frac{1}{\mu_1} \left(\frac{\partial E_r}{\partial n} - \frac{\partial E_n}{\partial r} \right)_1 = \frac{1}{\mu_2} \left(\frac{\partial E_r}{\partial n} - \frac{\partial E_n}{\partial r} \right)_2 \quad (14)$$

$$\frac{1}{\mu_1} \left(\frac{\partial E_n}{\partial \lambda} - \frac{\partial E_\lambda}{\partial n} \right)_1 = \frac{1}{\mu_1} \left(\frac{\partial E_n}{\partial \lambda} - \frac{\partial E_\lambda}{\partial n} \right)_2 \quad (15)$$

Provided that Equations (14) and (15) are satisfied, Equation (8) will be satisfied.

THE ENERGY FUNCTIONAL

Consider the functional

$$F(\bar{E}) = \int \frac{1}{\mu} (\nabla \times \bar{E})^2 d\Omega - \int \frac{k^2}{\mu} \bar{E}^2 d\Omega . \quad (16)$$

We shall show that this functional may be used to solve for the electric field in wave problems *provided that the tangential component of \bar{E} is made continuous.*

To minimize $F(\bar{E})$, let $\bar{E} = \bar{E}_{ex} + \epsilon \bar{\xi}$ where \bar{E}_{ex} is the exact solution of the wave Equation (6), ϵ is a number, and $\bar{\xi}$ is an arbitrary vector function. The first variation of $F(\bar{E})$ is

$$\begin{aligned} \delta F(\bar{E}) &= \frac{\partial F(\bar{E}_{ex} + \epsilon \bar{\xi})}{\partial \epsilon} \Big|_{\epsilon=0} \\ &= \int \frac{1}{\mu} (\nabla \times \bar{\xi}) \cdot (\nabla \times \bar{E}_{ex}) d\Omega - \int \frac{k^2}{\mu} \bar{\xi} \cdot \bar{E}_{ex} d\Omega . \end{aligned} \quad (17)$$

By integrating the vector identity

$$\nabla \cdot (\bar{a} \times \bar{b}) = (\nabla \times \bar{a}) \cdot \bar{b} - \bar{a} \cdot (\nabla \times \bar{b}) \quad (18)$$

we find that

$$\oint (\bar{a} \times \bar{b}) \cdot \bar{dS} = \int [(\nabla \times \bar{a}) \cdot \bar{b} - \bar{a} \cdot (\nabla \times \bar{b})] d\Omega . \quad (19)$$

Thus (17) is converted to

$$\begin{aligned} \delta F(\bar{A}) &= \int \bar{\xi} \cdot \left[\nabla \times \frac{1}{\mu} \nabla \times \bar{E}_{ex} - \frac{k^2}{\mu} \bar{E}_{ex} \right] d\Omega \\ &+ \oint \left(\bar{\xi} \times \frac{1}{\mu} \nabla \times \bar{E}_{ex} \right) \cdot \bar{dS} . \end{aligned} \quad (20)$$

Since \bar{E}_{ex} satisfies Equation (6) exactly, the volume integral in (20) drops out, leaving

$$\delta F(\bar{E}) = \oint \left(\bar{\xi} \times \frac{1}{\mu} \nabla \times \bar{E}_{ex} \right) \cdot \bar{dS} = -j\omega \oint (\bar{\xi} \times \bar{H}) \cdot \bar{dS} . \quad (21)$$

Finally, setting the first variation of $F(\bar{E})$ equal to zero yields

$$\oint (\bar{\xi} \times \bar{H}) \cdot \bar{dS} = 0 . \quad (22)$$

Equation (22) provides the natural boundary conditions for the functional.

NATURAL BOUNDARY CONDITIONS

Evaluating Equation (22) by components yields

$$\oint (\xi_r H_\lambda - \xi_\lambda H_r) dS = 0 . \quad (23)$$

In terms of the electric field \bar{E} this is

$$\oint \left[\xi \frac{1}{\mu} \left(\frac{\partial E_r}{\partial n} - \frac{\partial E_n}{\partial r} \right) - \xi_\lambda \frac{1}{\mu} \left(\frac{\partial E_n}{\partial \lambda} - \frac{\partial E_\lambda}{\partial n} \right) \right] dS = 0 . \quad (24)$$

On exterior boundaries, if we set the tangential components of \bar{E} equal to a given value, then ξ_r and ξ_λ are zero and Equation (24) is satisfied. On the other hand, along boundaries where we leave ξ_r and ξ_λ to be arbitrary, we will automatically obtain a solution for \bar{E} that satisfies

$$\bar{E}_n \times \bar{H} = 0 . \quad (25)$$

On interior boundaries, if we impose continuity of the tangential component of \bar{E} then we will have that

$$\xi_r|_1 = \xi_r|_2$$

$$\xi_\lambda|_1 = \xi_\lambda|_2 . \quad (26)$$

For boundaries, Equation (24) yields

$$\begin{aligned} & \int \xi_r \left[\frac{1}{\mu_1} \left(\frac{\partial E_r}{\partial n} - \frac{\partial E_n}{\partial r} \right)_1 - \frac{1}{\mu_1} \left(\frac{\partial E_r}{\partial n} - \frac{\partial E_n}{\partial r} \right)_2 \right] dS \\ & - \int \xi_\lambda \left[\frac{1}{\mu_1} \left(\frac{\partial E_n}{\partial \lambda} - \frac{\partial E_\lambda}{\partial n} \right)_1 - \frac{1}{\mu_2} \left(\frac{\partial E_n}{\partial \lambda} - \frac{\partial E_\lambda}{\partial n} \right)_2 \right] dS = 0 . \end{aligned} \quad (27)$$

Since ξ_r and ξ_λ are arbitrary on interior boundaries, Equation (27) yields exactly the correct interface conditions (14) and (15).

We note that the continuity of the normal component of \vec{E} is not required in the above formulation. In fact, imposing continuity on the normal component of \vec{E} is wrong because $\vec{1}_n \cdot \vec{E}$ is discontinuous at material boundaries. The beauty of the procedure presented in this report is derived from this fact: if one allows the normal component of the electric field to be discontinuous imposing continuity of only tangential component, then the amount of discontinuity in the normal component is automatically given by the natural boundary conditions in the variational principle.

TANGENTIAL CONTINUITY

It has been the usual practice in the finite element solution of vector field problems to create a scalar approximation for each vector component separately. In view of the above analysis, we must do something entirely different: we must generate vector-valued finite elements that provide continuity of only the tangential component of the field. No finite elements having this property have been published previously.

In the two-dimensions, the idea is the following: consider the arbitrary triangular finite element presented in Figure 1. The three unit vectors $\vec{1}_i$, $i = 1, 2, 3$, parallel to the three sides of the element are

$$\vec{1}_i = \frac{1}{h_i} (b_i \vec{1}_y + c_i \vec{1}_x) \quad (28)$$

where b_i and c_i are the usual parameters

$$b_i = y_{i1} - y_{i2} \quad (29)$$

$$c_i = x_{i2} - x_{i1} \quad (30)$$

and h_i represents the length of side i

$$h_i^2 = b_i^2 + c_i^2 \quad (31)$$

We note here that the h_i may also be written in terms of the triangle vertex angles θ_i as

$$h_i^2 = \Delta(\cot\theta_{i1} + \cot\theta_{i2}) \quad (32)$$

where Δ is plus or minus twice the triangle area

$$\Delta = c_{i2}b_{i1} - c_{i1}b_{i2} \quad (33)$$

The dot product of \bar{I}_i and the field vector \bar{E} evaluated on side i is the tangential component of \bar{E} on that side. It is the quantity that we wish to make continuous for $i = 1, 2, 3$.

Now note that the tangential component of \bar{E} evaluated on side i is a one-dimensional scalar and can therefore be approximated by one-dimensional N 'th order interpolation polynomials

$$\bar{I}_i \cdot \bar{E}|_{side\ i} = \sum_{k=0}^N e_k^i \beta_k^i \quad (34)$$

where e_k^i are coefficients and β_k^i are N 'th order interpolation polynomials. We note that since triangles have three sides, and since there are $(N+1)$ parameters on each side, that there are $3(N+1)$ coefficients e_k^i .

The β_k^i may be written in terms of the Silvester polynomials

$$P_0(\zeta) = 1$$

$$P_m(\zeta) = \prod_{j=1}^m \left(\frac{N\zeta - j + 1}{j} \right), \quad m \pm 1 \quad (35)$$

as

$$\beta_k^i = P_{N-k}(\zeta_{i1}) P_k(\zeta_{i2}) \quad (36)$$

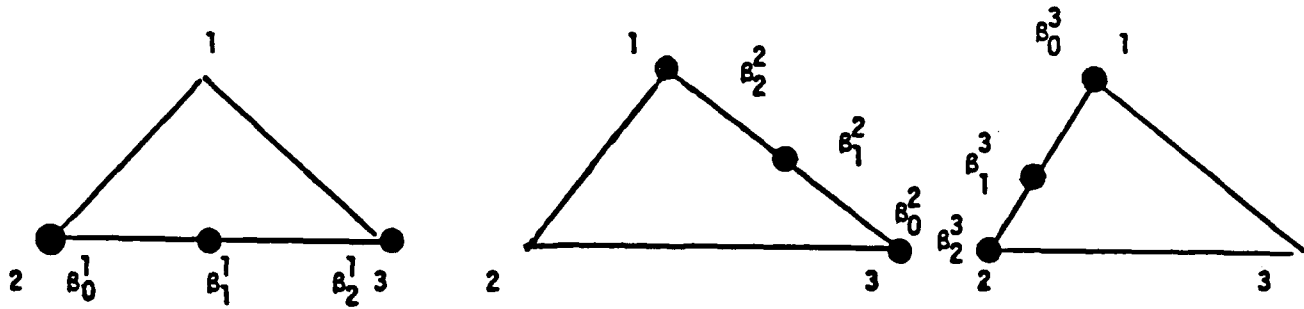
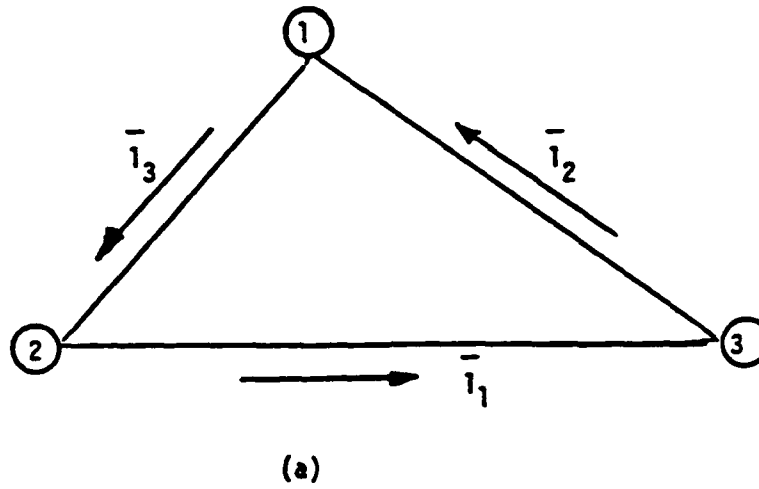


Figure 1. (a) The unit vectors $\bar{1}_i$ for an arbitrary triangle.

(b) The interpolation nodes corresponding to $\bar{1}_i \cdot \bar{E}$ for the case $N = 2$.

For example, if $i = 1$ and $N = 2$, we obtain

$$\beta_0^1 = \zeta_2(2\zeta_2 - 1)$$

$$\beta_1^1 = 4\zeta_2\zeta_3$$

$$\beta_2^1 = \zeta_3(2\zeta_3 - 1) . \quad (37)$$

The location of the interpolation nodes corresponding to these polynomials are indicated in Figure 1(b).

VECTOR BASIS FUNCTION

Finite elements possessing the desired tangential continuity are provided by the following theorem:

Theorem:

Let \bar{E} be approximated by the vector

$$\begin{aligned} \bar{E} = & \bar{I}_x \frac{1}{\Delta} \sum_{i=1}^3 h_i \left\{ b_{i2} \gamma_{N-1}^i - b_{i1} \gamma_N^i \right\} \\ & + \bar{I}_y \frac{1}{\Delta} \sum_{i=1}^3 h_i \left\{ c_{i2} \gamma_{N-1}^i - c_{i1} \gamma_N^i \right\} \end{aligned} \quad (38)$$

where

$$\begin{aligned} \gamma_{N-1}^i &= \sum_{k=0}^{N-1} e_k^i \beta_k^i \\ \gamma_N^i &= e_N^i \beta_N^i . \end{aligned} \quad (39)$$

Then

$$\bar{I}_i \cdot \bar{E}|_{side \ i} = \sum_{k=0}^N e_k^i \beta_k^i . \quad (40)$$

Proof:

We will show that (40) is true on side 2; the proof for sides 2 and 3 is very similar. Evaluating $\bar{\Gamma}_1 \cdot \bar{E}$ gives

$$\begin{aligned} \bar{\Gamma}_1 \cdot \bar{E} &= \frac{1}{\Delta} \left\{ c_1 b_3 \gamma_{N-1}^1 - c_1 b_2 \gamma_N^1 - b_1 c_3 \gamma_{N-1}^1 + b_1 c_2 \gamma_N^1 \right\} \\ &+ \frac{1}{\Delta} \frac{h_2}{h_1} \left\{ -c_1 b_3 \gamma_N^2 + b_1 c_3 \gamma_N^2 \right\} \\ &+ \frac{1}{\Delta} \frac{h_3}{h_1} \left\{ c_1 b_2 \gamma_{N-1}^3 - b_1 c_2 \gamma_{N-1}^3 \right\}. \end{aligned} \quad (41)$$

On side 1, $\gamma_N^2 = 0$ and $\gamma_{N-1}^3 = 0$ by construction. Therefore on side 1 only the top row of Equation (41) survives. However, since $c_1 b_3 - b_1 c_3 = \Delta$ and $-c_1 b_2 + b_1 c_2 = \Delta$, Equation (41) yields

$$\bar{\Gamma}_1 \cdot \bar{E}|_{side\ 1} = \gamma_{N-1}^1 + \gamma_N^1 \quad (42)$$

which is the same as (40).

THE CASE $N = 1$

For $N = 1$, we find that $\beta_o^i = \zeta_{i1}$ and $\beta_i^i = \zeta_{i2}$. Thus (38) becomes

$$\begin{aligned} \bar{E} &= \bar{\Gamma}_x \sum_{i=1}^3 \frac{h_i}{\Delta} \left\{ e_o^i b_{i2} \zeta_{i1} - e_1^i b_{i1} \zeta_{i2} \right\} \\ &+ \bar{\Gamma}_y \sum_{i=1}^3 \frac{h_i}{\Delta} \left\{ e_o^i c_{i2} \zeta_{i1} - e_1^i c_{i2} \zeta_{i2} \right\}. \end{aligned} \quad (43)$$

Since $\zeta_i = \frac{1}{\Delta} (a_1 + b_o x + c_i y)$, we can rewrite this as

$$\bar{E} = \frac{\bar{\Gamma}_x}{\Delta} (f_x + g_x x + h_x y) + \frac{\bar{\Gamma}_y}{\Delta} (f_y + g_y x + h_y y) \quad (44)$$

where

$$f_x = \sum_{i=1}^3 h_i (e_o^i b_{i2} a_{i1} - e_1^i b_{i1} a_{i2})$$

$$g_x = \sum_{i=1}^3 h_i (e_o^i - e_1^i b_{i1} b_{i2})$$

$$h_x = \sum_{i=1}^3 h_i (e_o^i b_{i2} c_{i1} - e_1^i b_{i1} c_{i2}) \quad (45)$$

$$f_y = \sum_{i=1}^3 h_i (e_o^i c_{i2} a_{i1} - e_1^i c_{i1} a_{i2})$$

$$g_y = \sum_{i=1}^3 h_i (e_o^i c_{i2} b_{i1} - e_1^i c_{i1} b_{i2})$$

$$h_y = \sum_{i=1}^3 h_i (e_o^i - e_1^i c_{i1} c_{i2}) \quad (46)$$

Thus

$$\nabla \cdot \bar{E} = \frac{1}{\Delta} (g_x + h_y) \quad (47)$$

$$\nabla \times \bar{E} = \frac{1}{\Delta} (g_y - h_x) \bar{I}_z \quad (48)$$

and

$$\int |\nabla \times \bar{E}|^2 d\Omega = \frac{1}{2\Delta} (g_y^2 - 2g_y h_x + h_x^2) \quad (49)$$

THE CASE $N = 0$

Although $N = 0$ is not permitted in Equation (38), zeroth order tangential continuous finite elements may be obtained by setting $e_o^i = e_1^i = e^i$ in Equation (43). The result is

$$\begin{aligned} \bar{E} = & \frac{\bar{I}_x}{\Delta} \sum_{i=1}^3 e^i h_i (b_{i2} s_{i1} - b_{i1} s_{i2}) \\ & + \frac{\bar{I}_y}{\Delta} \sum_{i=1}^3 e^i h_i (c_{i2} s_{i1} - c_{i1} s_{i2}) . \end{aligned} \quad (50)$$

In this case $g_x = 0$, $h_y = 0$ and $h_x = -g_y = g$ and (44) becomes

$$\bar{E} = \frac{\bar{I}_x}{\Delta} (f_x + gy) + \frac{\bar{I}_y}{\Delta} (f_y - gx) . \quad (51)$$

For this element we find that

$$\nabla \cdot \bar{E} = 0 \quad (52)$$

$$\nabla \times \bar{E} = -2g \, z/\Delta \quad (53)$$

and

$$\int |\nabla \times \bar{E}|^2 d\Omega = \frac{2}{\Delta} g^2 . \quad (54)$$

3-D VECTOR ELEMENT

We define the tangential component of the field vector at side i to be positive when it is parallel to the unit vector l_i . However, to have a consistent sign of the field vector, one has to assign the tangential vectors globally, not locally. An example of such vector mesh is shown in Figure 2. It is, of course, possible to have other vector mesh patterns besides the one shown; these patterns are related through a group transformation. For example, the matrix P transforming the vector (e^1, e^2, e^3) into $(-e^1, e^2, e^3)$ is defined as

$$(e^1, e^2, e^3) P = (-e^1, e^2, e^3) \quad \text{where } P = \begin{pmatrix} -1 & 0 & 0 \\ 0 & 1 & 0 \\ 0 & 0 & 1 \end{pmatrix} \quad (55)$$

The corresponding element matrices on the transformed mesh are given as follows:

$$\begin{aligned} S^1 &= \text{PSP} \\ T^1 &= \text{PTP} \end{aligned} \quad (56)$$

One can prove that the following field vector preserves the continuity of the tangential component.

$$\begin{aligned} E_x &= \frac{1}{V} \sum_{i < j}^4 \gamma_{ij} [b_j \gamma_{N-1}^{ij} - b_i \gamma_N^{ij}] \\ E_y &= \frac{1}{V} \sum_{i < j}^4 \gamma_{ij} [c_j \gamma_{N-1}^{ij} - c_i \gamma_N^{ij}] \\ E_z &= \frac{1}{V} \sum_{i < j}^4 \gamma_{ij} [d_j \gamma_{N-1}^{ij} - d_i \gamma_N^{ij}] \end{aligned} \quad (57)$$

where

$$\gamma_{N-1}^{ij} = \sum_{k=0}^{N-1} \beta_k^{ij} e_k^{ij},$$

$$\gamma_N^{ij} = \beta_N^{ij} e_N^{ij},$$

$$\beta_k^{ij} = P_{N-k}(\xi_i) P_k(\xi_j)$$

$$b_i = (-1)^{i+1} \begin{vmatrix} y_{jk} & y_{kl} \\ z_{jk} & z_{kl} \end{vmatrix}$$

$$c_i = (-1)^{i+1} \begin{vmatrix} z_{jk} & z_{kl} \\ x_{jk} & x_{kl} \end{vmatrix}$$

$$d_i = (-1)^{i+1} \begin{vmatrix} x_{jk} & x_{kl} \\ y_{jk} & y_{kl} \end{vmatrix}$$

$$x_{jk} = x_j - x_k,$$

$$y_{jk} = x_j - x_k,$$

$$z_{jk} = z_j - z_k$$

$$\gamma_{jk} = (x_{ik}^2 + y_{jk}^2 + z_{jk}^2)^{\frac{1}{2}} \quad (58)$$

and V is 6 times the volume of the tetrahedra. Then

$$\hat{l}_{ij} \cdot \vec{E} |_{edge\ ij} = \sum_{k=0}^N e_k^{ij} \beta_k^{ij} \quad (59)$$

where \hat{l}_{ij} is the unit edge vector on the edge ij , and

$$\hat{n}_i \times \vec{E}_1 |_{\xi_i=0} = \hat{n}_i \times \vec{E}_2 |_{\xi_i=0} \quad (60)$$

where (1) and (2) indicate two adjacent tetrahedra with a common face i , and \hat{n}_i is the corresponding unit normal vector.

THE CASE $N = 0$

In this case,

$$\begin{aligned} E_x &= \frac{1}{V} \sum \gamma_{ij} [b_i \xi_i - b_j \xi_j] e^{ij} \\ F_y &= \frac{1}{V} \sum \gamma_{ij} [c_j \xi_i - c_i \xi_j] e^{ij} \end{aligned} \quad (61)$$

Let us define

$$\tilde{e}_6 = (e_{12}, e_{13}, e_{14}, e_{23}, e_{24}, e_{34}) \quad (62)$$

Then, the matrix elements of S are

$$\begin{aligned} (S)_{ij,kl} &= \frac{2}{3V} \gamma_{ij} \gamma_{kl} \text{Sign}(ij) \text{Sign}(kl) \\ &\quad (X_{\widetilde{ij}} X_{\widetilde{kl}} + Y_{\widetilde{ij}} Y_{\widetilde{kl}} + Z_{\widetilde{ij}} Z_{\widetilde{kl}}) \end{aligned} \quad (63)$$

where the function $\text{Sign}(ij) = 1$ when $i-j \pm 2$, and is -1 otherwise, and \widetilde{ij} means the complementary index of ij e.g., $\widetilde{12}=34$, $\widetilde{13}=24$, and $\widetilde{34}=12$.

And the matrix elements of T are

$$(T)_{ij,kl} = \frac{1}{120V} \gamma_{ij} \gamma_{kl} (W_{jl} K_{ik} - W_{jk} K_{il} - W_{il} W_{jk} + W_{ik} K_{jl}) . \quad (64)$$

Where $W_{ij} = 2$ when $i = j$, 1 otherwise, and

$$K_{ij} = b_i b_j + c_i c_j + d_i d_j . \quad (65)$$

APPLICATION TO DIELECTRIC-LOADED WAVEGUIDES

I. THEORY

Assuming the wave travels in Z direction, one can write \bar{E} as:

$$\bar{E} = \left(\bar{e}_t(x,y) + j \bar{e}_z(x,y) \right) e^{-j\beta z} \quad j4z \quad (66)$$

where $\bar{e}_t = e_x \hat{x} + e_y \hat{y}$ and β is the propagation constant.

Substituting (66) into (16) yields

$$F = \int \frac{1}{\mu_r} \left[\beta^2 |\bar{e}_t|^2 + |\nabla \times \bar{e}_t|^2 + |\nabla e_z|^2 - 2\beta \left(e_x \frac{\partial e_z}{\partial x} + e_y \frac{\partial e_z}{\partial y} \right) \right] - \epsilon_v k_o^2 (|\bar{e}_t|^2 + |\bar{e}_z|^2) d\Omega . \quad (67)$$

Defining

$$\begin{aligned} \tilde{e}_t, T_t, \underline{e}_t &= \int |\bar{e}_t|^2 d\Omega \\ \tilde{e}_z, T_z, \underline{e}_z &= \int |\bar{e}_z|^2 d\Omega \\ \tilde{e}_t, S_t, \underline{e}_t &= \int |\nabla \times \bar{e}_t|^2 d\Omega \\ \tilde{e}_z, S_z, \underline{e}_z &= \int |\nabla e_z|^2 d\Omega \end{aligned} \quad (68)$$

and

$$\begin{pmatrix} \tilde{e}_t, \tilde{e}_z \end{pmatrix} \begin{bmatrix} 0 & \beta W^+ \\ \beta W & 0 \end{bmatrix} \begin{pmatrix} \underline{e}_t \\ \underline{e}_z \end{pmatrix} = \int -2\beta \left(e_x \frac{\partial e_z}{\partial x} + e_y \frac{\partial e_z}{\partial y} \right) d\Omega \quad (69)$$

gives

$$F = \tilde{e} K \underline{e} - k_o^2 \tilde{e} M \underline{e} \quad (70)$$

where

$$\tilde{e} = (\tilde{e}_t, \tilde{e}_z)$$

$$K = \frac{1}{\mu r} \begin{bmatrix} \beta^2 T_t + S_t & \beta W^+ \\ \beta W & S_z \end{bmatrix} \quad (71)$$

and

$$M = \begin{bmatrix} T_t & 0 \\ 0 & T_z \end{bmatrix} \quad (72)$$

The first derivative with respect to \tilde{e} gives

$$K \underline{e} = R_o^2 M \underline{e} \quad (73)$$

II. RESULT

Taking a rectangular waveguide half-filled with dielectric, as studied by Konrad, as an example, we approximate the transverse component of the field vector using zeroth-order vector elements and the longitudinal component of the field vector using first-order scalar element, as shown in Figure 1. Unlike Konrad's result, spurious modes do not occur either above the air line or below the air. It is interesting to note that Konrad had incorrectly identified some spurious modes as physical ones.

APPLIED TO A CAVITY PROBLEM

A unit, empty cubic cavity was modeled by the zeroth-order 3-D vector element. As shown in Figure 2, the agreement is reasonable. The result also shows the convergence as the mesh becomes finer. Opposed to the result obtained from the traditional method, the convergence is simply destroyed by the fact that the number of spurious modes increases with the number of the degree of freedoms. We also model a dielectric-loaded cavity and the result is again reasonably good.

THE EVALUATION OF S^* AND T^*

The S^* matrix is related to the calculation of

$$\int |\nabla \times E|^2 d\Omega = \frac{2}{\Delta} g^2 \quad (74)$$

where

$$g = -\sum_{i=1}^3 h_i e^i \quad (75)$$

Let us define

$$\tilde{h} = (h_1 \ h_2 \ h_3) \text{ and } \underline{e} = \begin{pmatrix} e^1 \\ e^2 \\ e^3 \end{pmatrix}. \quad (76)$$

Then,

$$g = -\tilde{h} \ \underline{e} \quad (77)$$

and

$$g^2 = \tilde{e} \ \underline{h} \ \tilde{h} \ \underline{e}. \quad (78)$$

Since

$$h_i = \sqrt{\cot \theta_{i1} + \cot \theta_{i2}}, \quad (79)$$

\underline{h} can be written as

$$\underline{h} = \sqrt{\Delta} \ \underline{m} \quad (80)$$

$$\text{where } \underline{m} = \begin{pmatrix} m_1 \\ m_2 \\ m_3 \end{pmatrix} \quad (81)$$

and

$$m_i = \sqrt{\cot \theta_{i1} + \cot \theta_{i2}}. \quad (82)$$

Substituting Equation (81) into Equation (80) gives

$$g^2 = \Delta \ \tilde{e} \ \underline{m} \ \tilde{m} \ \underline{e} \quad (83)$$

From Equation (74), S^* is

$$S^* = 2 \ \underline{m} \ \tilde{m}. \quad (84)$$

On the other hand, the T^* matrix is related to

$$\int |E|^2 \ d\Omega = \frac{1}{\Delta^2} \int \left(\left[\sum_{i=1}^3 h_i e^i (b_{i2} \xi_{i1} - b_{i1} \xi_{i2}) \right]^2 + \left[\sum_{i=1}^3 h_i e^i (c_{i1} \xi_{i1} - c_{i1} \xi_{i2}) \right]^2 \right) d\Omega. \quad (85)$$

The first term can be written in the following format:

$$\left[\sum_{i=1}^3 h_i e^{i(b_{i2}\xi_{i1} - b_{i1}\xi_{i2})} \right]^2 = \Delta \tilde{e} K_1 e \quad (86)$$

where

$$K_1 = \begin{bmatrix} m_1 m_1 (b_3 \xi_2 - b_1 \xi_3)^2 & m_1 m_2 (b_3 \xi_2 - b_1 \xi_3) & m_1 m_2 (b_3 \xi_2 - b_2 \xi_3) \\ & x(b_1 \xi_3 - b_3 \xi_3) & x(b_2 \xi_1 - b_1 \xi_2) \\ & m_2 m_2 (b_1 \xi_3 - b_3 \xi_1)^2 & m_2 m_3 (b_1 \xi_3 - b_3 \xi_1) \\ & & x(b_1 \xi_1 - b_1 \xi_2) \\ & & m_3 m_3 (b_2 \xi_1 - b_1 \xi_2)^2 \end{bmatrix} \quad (87)$$

The integral of K_1 is

$$\int K_1 d\Omega = \frac{\Delta}{24} \begin{bmatrix} m_1 m_1 (2b_3^2 - 2b_3 b_2 + 2b_2^2) \\ m_2 m_1 (-2b_1 b_2 - 2b_3^2) & m_2 m_2 (2b_1^2 - 2b_1 b_3 + b_3^2) \\ m_3 m_1 (-2b_3 b_1 - 2b_2^2) & m_3 m_2 (-2b_3 b_2 - 2b_1^2) & m_2 m_3 (2b_1^2 - 2b_1 b_2 + 2b_2^2) \end{bmatrix} \quad (88)$$

By the same token, the second term becomes

$$\left[\sum_{i=1}^3 h_i e^{i(c_{i2}\xi_{i1} - c_{i1}\xi_{i2})} \right]^2 = \Delta \tilde{e} K_2 e \quad (89)$$

and the integral of K_2 is

$$\int K_2 d\Omega = \frac{\Delta}{24} \begin{bmatrix} m_1 m_1 (2c_3^2 - 2c_3 c_2 + 2c_2^2) \\ m_2 m_1 (-2c_1 c_2 - 2c_3^2) & m_2 m_2 (2c_1^2 - 2c_1 c_3 + c_3^2) \\ m_3 m_1 (-2c_3 c_1 - 2c_2^2) & m_3 m_2 (-c_3 c_2 - 2c_1^2) & m_3 m_3 (2c_1^2 - 2c_1 c_2 + 2c_2^2) \end{bmatrix} \quad (90)$$

By applying the identities

$$\begin{aligned} b_i b_{i1} + c_i c_{i1} &= \Delta \\ \cot \theta_{i2} & \quad i \neq i^1 \end{aligned} \quad (91)$$

and

$$\begin{aligned} b_i^2 + c_i^2 &= \Delta \\ (\cot \theta_{i1} + \cot \theta_{i2}) & \end{aligned} \quad (92)$$

to the sum of and , Eq. becomes

$$\int |\bar{e}|^2 d\Omega =$$

$$\frac{\Delta}{24} \tilde{e} \begin{bmatrix} m_1 m_1 [2m_1 m_1 + 6 \cot \theta_1] & & \\ m_2 m_1 [2 \cot \theta_3 - 2m_3 m_3] & m_2 m_2 [2m_2 m_2 + 6 \cot \theta_2] & \\ m_3 m_1 [2 \cot \theta_2 - 2m_2 m_2] & m_3 m_2 [2 \cot \theta_1 - 2m_1 m_1] & m_3 m_3 [2m_3 m_3 + 6 \cot \theta_3] \end{bmatrix} \tilde{e} \quad (93)$$

therefore,

$$T^* = \frac{\Delta}{24} \begin{bmatrix} & & \\ & & \\ & & \end{bmatrix} . \quad (94)$$

APPENDIX C - C^1 QUADRATIC INTERPOLATION FOR DERIVATIVE CONTINUOUS FINITE ELEMENT APPROXIMATIONS

ABSTRACT

A highly efficient procedure for generating smooth surfaces over arbitrarily spaced data points is developed in this appendix. The procedure uses quadratic polynomials for the construction of derivative continuous surfaces rather than the cubic polynomials generally employed previously. It is based on a subdivision procedure, dividing each triangle in a triangulation of the data points into six subtriangles and fitting a quadratic Bezier surface patch over each subtriangle. It requires only function and first derivative values at the data points and is easily implemented by means of simple formulas for the Bezier coefficients. Since two-dimensional quadratic polynomials contain only six terms, while ten terms are required to evaluate a cubic, the new procedure provides a major improvement in the efficiency of algorithms for representing electromagnetic fields.

INTRODUCTION

The generation of smooth surfaces that interpolate to prescribed values of a two-dimensional function at an arbitrary point set is one of the central topics of computer-aided geometric design (CAGD). Early work focused on the Coon's patch as the preferred method of generating C^1 surfaces over rectangular and triangular grids [1]; more recently, because of their easy geometrical interpretation, techniques for generating smooth surfaces based on Bezier polynomials have become popular [2].

To date, however, the preponderance of work in this area has been based on the considerable flexibility of cubics for providing smooth curves; relatively little work exists for using quadratic polynomials to achieve similar results. While the cubics developed previously using either the Coon's patch or the Bezier technique provide excellent results, they have three drawbacks:

- (1) they are relatively complicated;
- (2) they require either that a "twist condition" be satisfied at the data points¹ or that mid-side derivatives be given²; and
- (3) compared to quadratics, they are expensive to compute.

We examine here the requirements for C^1 interpolation by quadratics using the Bezier technique and show that a simple, efficient and accurate algorithm exists for generating such surfaces. The algorithm requires only function and derivative values at an arbitrary set of points; no mid-side or twist derivatives are employed. Further, the new algorithm is considerably faster for drawing smooth surfaces than are algorithms based on evaluating cubic polynomials since fewer operations are required to evaluate quadratic polynomials than is required for cubics. Indeed, it may be argued that the new procedure is optimal for C^1 surface interpolation since quadratics are the lowest order polynomials for which smooth interpolation is possible.

The pioneering work on C^1 interpolation by quadratic polynomials is by Powell and Sabin [3]. They showed in 1977 that C^1 surfaces could be produced over triangular data points by subdividing the original triangles into either six or twelve subtriangles. Their procedure has, however, not been widely employed due to its complexity. Sibson and Thomson⁴ have also introduced a quadratic C^1 interpolation procedure but their method is limited to treating only rectangular arrays of data points. The method developed in this paper does not have any geometrical restrictions and therefore is ideal for design purposes. The potential of quadratic surface patches in CAGD has also been recognized and is discussed in a recent paper by Sederberg and Anderson⁵.

BEZIER POLYNOMIALS

The Bernstein-Bezier approach to surface modeling is well known and is described in some detail in a comprehensive review paper by Bohm, Farin and Kahmann [6]. With regard to surface modeling, Bezier polynomials provide the important property that C^1 continuity can be ensured between triangular patches by requiring that each pair of adjacent subtriangles in the Bezier net be coplanar. This is both conceptually and computationally a simple task, and has therefore great appeal for constructing methods of smooth interpolation.

For quadratics, the Bernstein-Bezier surface patch over triangles is defined as follows

$$f(x,y) = f(s_1, s_2, s_3) = \sum_{\substack{i+j+k=2 \\ i,j,k \geq 0}} \frac{2!}{i!j!k!} s_1^i s_2^j s_3^k \phi_{ijk} \quad (1)$$

where the ξ_i are the homogeneous or barycentric or triangle area coordinates of projective geometry^[7] and the coefficients ϕ_{ijk} are the control vertices of the Bezier net. Note that unlike the case with ordinary Lagrange interpolation, the coefficients ϕ_{ijk} do not necessarily provide values of $f(x, y)$ at the nodal points; rather, it can be shown that the surface patch will lie in the convex hull of its Bezier net^[6].

The constraints on the control vertices ϕ_{ijk} in neighboring triangles to ensure derivative continuity across the interface are derived in Reference 2. The geometric interpretation of these constraints is illustrated in Figure 1. In order to have C^1 continuity between quadratic Bezier patches, each pair of subtriangles of the Bezier net that shares a common boundary — the two shaded quadrilaterals in the figure — must be planar.

SUBDIVISION PROCEDURE

Consider an arbitrary set of points P on a plane, as illustrated in the example in Figure 2(a). This point set may be triangulated in a number of ways; we have employed Delaunay triangulation^[8] to illustrate a possible subdivision in Figure 2(b), however other triangulations may be employed if desired.

We assume that position and tangent plane data are given on P . Let Q represent a new set of points chosen arbitrarily so that each triangle T_i contains one and only one point Q_i , $i=1, \dots, n_t$, where n_t represents the number of triangles in the mesh. By connecting each point Q_i with the associated triangle vertices and with the three neighboring triangle interior points Q_j , each interior triangle is subdivided into six triangles as shown in Figure 2(c). Boundary triangles are subdivided into six by adding one point B_i at an arbitrary location along each exterior triangle boundary.

Consider a typical pair of interior triangles as illustrated in Figure 3. The quadratic Bezier net further subdivides these triangles as indicated. According to the requirements for derivative continuity, the Bezier net of each of the shaded areas must be planar in order to achieve C^1 continuity. The question is: Is it possible to construct such a figure, keeping in mind the interconnections between these and other elements?

With regard to the original triangle vertices, it will be noticed that the plane of the Bezier net surrounding each vertex is completely defined by the data specified at the vertex. This leaves three shaded regions to examine: Two triangular patches centered on the interior points Q_1 and Q_2 , and a diamond-shaped region $efgh$ spanning the interface between the elements.

The triangular patches centered on Q_1 and Q_2 are easily made planar by requiring that its three edges form straight lines and that the points Q_i lie in the plane of these lines. The conditions for the region $efgh$ at the center of the common triangle edges to be planar are more complicated and are provided by the following lemma:

Lemma. Let A, B, C and D be any four points in three-dimensional space as shown in Figure 4. Further, let e, f, g and h be points along the line segments \overline{AB} , \overline{BC} , \overline{CD} and \overline{DA} , respectively, having the properties that the points e and g divide the line segments \overline{AB} and \overline{DC} in equal ratios.

$$\frac{\overline{Ae}}{\overline{AB}} = \frac{\overline{Dg}}{\overline{DC}} = \gamma_1 \quad (2)$$

and that f and h divide \overline{BC} and \overline{AD} in equal ratios.

$$\frac{\overline{Bf}}{\overline{BC}} = \frac{\overline{Ah}}{\overline{AD}} = \gamma_2 \quad (3)$$

Then the four points e, f, g and h are coplanar.

Proof: Without loss of generality, we may adopt a Cartesian coordinate system such that A is at the origin, B lies on the x axis and C lies in the (x, y) plane. Then the coordinates of A, B, C and D are

$$\begin{aligned} A &= (0, 0, 0) \\ B &= (b, 0, 0) \\ C &= (c_1, c_2, 0) \\ D &= (d_1, d_2, d_3) \end{aligned} \quad (4)$$

Vectors to the points $e-h$ are given by

$$\begin{aligned} \overline{e} &= \gamma_1 \overline{B} = \gamma_1 b \overline{I}_x \\ \overline{f} &= \gamma_2 \overline{C} + (1-\gamma_2) \overline{B} \\ &= (\gamma_2 c_1 + b - \gamma_2 b) \overline{I}_x + \gamma_2 c_2 \overline{I}_y \\ \overline{g} &= \gamma_1 \overline{C} + (1-\gamma_1) \overline{D} \\ &= (\gamma_1 c_1 + d_1 - \gamma_1 d_1) \overline{I}_x + (\gamma_1 c_2 + d_2 - \gamma_1 d_2) \overline{I}_y \\ &\quad + (d_3 - \gamma_1 d_3) \overline{I}_z \\ \overline{h} &= \gamma_2 \overline{D} = \gamma_2 d_1 \overline{I}_x + \gamma_2 d_2 \overline{I}_y + \gamma_2 d_3 \overline{I}_z \end{aligned} \quad (5)$$

We need to show that the vector \overline{eg} is a linear combination of the vectors \overline{ef} and \overline{eh}

$$\overline{eg} = \alpha \overline{ef} + \beta \overline{eh} \quad (6)$$

The x , y and z components of equation (6) are

$$\begin{aligned} \gamma_1 c_1 + d_1 - \gamma_1 d_1 - \gamma_1 b &= \alpha(\gamma_2 c_1 + b - \gamma_2 b - \gamma_1 b) \\ &\quad + \beta(\gamma_2 d_1 - \gamma_1 b) \\ \gamma_1 c_2 + d_2 - \gamma_1 d_2 &= \alpha \gamma_2 c_2 + \beta \gamma_2 d_2 \\ d_3 - \gamma_1 d_3 &= \beta \gamma_2 d_3 \end{aligned} \quad (7)$$

Rearranging yields

$$\begin{aligned} (\gamma_1 - \alpha \gamma_2) c_1 + (1 - \gamma_1 - \beta \gamma_2) d_1 + (-\gamma_1 - \alpha + \alpha \gamma_2 + \alpha \gamma_1 + \beta \gamma_1) b &= 0 \\ (\gamma_1 - \alpha \gamma_2) c_2 + (1 - \gamma_1 - \beta \gamma_2) d_2 &= 0 \\ (1 - \gamma_1 - \beta \gamma_2) d_3 &= 0 \end{aligned} \quad (8)$$

Since the c_i and d_i are arbitrary, it follows that

$$\begin{aligned} \gamma_1 &= \alpha \gamma_2 \\ 1 &= \gamma_1 + \beta \gamma_2 \end{aligned} \quad (9)$$

Solving this for α and β gives

$$\begin{aligned} \alpha &= \gamma_1 / \gamma_2 \\ \beta &= (1 - \gamma_1) / \gamma_2 \end{aligned} \quad (10)$$

Since b is also arbitrary, we must also have that

$$-\gamma_1 - \alpha + \alpha \gamma_2 + \alpha \gamma_1 + \beta \gamma_1 = 0 \quad (11)$$

The reader may verify that equation (10) also satisfies equation (11).

By construction, the quadrilateral $ABCD$ satisfies the requirements of the above lemma. It follows that C^1 continuity is achieved for any location of the points Q_i by requiring the shaded regions around the original points P_i and around the interior points Q_i to be planar, and by requiring the Bezier node E to lie in the plane of the region $efgh$.

A FORMULA FOR C^1 QUADRATICS

We now proceed to derive a formula for the Bezier coefficients ϕ_i on the subdivided grid. For this purpose, consider the triangle T shown in Figure 5. In this figure, Q is the interior point in triangle T and U , V and W are the interior points in the neighboring triangles. The points Q , U , V and W may be expressed in terms of the Barycentric coordinates of triangle T as

$$\begin{aligned} Q &: (q_1, q_2, q_3) \\ U &: (u_1, u_2, u_3) \\ V &: (v_1, v_2, v_3) \\ W &: (w_1, w_2, w_3). \end{aligned} \tag{12}$$

Since the points U , V and W are outside triangle T , their coordinates will not be limited to the usual homogeneous range $0 \leq \zeta \leq 1$.

LOCATING THE POINT COORDINATES

Our first task is to determine the coordinates of the Bezier nodes B_i . To simplify the algebra, let α , β and γ be the following ratios

$$\begin{aligned} \alpha &= \frac{d_{7,6}}{d_{7,5}} \\ \beta &= \frac{d_{3,2}}{d_{3,7}} \\ \gamma &= \frac{d_{6,4}}{d_{6,3}} \end{aligned} \tag{13}$$

where $d_{i,j}$ represents the distance between nodes i and j . Now note that the line $\overline{B_1 U}$ is described by

$$\zeta_i = (u_i - q_i)t + q_i, \quad i = 1, 2, 3 \tag{14}$$

for $0 \leq t \leq 1$. At node B_6 , $\zeta_1 = 0$ so that

$$t = -q_1 / (u_1 - q_1). \tag{15}$$

Thus, substituting (15) into (14) gives the coordinates of B_6 as

$$B_6: (0, \alpha, 1-\alpha) \tag{16}$$

where

$$\alpha = \frac{q_2 u_1 - q_1 u_2}{u_1 - q_1} \quad (17)$$

In the same way, we find that

$$B_2: (1-\beta, 0, \beta)$$

$$B_4: (\gamma, 1-\gamma, 0) \quad (18)$$

where

$$\beta = \frac{q_3 v_2 - q_2 v_3}{v_2 - q_2}$$

$$\gamma = \frac{q_1 w_3 - q_3 w_1}{w_3 - q_3} \quad (19)$$

The coordinates of the remaining nodes are found by noting that they are located midway between nodes with known coordinates. For example, the coordinates of B_9 are the average of the coordinates of B_3 and B_4

$$B_9: \left(\frac{1+\gamma}{2}, \frac{1-\gamma}{2}, 0 \right) \quad (20)$$

B_{15} is located at the average of the coordinates of B_1 and B_3

$$B_{15}: \left((1+q_1)/2, q_2/2, q_3/2 \right) \quad (21)$$

and B_{16} is at the average of B_4 and B_1

$$B_{16}: \left(\frac{\gamma+q_1}{2}, \frac{1-\gamma+q_2}{2}, \frac{q_3}{2} \right) \quad (22)$$

Similar results are obtained for the other nodal coordinates.

COMPUTING FUNCTION VALUES

By definition, we are given the function values and the values of its x and y derivatives at the three vertices. The value at node 9 is

$$\phi_9 = \phi_3 + (\nabla \phi|_3 \cdot \bar{I}_{3,9}) d_{3,9} \quad (23)$$

where $\bar{I}_{i,j}$ is the unit vector from node i to node j

$$\bar{I}_{ij} = \frac{1}{d_{ij}} \left[(x_j - x_i) \bar{I}_x + (y_j - y_i) \bar{I}_y \right] \quad (24)$$

From Equation (20) we know that

$$\begin{aligned} x_9 &= \left(\frac{1+\gamma}{2} \right) x_3 + \left(\frac{1-\gamma}{2} \right) x_4 \\ y_9 &= \left(\frac{1+\gamma}{2} \right) y_3 + \left(\frac{1-\gamma}{2} \right) y_4 \end{aligned} \quad (25)$$

It follows that

$$\bar{\Gamma}_{3,9} = \frac{(1-\gamma)}{2d_{3,9}} \left[(x_5-x_3) \bar{\Gamma}_x + (y_5-y_3) \bar{\Gamma}_y \right]. \quad (26)$$

Thus, Equation (23) yields

$$\phi_9 = \phi_3 + \frac{1}{2}(1-\gamma)(x_5-x_3) \frac{\partial \phi}{\partial x}|_3 + \frac{1}{2}(1-\gamma)(y_5-y_3) \frac{\partial \phi}{\partial y}|_3. \quad (27)$$

In the same way we find that

$$\begin{aligned} \phi_8 &= \phi_3 + \frac{\beta}{2}(x_7-x_3) \frac{\partial \phi}{\partial x}|_3 + \frac{\beta}{2}(y_7-y_3) \frac{\partial \phi}{\partial y}|_3 \\ \phi_{11} &= \phi_5 + \frac{(1-\alpha)}{2}(x_7-x_5) \frac{\partial \phi}{\partial x}|_5 + \frac{(1-\alpha)}{2}(y_7-y_5) \frac{\partial \phi}{\partial y}|_5 \\ \phi_{10} &= \phi_5 + \frac{\gamma}{2}(x_3-x_5) \frac{\partial \phi}{\partial x}|_5 + \frac{\gamma}{2}(y_3-y_5) \frac{\partial \phi}{\partial y}|_5 \\ \phi_{13} &= \phi_7 + \frac{1-\beta}{2}(x_3-x_7) \frac{\partial \phi}{\partial x}|_7 + \frac{(1-\beta)}{2}(y_3-y_7) \frac{\partial \phi}{\partial y}|_7 \\ \phi_{12} &= \phi_7 + \frac{\alpha}{2}(x_5-x_7) \frac{\partial \phi}{\partial x}|_7 + \frac{\alpha}{2}(y_5-y_7) \frac{\partial \phi}{\partial y}|_7 \end{aligned} \quad (28)$$

Also

$$\begin{aligned} \phi_{15} &= \phi_3 + \frac{1}{2} [(q_1-1)x_3 + q_2x_5 + q_3x_7] \frac{\partial \phi}{\partial x}|_3 + \frac{1}{2} [(q_1-1)y_3 + q_2y_5 + q_3y_7] \frac{\partial \phi}{\partial y}|_3 \\ \phi_{17} &= \phi_5 + \frac{1}{2} [q_1x_3 + (q_2-1)x_5 + q_3x_7] \frac{\partial \phi}{\partial x}|_5 + \frac{1}{2} [q_1y_3 + (q_2-1)y_5 + q_3y_7] \frac{\partial \phi}{\partial y}|_5 \\ \phi_{19} &= \phi_7 + \frac{1}{2} [q_1x_3 + q_2x_5 + (q_3-1)x_7] \frac{\partial \phi}{\partial x}|_7 + \frac{1}{2} [q_1y_3 + q_2y_5 + (q_3-1)y_7] \frac{\partial \phi}{\partial y}|_7 \end{aligned} \quad (29)$$

The remaining nodal values are computed by using linear interpolation. First, note that

$$\frac{d_{12,6}}{d_{12,11}} = \frac{d_{19,18}}{d_{19,17}} = \frac{d_{7,6}}{d_{7,5}} = \alpha. \quad (30)$$

Therefore, the line segments B_{11}, B_6, B_{12} and B_{17}, B_{18}, B_{19} will be straight provided that

$$\begin{aligned} \phi_6 &= (1-\alpha)\phi_{12} + \alpha\phi_{11} \\ \phi_{18} &= (1-\alpha)\phi_{19} + \alpha\phi_{17}. \end{aligned} \quad (31)$$

Similarly

$$\begin{aligned} \phi_2 &= (1-\beta)\phi_8 + \beta\phi_{13} \\ \phi_{14} &= (1-\beta)\phi_{15} + \beta\phi_{19} \\ \phi_4 &= (1-\gamma)\phi_{10} + \gamma\phi_9 \\ \phi_{16} &= (1-\gamma)\phi_{17} + \gamma\phi_{15}. \end{aligned} \quad (32)$$

The only remaining unknown value is that of the interior node Q , alternatively labeled as B_1 . The

Bezier net of this node must lie in the plane of the triangle B_{15}, B_{17}, B_{19} . We note that the homogeneous coordinates of Q are identical in both the original triangle B_3, B_6, B_7 and in the central subtriangle B_{15}, B_{17}, B_{19} . Therefore the value of Q is

$$\phi_1 = q_1\phi_{15} + q_2\phi_{17} + q_3\phi_{19}. \quad (33)$$

In view of the above lemma and the proceeding discussion, we have established the following theorem:

Theorem: Let J be an arbitrary triangulation of an arbitrary set of points P in a plane. Further, let function and first x and y derivative values be specified on P . Then a piecewise quadratic C^1 surface is formed by placing a point Q_i at an arbitrary location inside each triangle, thereby subdividing each triangle into six triangles, and evaluating the Bezier coefficients of the quadratic polynomials on the subdivided triangles according to the formulas in equations (27)-(29) and (31)-(33).

SPECIAL CASES

While the above theorem provides complete flexibility in choosing the locations of the interior subdivision points Q_i , it is appropriate to choose specific locations for these points in computer implementations. Two logical locations for these points are (1) the triangle centroids, and (2) the centers of the triangle inscribed circles. We note that although the centers of the triangle circumcircles have a special meaning in the commonly used Delaunay triangulation procedure, these circumcenters represent a poor choice for our algorithm since they may fall outside the triangle being subdivided.

THE CENTROID ALGORITHM

If Q_i is chosen to be the centroid of triangle i then its homogeneous coordinates are $q_1 = q_2 = q_3 = \frac{1}{3}$. In this case, we find that

$$\alpha = \frac{u_1 - u_2}{3u_1 - 1}$$

$$\beta = \frac{v_2 - v_3}{3v_2 - 1}$$

$$\gamma = \frac{w_3 - w_1}{3w_3 - 1}. \quad (34)$$

A typical surface generated by the centroid algorithm is presented in Figure 6. Figure 6(a) shows an irregular triangulation of 18 data points with each original triangle subdivided into six triangles by using the centroids. Figure 6(b) presents a typical C^1 quadratic surface produced over the irregular triangular grid obtained by specifying function and derivative values at the vertices. As is apparent from this figure, very complicated shapes may be produced by using only a few elements.

THE INSCRIBED CIRCUMCENTER ALGORITHM

As is well known, the lines connecting the center of an inscribed circle to the triangle vertices bisects the enclosed angles at the vertices. Referring to Figure 7 and using the area properties of triangle homogeneous coordinates, we find that

$$q_m = \frac{A_{m1} + A_{m2}}{|\Delta|} \quad (35)$$

where A_i is the area of the subtriangle indicated in Figure 7, Δ is the determinate

$$\Delta = \frac{1}{2} \begin{vmatrix} 1 & 1 & 1 \\ x_1 & x_2 & x_3 \\ y_1 & y_2 & y_3 \end{vmatrix} \quad (36)$$

and the subscripts $m, m1, m2$ are cyclic modulo three. Since $A_i = \frac{1}{2}r^2 \cot \theta_i$, Equation (35) yields

$$q_m = \frac{1}{2}r^2 (\cot \theta_{m1} + \cot \theta_{m2}) / |\Delta|. \quad (37)$$

Using the cotangent identity

$$\cot \theta_{m1} + \cot \theta_{m2} = \left[(x_{m1} - x_{m2})^2 + (y_{m1} - y_{m2})^2 \right] / 2|\Delta| \quad (38)$$

results in the equation

$$q_m = \frac{1}{4}r^2 \left[(x_{m1} - x_{m2})^2 + (y_{m1} - y_{m2})^2 \right] / |\Delta|^2. \quad (39)$$

Equation (39) may then be used to evaluate α , β , and γ in Equations (17) and (19).

A QUADRATIC HONEYCOMB ALGORITHM

Farin has published a C^1 surface generation procedure for data points arranged in a hexagonal or "honeycomb" pattern.^[9] He developed this procedure by using the properties of cubic Bezier polynomials. We shall now develop a similar algorithm based on the properties of quadratic Bezier polynomials.

With a regular array of hexagons, a triangulation can be associated as described in Figure 8. The vertices of the hexagons may be partitioned into the two groups C_1, C_3, C_5 and C_2, C_4, C_6 . We can then create two new triangulations, both of which consist of triangles of identical size and shape, one triangulation based on the points C_1, C_3, C_5 and the other on the points C_2, C_4, C_6 . Following the approach of Farin, we let each group of hexagon vertices that define the new triangulations form a plane in three dimensions such that the vertex values correspond to the specified values on the honeycomb grid. By insisting that the control vertices of the Bezier net at the corners of the original triangle lie on the average of these two planes, we can express each control vertex as a weighted sum of the values at the honeycomb vertices. In particular, choosing the interior points Q_i to be the triangle centroids, the following simple formulas are obtained

$$\begin{aligned} \phi_7 &= \frac{1}{6} (C_1 + C_2 + C_3 + C_4 + C_5 + C_6) \\ \phi_{10} &= \frac{1}{12} (4C_1 + 3(C_2 + C_6) + C_5 + C_3) \\ \phi_{12} &= \frac{1}{24} (7(C_1 + C_6) + 4(C_2 + C_5) + C_3 + C_4) \end{aligned} \quad (40)$$

By symmetry, identical formulas are obtained for the other two corners of the original triangle. The remaining control vertices are obtained by enforcing the interior C^1 conditions described in previous sections. Thus we see that Farin's construction is equivalent to giving position and tangent plane data at the triangle vertices, although, in fact, no derivative values are specified on the honeycomb at all.

Figure 9 provides an example of surface generated by the quadratic honeycomb algorithm where only function values at the vertices of the honeycomb grid were specified.

CONCLUSIONS

Although quadratics have often been dismissed as candidates for C^1 data interpolation, they are in fact ideal for such application. The numerical values of a quadratic C^1 surface are controlled purely by function and first derivative values at the data points; this surface is defined independently of the mid-side and twist derivative conditions required by cubics. In the event that the data points are arranged in a regular hexagonal array, a very simple formula exists for the surface purely in terms of surface values at the honeycomb vertices.

The main advantage of the procedure developed in this appendix is its efficiency. Quadratic polynomials in two-dimensions contain only six terms compared to the ten terms required for two-dimensional cubics. Although the algorithm in this paper requires that each data triangle be divided into six quadratic subtriangles to ensure C^1 continuity, while previous approaches are based on a subdivision into three cubics, the number of subtriangles required by the surface is less important than the order of the polynomial used. The reason for this is that a particular subtriangle in a surface description can be located very quickly; a much greater time is required to draw the surface once the subtriangle is determined.

A second advantage of the quadratic approach in this appendix is its simplicity. Surfaces are obtained by generating an arbitrary triangulation of the data points, subdividing each triangle into six, and using the formulas derived in this paper. Since there are only six terms in a quadratic, the formulas defining the quadratic surfaces defined in this appendix involve relatively few fundamental coefficients.

REFERENCES

1. Barnhill, R.E., "Computer Aided Surface Representation and Design," *Surfaces in CAGD*, R.E. Barnhill, W. Boehm (eds.), North-Holland Publishing Co., 1983.
2. Farin, G., "Smooth Interpolation to Scattered 3D Data," *Surfaces in CAGD*, R.E. Barnhill, W. Boehm (eds.), North-Holland Publishing Co., 1983.
3. Powell, M. and M. Sabin, "Piecewise Quadratic Approximation on Triangles," *ACM Transactions on Mathematical Software*, Vol. 3, 1977, pp. 316-325.
4. Sibson, R. and G. Thomson, "A Seamed Quadratic Element for Contouring," *The Computer Journal*, Vol. 24, No. 4, 1981, pp. 378-382.
5. Sederberg, T. and D. Anderson, "Steiner Surface Patches," *IEEE Computer Graphics and Applications*, Vol. 5, No. 5, 1985, pp. 23-36.
6. Boehm, W., G. Farin and J. Kahmann, "A Survey of Curve and Surface Methods in CAGD," *Computer Aided Geometric Design 1*, 1984, pp. 1-60.

7. Maxwell, E.A., *General Homogeneous Coordinates*, Cambridge University Press, 1960.
8. Lee, D. and B.J. Schacter, "Two Algorithms for Constructing a Delaunay Triangulation," *International Journal of Computer and Information Sciences*, Vol. 9, No. 3, 1980, pp. 219-242.
9. Farin, G., "Designing C^1 Surfaces Consisting of Triangular Cubic Patches," *Computer Aided Design*, Vol. 14, No. 5, 1982, pp. 253-256.

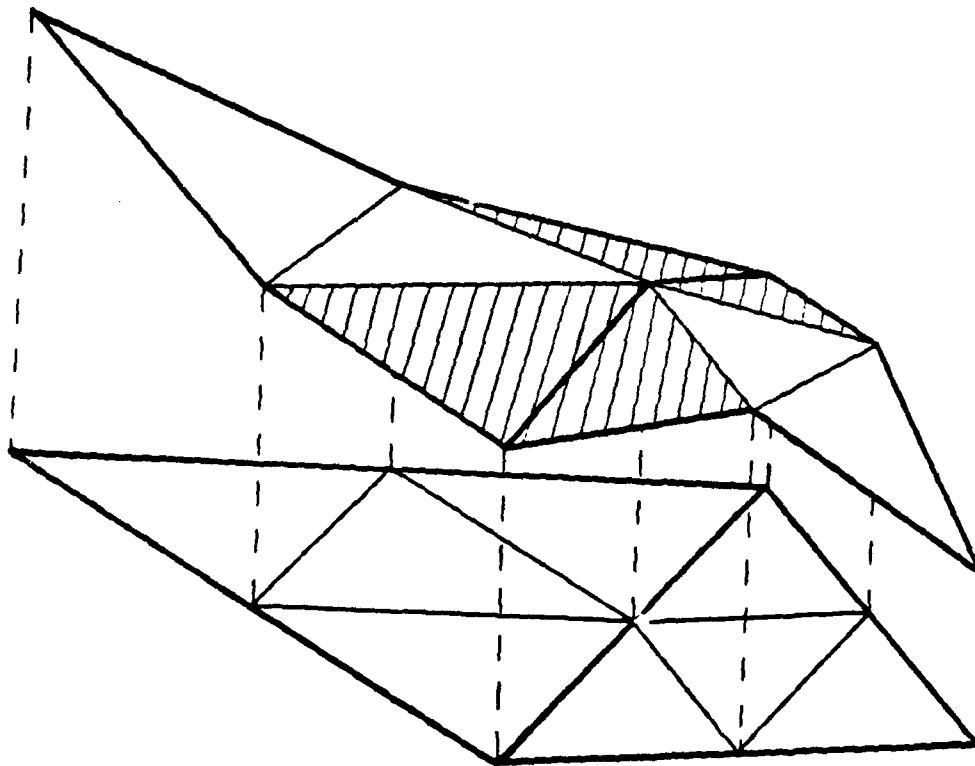


Figure 1: Two neighboring triangles showing the associated quadratic Bezier nets and a typical control surface. The shaded areas on the control surface must be planar for derivative continuity.

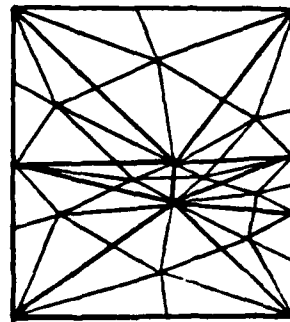
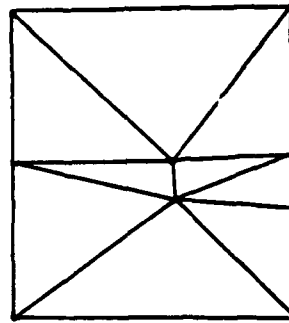
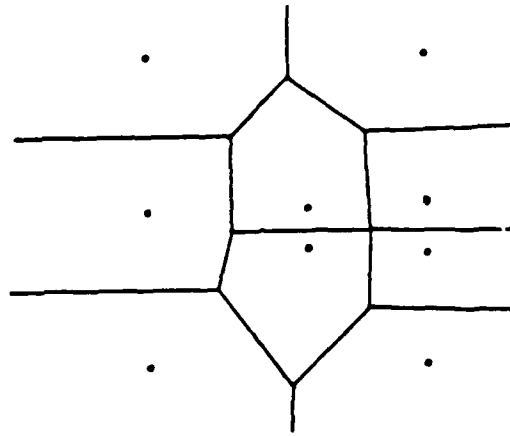


Figure 2: (a) A representative set of points showing the Voronoi polygons.
 (b) The Delaunay triangulation of the points in (a). (c) Subdivision of the triangles in (b) into six subtriangles.

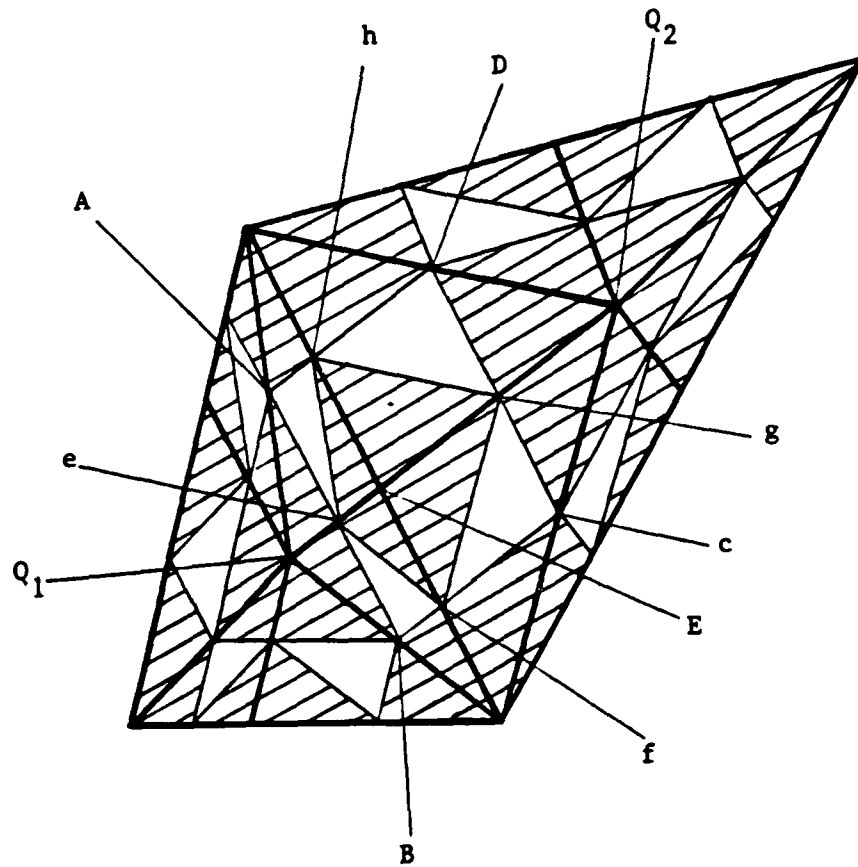


Figure 3: The Bezier net for two subdivided triangles. Each of the shaded areas must be coplanar for derivative continuity of the associated quadratic surface.

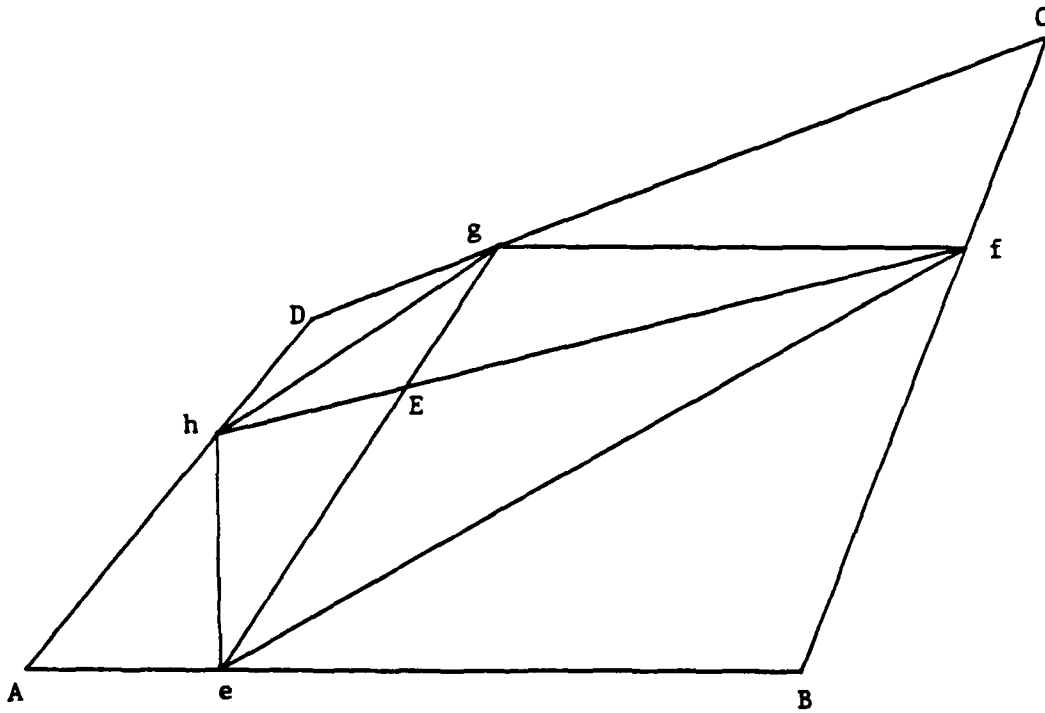


Figure 4: Geometry of the region at the center of the common triangle edge.

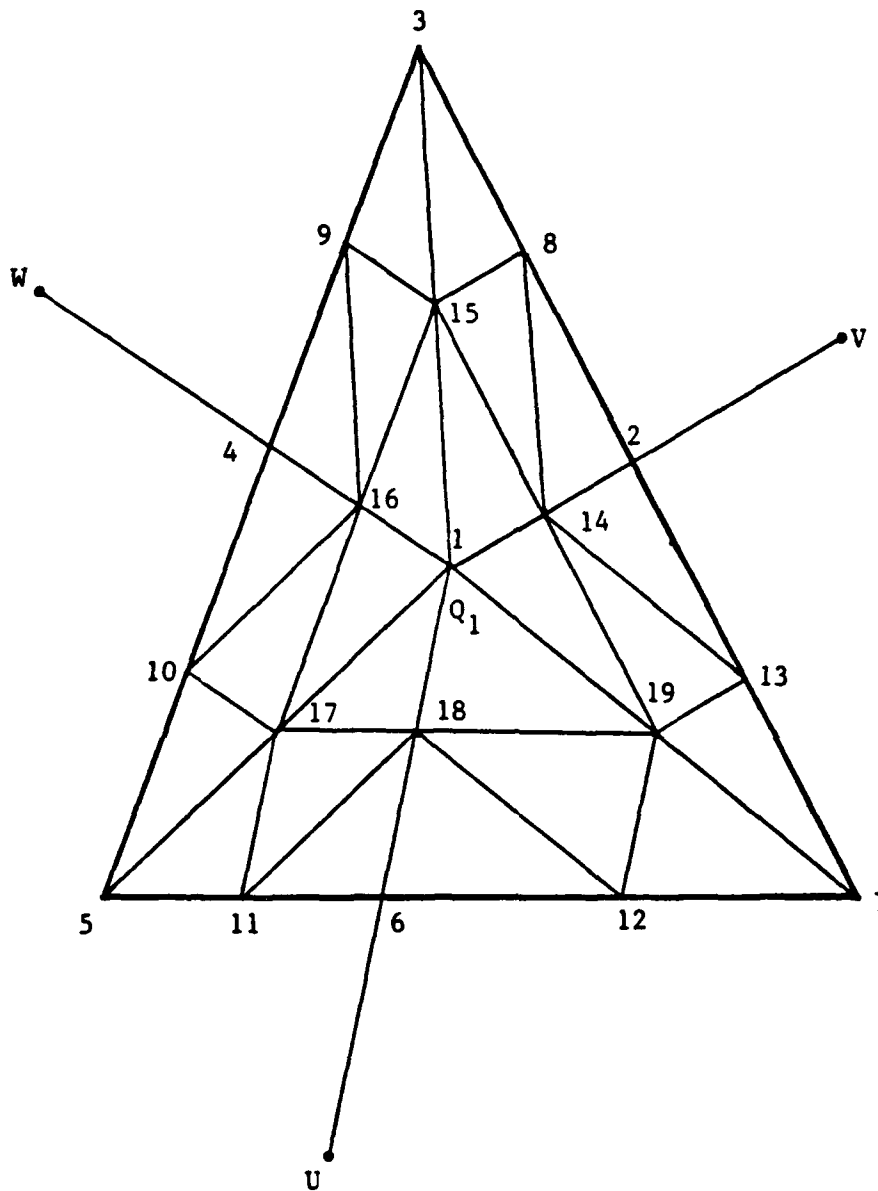


Figure 5: Node numbering scheme for a triangle subdivided into six Bezier quadratics. In subtriangle i , the node numbers are given by the formula $\{1, (13+i), (14+i \bmod 6), (1+i), (7+i), (2+i \bmod 6)\}$

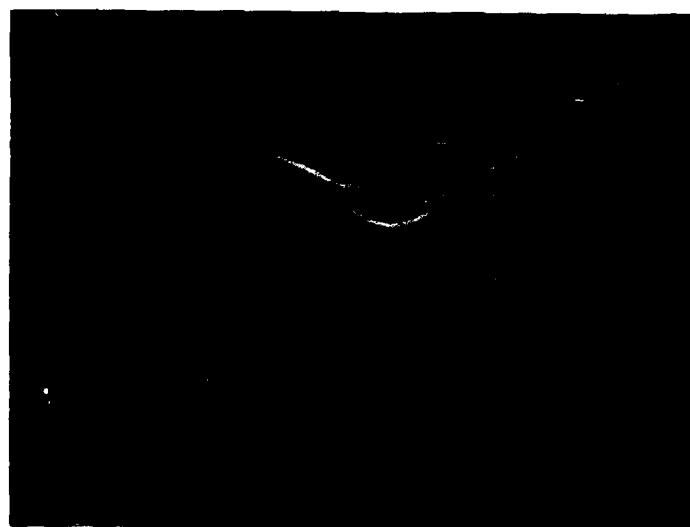
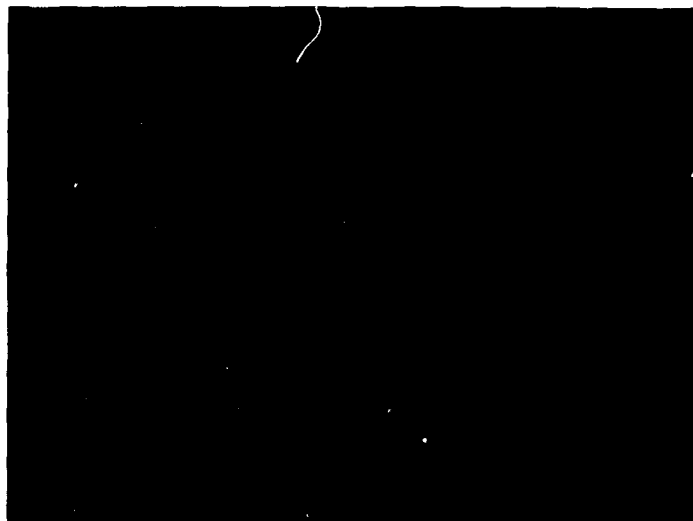


Figure 6: (a) The triangulation and corresponding Bezier net used to generate an arbitrary C^1 surface. (b) A complex C^1 quadratic surface obtained by specifying random function and derivative values at the data points.

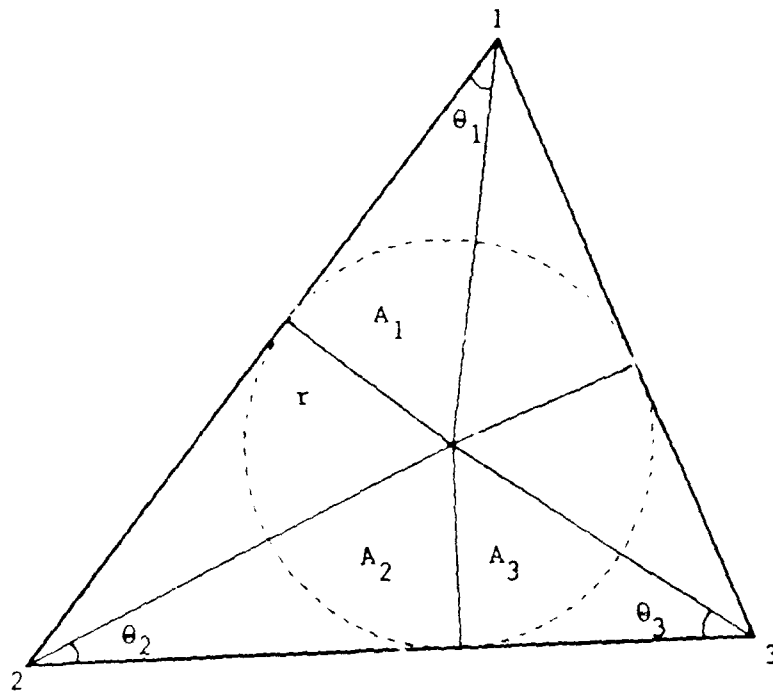


Figure 7: The circumcenter of an inscribed circle bisects the triangle vertex angles.

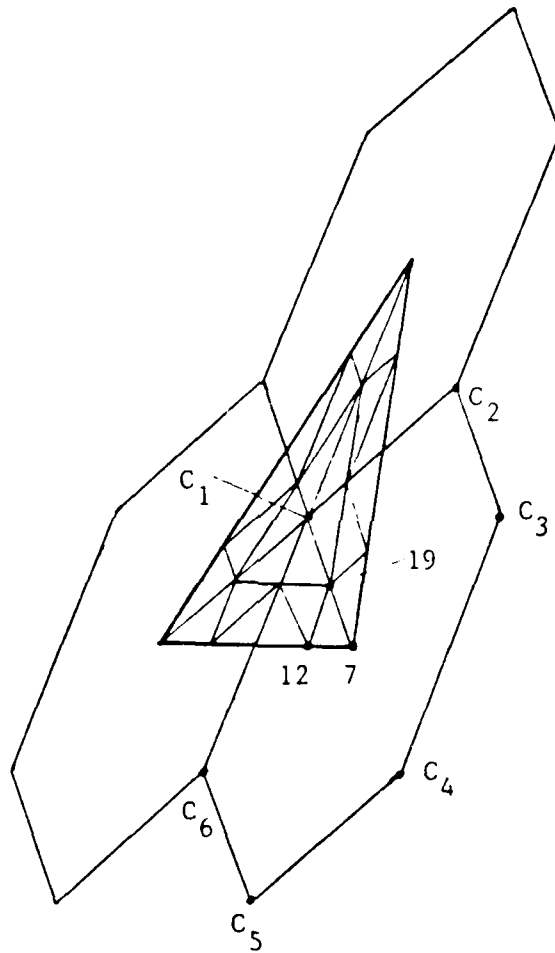


Figure 8: The centroids of three adjacent hexagons may be used to form a triangle. In this figure, this triangle has been divided into six triangles with the associated quadratic Bezier net superimposed.

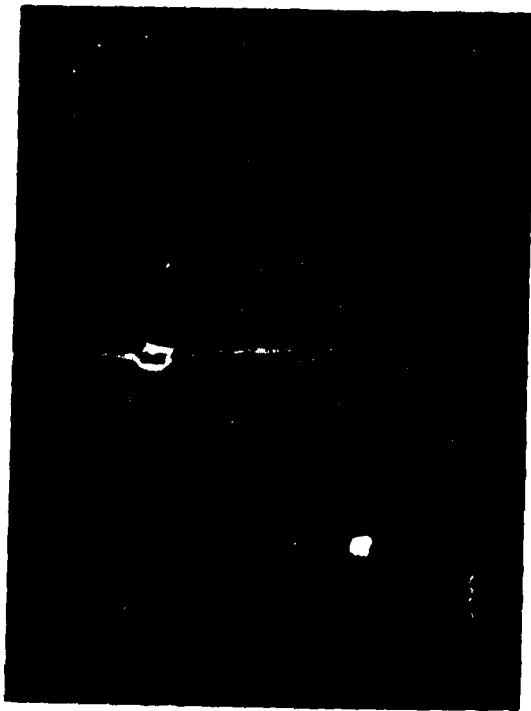


Figure 9 (a)

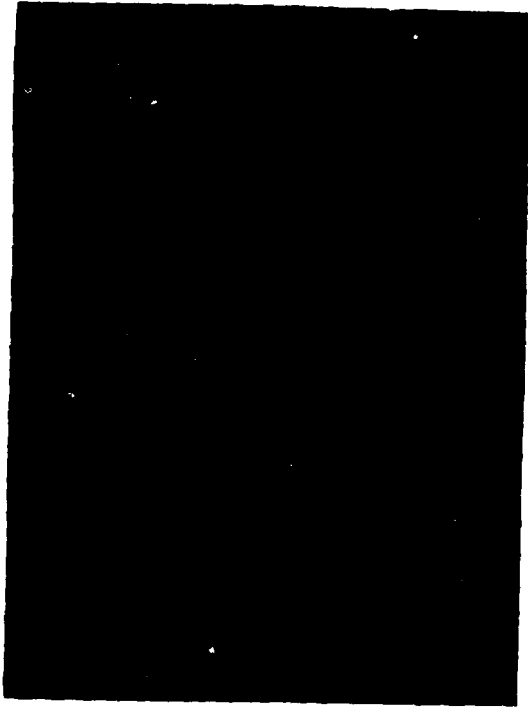


Figure 9 (b)



Figure 9 (c)

Figure 9: (a) A hexagonal array and associated triangulation for use in the honeycomb algorithm. (b) Control surface produced by setting two hexagon vertices to minus one and setting the others to zero. (c) The associated quadratic surface.

APPENDIX D - ELIMINATING SPURIOUS SOLUTIONS IN ELECTROMAGNETIC WAVE PROBLEMS BY USING C^1 FINITE ELEMENTS

ABSTRACT

A novel approach to eliminating spurious or nonphysical solutions in finite element electromagnetic field analysis is presented in this appendix. In this method, C^1 or first derivative continuous finite elements are used to construct vector field solutions that are exactly divergence-free both within and across the edges of the elements. The appearance of spurious modes in high frequency analysis is generally attributed to the inability of the finite element field solutions to satisfy the divergence and boundary conditions required by Maxwell's equations. By using finite element vector field basis functions that satisfy the divergence and derivative continuity conditions exactly, spurious solutions are completely eliminated. In this appendix, this method is successfully applied to inhomogeneous dielectric waveguide problems. In addition, a new C^1 triangular finite element based on quadratics, the simplest of all possible general C^1 elements, is introduced for finite element analysis.

I. INTRODUCTION

The finite element analysis of waveguiding problems is one of the most important areas in computational high frequency electromagnetics. Different methods for analyzing dielectric-loaded waveguides and cavities have been proposed. They include vectorial finite element formulations in terms of the longitudinal-electric E_z and magnetic H_z field components [1]-[2] as well as formulations that are based on all three components of the field vectors [3]-[5]. From the beginning, it was recognized that a major difficulty in these analyses is the appearance of spurious or nonphysical solutions [1]-[5]. These spurious modes intermingle with the real physical solutions and make the distinction between correct and incorrect solutions very difficult. One cause of spurious modes is that the finite element vector solutions do not

satisfy the divergence-free condition $\nabla \cdot \vec{H} = 0$ [4]-[6] that is required by the physics of the problem. To remedy this difficulty, various methods that approximately impose the zero-divergence constraint in the finite element analysis have been proposed. The penalty function method [8]-[9], for instance, incorporates the condition $\nabla \cdot \vec{H} = 0$ to be satisfied in the least square sense in the variational functional. However, this method requires a suitable choice for the penalty coefficient. Recently a method that approximately enforces the zero-divergence condition via a Galerkin formulation has been introduced [10].

Still other methods that are based on approximating $\nabla \cdot \vec{H} = 0$ by finite difference [11] or by using vector field basis functions that are approximately divergence-free [12] have also been proposed.

Focusing only on procedures that set the divergence of \vec{H} to zero inside finite elements is, however, insufficient. The exact solutions of electromagnetic field problems are not only nondivergent inside each finite element, they are also nondivergent at inter-element boundaries. This means that a method of correctly specifying the derivative of the solution at the element edges must be developed.

In this paper, a very general approach for constructing finite element vector field basis functions that satisfy the zero-divergence condition both inside finite elements and across element edges is presented. Using this method, the problem of spurious solutions in waveguide problems is completely eliminated. The novelty of this approach is in the application of C^1 or first derivative continuous finite elements in electromagnetics. Although the Clough-Tocher C^1 cubic [13] is well known in structural analysis, the use

of C^1 elements has thus far been limited to mechanical engineering applications. However, in this paper, we shall demonstrate that C^1 elements can be used to construct vector fields that are exactly divergence-free, providing an alternative way of eliminating the long-standing problem of spurious modes in computational high frequency electromagnetics. Further, we introduce a new set of C^1 basis functions based on quadratic polynomials [14]-[15] for finite element work. These C^1 quadratics have the advantage of being lower order than the standard Clough-Tocher triangle.

II. FORMULATION

Consider a dielectric waveguide with arbitrary cross-section Ω in the x - y plane. With the time harmonic variation $e^{j\omega t}$ assumed throughout, the two Maxwell curl equations are:

$$\nabla \times \vec{E} = -j\omega\mu_0 \vec{H} \quad (1)$$

$$\nabla \times \vec{H} = j\omega\epsilon_0[\epsilon_r] \vec{E} \quad (2)$$

and $[\epsilon_r]$ denotes the relative permittivity tensor of the dielectric. We assume throughout that the relative permeability of the dielectric is unity. From (1) and (2) we obtain the vector wave equation

$$\nabla \times ([\epsilon_r]^{-1} \nabla \times \vec{H}) - k^2 \vec{H} = \vec{0} \quad (3)$$

where $k^2 = \omega^2 \mu_0 \epsilon_0$. In finite element analysis, this equation is replaced by the extremization of the functional [3]

$$F = \int_{\Omega} \left[(\nabla \times \vec{H})^* \cdot ([\epsilon_r]^{-1} \nabla \times \vec{H}) - k^2 \vec{H}^* \cdot \vec{H} \right] d\Omega. \quad (4)$$

At the stationary point of the functional (4), we obtain (3) as the Euler-Lagrange equation. The exact solution \vec{H} which satisfies (3) should in theory also satisfy $\nabla \cdot \vec{H} = 0$. This can be seen by taking the divergence of both sides of (3). However, problems arise when we obtain an approximate solution that does not satisfy (3) exactly and hence $\nabla \cdot \vec{H} \neq 0$. Solutions that do not even approximately satisfy $\nabla \cdot \vec{H} = 0$ are generally identified as spurious modes. To eliminate these spurious solutions, one can limit the subspace of trial functions \vec{H} in (4) to those that are exactly solenoidal in addition to satisfying the essential boundary conditions.

To obtain trial functions \vec{H} that satisfy $\nabla \cdot \vec{H} = 0$ a priori, it is mathematically straightforward to expand \vec{H} in general as

$$\vec{H} = \nabla \times \vec{\psi} = \nabla \times \left\{ [\psi_x(x,y) \vec{a}_x + \psi_y(x,y) \vec{a}_y + \psi_z(x,y) \vec{a}_z] e^{-j\beta z} \right\} \quad (5)$$

where β is the propagation constant in the longitudinal direction and ψ_x , ψ_y and ψ_z are scalar functions defined over Ω . While the preceding expansion is formally valid, it requires that each of the scalar function ψ have at least continuous first derivatives, that is, to be C^1 throughout the entire domain Ω . This is because even though $\nabla \cdot \bar{H} \equiv 0$ holds within the element, continuity of \bar{H} across element interfaces is required. Due to the differentiation in (5), C^1 continuity of ψ automatically implies continuity of \bar{H} throughout the entire domain Ω . In other words, the integral form of Gauss' law

$$\oint_s \bar{H} \cdot \bar{n} \, ds \equiv 0 \quad (6)$$

is identically satisfied for an arbitrary surface s within the waveguide, including surfaces that traverse element edges.

One can also appreciate the need for C^1 continuity by substituting (5) into (4) and so that F is written in terms of the trial function $\bar{\psi}$

$$F = \int_{\Omega} \left[(\nabla \times \nabla \times \bar{\psi})^* \cdot ([\epsilon_r]^{-1} \nabla \times \nabla \times \bar{\psi}) - k^2 (\nabla \times \bar{\psi})^* \cdot (\nabla \times \bar{\psi}) \right] d\Omega. \quad (7)$$

The functional (7) contains second derivatives of the scalar function ψ ; in order for such a functional to be integrable, C^1 continuity for ψ is required [13]. It is emphasized that standard C^0 Lagrangian polynomials are inadequate to yield an identically zero-divergence field \bar{H} ; such fields require at least C^1 continuity.

III. QUADRATIC C^1 TRIANGULAR FINITE ELEMENTS

The analysis presented in this paper is based on the recently developed C^1 quadratic triangular finite element that is described in [14]-[15]. Its construction is based on a subdivision principle. An interior point Q , such as the centroid, or more generally the triangle incenter, is selected for each element in the mesh. Then by joining each interior point to its element vertices and the interior points of neighboring elements, each element is subdivided into 6 subtriangles (Fig. 1). Over each subtriangle, a second order polynomial is defined using the Bernstein-Bezier representation [16]. After imposing C^1 continuity, the resulting C^1 element interpolates to the function and to the first x and y derivatives at the element vertices.

For the purpose of this paper, it is sufficient to summarize the linear relationship between the 19 Bezier coefficients ϕ , and the function and first derivatives data of $\phi(x,y)$ at the triangle vertices as given in Table 1.

IV. FINITE ELEMENT FORMULATION

In conventional finite element analysis, discretization of the functional (4) results in the general eigenvalue problem [3]

$$[S]\{H\} = k^2[T]\{H\} \quad (8)$$

where the components of the column vector $\{H\}$ are the values of H_x , H_y and H_z at the nodal points and the matrices $[S]$ and $[T]$ are given by

$$\{H\}^+ [S] \{H\} = \int_{\Omega} (\nabla \times \bar{H}^* \cdot ([\epsilon_r]^{-1} \nabla \times \bar{H}) \, d\Omega \quad (9)$$

$$\{H\}^+ [T] \{H\} = \int_{\Omega} (\bar{H})^* \cdot (\bar{H}) \, d\Omega. \quad (10)$$

According to (5), the vector $\{H\}$ is related to a column vector $\{P\}$ which contains the parameters describing the scalar C^1 functions ψ_i , $i = x, y, z$. This is represented by the "curl" matrix $[C]$

$$\{H\} = [C] \{P\}. \quad (11)$$

Substituting (11) into (9) and (10) results in a modified eigenvalue problem that guarantees $\nabla \cdot \bar{H} = 0$

$$[C]^T [S] [C] \{P\} = k^2 [C]^T [T] [C] \{P\}. \quad (12)$$

For the C^1 quadratic described in the previous section, the entries of $\{P\}$ are the function and first derivatives of ψ at the vertices of the element. The matrix $[C]$ is constructed for each element using (5) and the information provided in Table 1. The modified $[S]$ and $[T]$ matrices in (12) are then computed for each element and assembled to form the global matrices for the whole problem.

An equivalent procedure is to carry out the expansion in (7). The modified $[S]$ and $[T]$ matrices can then be computed directly without resorting to the congruence transformation in (12).

The extremization of the functional (4) requires the essential boundary condition $\bar{H} \cdot \bar{a}_n = 0$ to be satisfied along perfectly conducting surfaces. These boundary conditions on \bar{H} then correspond to constraints on the ψ 's in (5). Examples will be given in the next sections on the application of these constraints.

V. TEST EXAMPLES

A. EMPTY RECTANGULAR WAVEGUIDES

In the first example, we shall illustrate the present method by solving for the eigenmodes of an empty square metallic waveguide of width W . For the TM modes of the empty waveguide, we let $\psi_x = \psi_y = 0$ and write

$$\bar{H} = \nabla \times \psi_z(x, y) e^{-j\beta z} \bar{a}_z. \quad (13)$$

The essential boundary condition $\bar{H} \cdot \bar{a}_n = 0$ then implies that $\nabla \psi_z \cdot \bar{a}_t = 0$ where \bar{a}_t denotes the tangent vector to the metallic boundary Γ on the x - y plane. To enforce this condition, it is sufficient to impose $\psi_z = 0$ on Γ . In the same way, to solve for the TE modes we write

$$\bar{E} = \nabla \times \psi_z(x,y)e^{-j\beta z} \bar{a}_z \quad (14)$$

and require that $\bar{E} \cdot \bar{a}_t = 0$ on Γ . This is imposed by setting $\nabla \psi_z \cdot \bar{a}_n = 0$ on Γ .

The waveguide was discretized by using 81 C^1 elements; the first 10 TM modes computed are given in Table 2. It is interesting to note that even with a homogeneous guide, the classical analysis based on (8) yields several zero eigenvalues in addition to the correct nonzero values. It is these zero eigenvalues that shift to nonzero spurious frequencies if the guide is partially filled with dielectric. In contrast, the present method as based on (12) does not produce any "zero" eigenvalues with an empty waveguide. Every eigenvalue obtained corresponds to a physical solution. The next example shows that even with inhomogeneous dielectric waveguides, no spurious modes appear in the analysis.

B. DIELECTRIC-LOADED WAVEGUIDES

Consider a square metallic waveguide half-filled with dielectric. The dielectric has relative permittivity $\epsilon_r = 1.5$ and the geometry is shown in Fig. 2. Solving for the LSM modes of the guide we let $\psi_y = \psi_z = 0$ and write

$$\bar{H} = \nabla \times \psi_x(x,y)e^{-j\beta z} \bar{a}_x \quad (15)$$

The boundary conditions $\bar{H} \cdot \bar{a}_n = 0$ on Γ now correspond to $\psi_x = 0$ along $y = 0$ and $y = W$. In one test, 100 C^1 elements were used yielding a total of 319 unknowns. For $\beta W = 10$, the first ten eigenvalues from this test are given in Table 3 and compared to those obtained by Koshiba et al [8]. All solutions obtained by using the C^1 procedure correspond to physically correct solutions so that the problem of spurious modes is completely eliminated.

VI. CONCLUSION

A novel approach for eliminating spurious modes in waveguiding problems is presented. This method is based on the use of C^1 finite elements for constructing vector field solutions that are divergence-free. Unlike previous approaches that impose the zero-divergence condition approximately by modifying the variational procedure, field solutions from the present method satisfy the zero-divergence constraint exactly both inside and across the edges of the finite elements. It is found that in this way, spurious solutions do not occur.

This paper also introduces the use of C^1 quadratic triangles to finite element analysis. These quadratics are the simplest C^1 element possible and hence the most economical to use in many applications.

It should be noted that the method presented in this paper for constructing divergence-free finite element vector fields is a very general one. Its application is not limited to the two-dimensional waveguide problems considered. For instance, we are presently investigating the elimination of spurious modes in 3-D electromagnetic cavities by applying three-dimensional C^1 finite elements. The procedure can also be used to generate zero curl vector fields by changing the curl operator in (5) to the gradient operator.

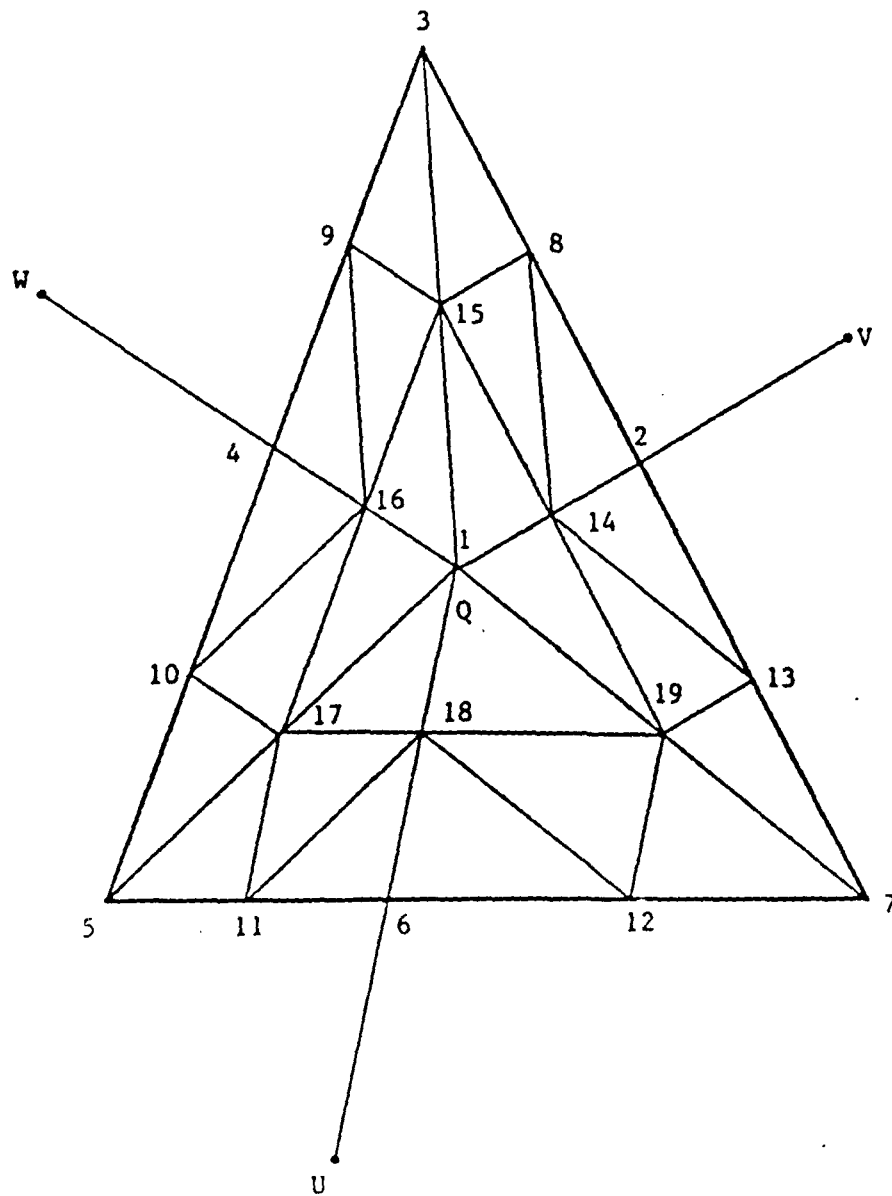


Figure 1: Node Numbering for Composite C^1 Quadratics.

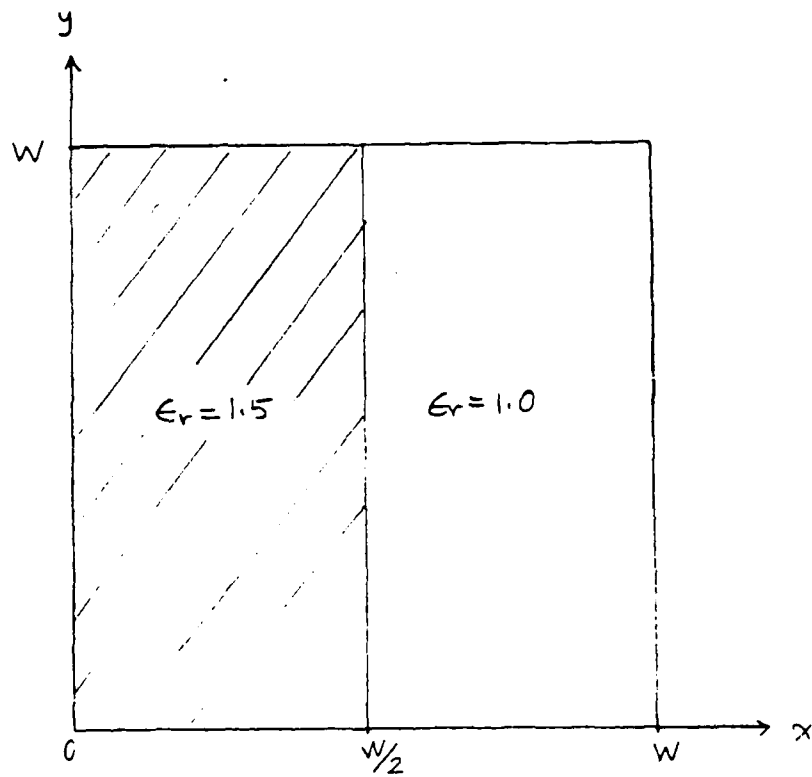


Figure 2: The Geometry of a Half-Filled Dielectric Waveguide

Table 1: Formulas for the Bezier Coefficients of Composite C^1 Quadratics Finite Elements

| ϕ_3 | $\frac{\partial \phi}{\partial x}_3$ | $\frac{\partial \phi}{\partial y}_3$ | ϕ_5 | $\frac{\partial \phi}{\partial x}_5$ | $\frac{\partial \phi}{\partial y}_5$ | ϕ_7 | $\frac{\partial \phi}{\partial x}_7$ | $\frac{\partial \phi}{\partial y}_7$ | |
|-------------|--------------------------------------|--------------------------------------|-----------------|--------------------------------------|--------------------------------------|------------------|--------------------------------------|--------------------------------------|------------------|
| ϕ_1 | q_1 | $q_1 a_1$ | $q_1 b_1$ | q_2 | $q_2 a_2$ | $q_2 b_2$ | q_3 | $q_3 a_3$ | $q_3 b_3$ |
| ϕ_2 | $(1-\beta)$ | $(1-\beta) a_4$ | $(1-\beta) b_4$ | | | | β | βa_9 | βb_9 |
| ϕ_3 | 1 | | | | | | | | |
| ϕ_4 | γ | γa_5 | γb_5 | $(1-\gamma)$ | $(1-\gamma) a_6$ | $(1-\gamma) b_6$ | | | |
| ϕ_5 | | | | 1 | | | | | |
| ϕ_6 | | | | α | αa_7 | αb_7 | $(1-\alpha)$ | $(1-\alpha) a_8$ | $(1-\alpha) b_8$ |
| ϕ_7 | | | | | | | 1 | | |
| ϕ_8 | 1 | a_4 | b_4 | | | | | | |
| ϕ_9 | 1 | a_5 | b_5 | | | | | | |
| ϕ_{10} | | | | 1 | a_6 | b_6 | | | |
| ϕ_{11} | | | | 1 | a_7 | b_7 | | | |
| ϕ_{12} | | | | | | | 1 | a_8 | b_8 |
| ϕ_{13} | | | | | | | 1 | a_9 | b_9 |
| ϕ_{14} | $(1-\beta)$ | $(1-\beta) a_1$ | $(1-\beta) b_1$ | | | | β | βa_3 | βb_3 |
| ϕ_{15} | 1 | a_1 | b_1 | | | | | | |
| ϕ_{16} | γ | γa_1 | γb_1 | $(1-\gamma)$ | $(1-\gamma) a_2$ | $(1-\gamma) b_2$ | | | |
| ϕ_{17} | | | | 1 | a_2 | b_2 | | | |
| ϕ_{18} | | | | α | αa_2 | αb_2 | $(1-\alpha)$ | $(1-\alpha) a_3$ | $(1-\alpha) b_3$ |
| ϕ_{19} | | | | | | | 1 | a_3 | b_3 |

where (q_1, q_2, q_3) denotes the simplex coordinates of Q and

$$a_1 = \frac{1}{2} [(q_1 - 1) x_3 + q_2 x_5 + q_3 x_7] \quad , \quad a_2 = \frac{1}{2} [q_1 x_3 + (q_2 - 1) x_5 + q_3 x_7]$$

$$a_3 = \frac{1}{2} [q_1 x_3 + q_2 x_5 + (q_3 - 1) x_7] \quad , \quad a_4 = \frac{\beta}{2} (x_7 - x_3)$$

$$a_5 = \frac{(1-\gamma)}{2} (x_5 - x_3) \quad , \quad a_6 = \frac{\gamma}{2} (x_3 - x_5)$$

$$a_7 = \frac{(1-\alpha)}{2} (x_7 - x_5) \quad , \quad a_8 = \frac{\alpha}{2} (x_5 - x_7)$$

$$a_9 = \frac{(1-\beta)}{2} (x_3 - x_7) \quad \alpha = d_{7,6}/d_{7,5}$$

$$\beta = d_{3,2}/d_{3,7}$$

$$\gamma = d_{5,4}/d_{5,3}$$

*The expressions for b_i are obtained from those of a_i by substituting y_j for x_j .

d_{ij} denotes distance between node i and node j .

Table 2: The First Ten TM Modes in a Square Waveguide

| TM Mode | C^1 Finite Element | Exact |
|---------|----------------------|---------|
| 1,1 | 4.4552 | 4.4429 |
| 1,2 | 7.0873 | 7.02481 |
| 2,1 | 7.0894 | 7.02481 |
| 2,2 | 8.9847 | 8.8858 |
| 1,3 | 10.1472 | 9.93459 |
| 3,1 | 10.1475 | 9.93459 |
| 2,3 | 11.5391 | 11.3272 |
| 3,2 | 11.5751 | 11.3272 |
| 1,4 | 13.4612 | 12.9531 |
| 4,1 | 13.4672 | 12.9531 |

Table 3: The First Ten LSM Modes for $\beta W = 10$ in the Dielectric Waveguide Shown in Figure 2.

| No. | C^1 Finite Element | Hayata et al. |
|-----|----------------------|---------------|
| 1 | 8.8109 | 8.8093 |
| 2 | 9.8834 | 9.3896 |
| 3 | 10.2751 | 10.2752 |
| 4 | 11.1073 | 11.1038 |
| 5 | 11.3835 | 11.2677 |
| 6 | 11.4685 | 11.4501 |
| 7 | 12.2654 | 11.9882 |
| 8 | 12.7957 | 12.6686 |
| 9 | 12.9510 | 12.8092 |
| 10 | 13.4298 | 12.9575 |

REFERENCES

1. S. Ahmed and P. Daly, "Finite-Element Methods for Inhomogeneous Waveguides", *Proc. Inst. Elec. Eng.*, Vol. 116, pp. 1661-1664, Oct. 1969.
2. Z.J. Cendes and P. Silvester, "Numerical Solution of Dielectric Loaded Waveguides: I - Finite-Element Analysis", *IEEE Trans. Microwave Theory Tech.*, Vol. MTT-18, pp. 1124-1131, Dec. 1970.
3. A. Konrad, "High-Order Triangular Finite Elements for Electromagnetic Waves in Anisotropic Media", *IEEE Trans. Microwave Theory Tech.*, Vol. MTT-25, pp. 353-360, May 1977.
4. J.B. Davies, F.A. Fernandez and G.Y. Phillippon, "Finite Element Analysis of All Modes in Cavities with Circular Symmetry", *IEEE Trans. Microwave Theory Tech.*, Vol. MTT-30, pp. 1975-1980, Nov. 1982.
5. B.M.A. Rahman and J.B. Davies, "Finite-Element Analysis of Optical and Microwave Waveguide Problems", *IEEE Trans. Microwave Theory Tech.*, Vol. MTT-32, pp. 20-28, Jan. 1984.
6. M. Hara, T. Wada, T. Fukasawa and F. Kikuchi, "Three-Dimensional Analysis of RF Electromagnetic Fields by Finite Element Method", *IEEE Trans. Magn.*, Vol. MAG-19, No. 6, pp. 2417-2420, 1983.
7. B.M.A. Rahman and J.B. Davies, "Penalty Function Improvement of Waveguide Solution by Finite Elements", *IEEE Trans. Microwave Theory Tech.*, Vol. MTT-32, pp. 922-928, Aug. 1984.
8. M. Koshiba, K. Hayata and M. Suzuki, "Vectorial Finite-Element without Spurious Solutions for Dielectric Waveguide Problems", *Electron. Lett.*, Vol. 20, pp. 409-410, May 1984.
9. J.P. Webb, "The Finite-Element Method for Finding Modes of Dielectric-Loaded Cavities", *IEEE Trans. Microwave Theory Tech.*, Vol. MTT-33, pp. 635-639, July 1985.
10. K. Hayata, M. Koshiba, M. Eguchi and M. Suzuki, "Vectorial Finite-Element Method without any Spurious Solutions for Dielectric Waveguiding Problems using Transverse Magnetic-Field Component", *IEEE Trans. Microwave Theory Tech.*, Vol. MTT-34, pp. 1120-1124, Nov. 1986.
11. N. Schulz, K. Bierwirth and F. Arndt, "Finite-Difference Analysis of Integrated Optical Waveguides without Spurious Mode Solutions", *Electron. Lett.*, Vol. 22, pp. 963-965, Aug. 1986.
12. A.J. Kobelansky and J.P. Webb, "Eliminating Spurious Modes in Finite-Element Waveguide Problems by using Divergence-Free Fields", *Electron. Lett.*, Vol. 22, pp. 569-570, May 1986.
13. G. Strang and G.J. Fix, An Analysis of the Finite Element Method, Prentice-Hall, Englewood Cliffs, NJ, 1973.
14. Z.J. Cendes and S.H. Wong, " C^1 Quadratic Interpolation over Arbitrary Point Sets", *IEEE Computer Graphics and Applications*, accepted for publication.

15. S.H. Wong and Z.J. Cendes, "A C^1 Quadratic Interpolant for Magnetic Field Computation", *IEEE Trans. Magn.*, Vol. MAG-22, pp. 1034-1036, Sept. 1986.
16. R.E. Barnhill and G. Farin, " C^1 Quadratic Interpolation over Triangles: Two Explicit Representations", *Int. J. Num. Meth. Engn.*, Vol. 17, pp. 1763-1778, 1981.

APPENDIX E - MODELING THE OPEN BOUNDARY CONDITION IN THE FINITE ELEMENT SOLUTION OF ELECTROMAGNETIC SCATTERING PROBLEMS

ABSTRACT

Electromagnetic scattering problems are solved in this appendix by using the finite element method within an artificial bound picture frame, and analytical expressions in the exterior region. Two schemes for coupling the solutions in the two regions are proposed, namely, a "two-boundary approach" and a "transfinite elements approach." The two boundary approach, as implied by the name, employs two boundaries in the solution procedure and the superposition theorem to determine the proper linear combination of modes for the problem. By allowing the exterior region and the finite element solution region to overlap, the coefficients in the modal expansion are determined. As for the transfinite element method, it is based on variational principles, choosing different basis functions for the finite elements solution region and for the exterior region. The application of the two boundary approach to waveguide junction problems as well as to object scattering problems is presented here. Application of the transfinite element method to electrostatic problems and to object scattering problems are also studies.

SECTION 1 INTRODUCTION

1.1 OPEN BOUNDARY SCATTERING PROBLEMS

A number of important electromagnetic problems involve the bistatic scattering of electromagnetic fields from metal and dielectric objects in open regions. The primary categories of these scattering problems are the following:

1. Radiation from antennas.
2. Electromagnetic scattering from arbitrarily shaped and inhomogeneous penetrable bodies.
3. Microwave planar integrated circuits.
4. Waveguide junctions.

In these problems, knowledge of the field distribution is important in two different regions: (1) at a very great distance from the scattering object and (2) within the vicinity of the scatterer itself.

Since the geometry of electromagnetic scatterers is in general complicated and often three-dimensional, numerical methods are preferred for their analysis. These methods may be divided into two groups: (1) integral equation methods, and (2) differential equation methods. Of these two approaches, by far the most commonly used has been the integral approach, popularized by Harrington with his monograph "Fields Computation by Moment Methods".¹ However, despite their popularity, integral methods have failed to solve a number of important scattering problems, most notably those involving large or complicated variations in permeability and/or permittivity.

On the other hand, in other engineering disciplines, differential methods have been very successful in modeling large, complicated inhomogeneous structures. Differential methods appear to have an advantage precisely where integral methods are weak - namely in modeling the interface condition between media with different properties. They have had limited application to scattering problems for only one reason: differential methods cannot accomodate easily the open

or infinite region encountered in scattering problems. While a number of procedures to model open boundary conditions with differential methods have been proposed and will be reviewed below, none of the existing methods is completely satisfactory in terms of simplicity, ease of use, and efficiency.

The purpose of this appendix is to develop new methods of modeling electromagnetic scattering from complicated shapes. We employ the finite element method to model the fields in the near field scattering region and develop two new ways to model the open region enclosing the scatterer. This appendix is restricted to considering electromagnetic scattering problems to two dimensions. We specifically treat the scattering that appears at waveguide junctions and from cylindrical scatterers in free space. However, the methods developed in this report will also be useful for solving the general electromagnetic scattering problems.

1.2. MODELING THE OPEN BOUNDARY CONDITION

Since finite element methods are best suited to modeling electromagnetic fields in the immediate vicinity of the scatterer, some method of representing the fields in the infinite region must be developed, as well as procedures for coupling the finite element solution region to the infinite region. With regard to waveguide junction scattering, such procedures were developed relatively early and are known by the name modal analysis technique^{2,3,4}. The idea behind this method is to replace the waveguide discontinuity problem by two appropriate semi-infinite uniform waveguides separated by a so-called "discontinuity region". Muilwyk and Davies⁵ adapted an experimental procedure proposed by Montgomery et al⁶ for finding the scattering parameters of a discontinuity by locating the nulls of its standing wave patterns. They solved the field problems in the discontinuity region by using the finite-difference method. A deficiency in the method proposed by Muilwyk and Davies is that finding the locations of the nulls in the standing wave pattern is a trial and error procedure and on each trial an eigenvalue problem must be solved.

Marin⁷ has applied the finite element method to solve the scattering problems with lossy scatterers. A nonlocal boundary condition was employed to derive a variational formulation of the scattering problem, and the finite element method was applied to determine the approximation to the near fields. Scattering amplitudes are determined by means of an integral representation obtained from Green's formula and properties of the nonlocal boundary operator. But the complexity of the calculation for the nonlocal boundary operator has limited the usage of this method. Recently Koshiba and Suzuki⁸ proposed a better way of using the integral technique for solving the problem of a H-plane waveguide junction containing lossy ferrite posts of arbitrary shape. The procedure is to consider two planes in each port and then to relate the unknowns on

these two planes using an integral equation procedure. The result is a set of equations that are combined with the equations obtained from the finite element method and solved directly for the field values inside the discontinuity region. Unfortunately the resulting matrix equation is complex and non-symmetric even for the lossless cases.

With regard to open cylindrical scattering problems, a common feature in numerical modeling methods is the subdivision of the problem into a finite, closed region called a "picture frame" and the surrounding open space. A finite element or finite difference approximation is then made for the fields within the picture frame and some device used to couple the exterior field boundary condition to the picture frame boundary.

In one approach, proposed by Silvester and Hsieh⁹ for electrostatics problems, a single picture frame is defined and the energy functional of the entire region exterior to the picture frame evaluated and added to the interior region energy functional. The solution is therefore involves the electrostatic field in all space, but by a judicious choice of exterior field approximation functions explicitly solves for the field only in the region interior to the picture frame. A major difficulty with this formulation, however is that the integrand along the picture frame boundary is singular and difficult to compute. In another approach, proposed by McDonald and Wexler¹⁰, two concentric picture frames are defined and the integral equation relating the potentials between the two picture frames is used to specify the boundary conditions. Fields outside of the outer picture frame are never considered in the solution process; the integral equation merely provides a relationship between internal field values. However, the energy functional in the exterior region can be evaluated by using an integral transformation and weighted Gaussian quadrature formulas. The programming requirements of this procedure are also relatively difficult and this has limited its application. By using the mode decomposition technique, Chang and Mei¹¹ presented a method which they called "unimoment method" to calculate the scattered fields of dielectric cylinders of arbitrary cross section or of inhomogeneous material. The basic technique of the method is to use the finite element method inside a circular picture frame, and to expand the fields outside in cylindrical harmonics. Coupling the interior and exterior solutions is performed by matching the interior and exterior fields with respect to both the function values and the normal derivative values on the circle. There are two disadvantages with this method: first for N expansion functions in the exterior region, $2 \times N$ boundary value problems must be solved as the basis functions; second, derivatives of the finite element solutions for each mode on the boundary must be calculated.

Bettess¹² in 1977 proposed a procedure he dubbed "infinite elements". In this method, a series of shape functions analogous to Lagrange polynomials but including an exponential decay term

are generated. The approximate interpolation functions are unbounded geometrically hence the name "infinite elements". Unfortunately the accuracy of this method depends on the ability of the user to place the right decay factor in the infinite elements. Also forming such infinite elements is relatively inefficient and complex so that usage of this method is relatively limited.

A somewhat better group of methods, are called "ballooning" and its variants. Ballooning was invented by Silvester¹³ for modeling the Laplacian problems of the open type. It also employs a picture frame to limit the size of the finite element mesh; however, in this case the exterior boundary is modeled by using uniform layers of finite elements on the outside. Unfortunately, this method has deficiencies as well: first the algorithm is not efficient when applied to the wave equation; second the field values outside the picture frame can not be obtained easily. Dasgupta¹⁴ extended the ballooning algorithm into the cloning algorithm. In cloning, the formulation has led to a quadratic matrix equation. The unknown relates to the desired matrix pertaining to the infinite or semi-infinite region. The major contribution of the cloning method is that no analytical expressions are required to supply the Sommerfeld radiation condition. But in order to obtain the unknown matrix, a set of quadratic eigenvalue problems has to be solved. More recently, a method called "infinitesimal scaling" has been proposed by Hurwitz^{15,16,17}. The infinitesimal scaling method seeks to determine the coefficient matrix which expresses the contribution of an element to the global functional in terms of the solution values on the boundary nodes by using a scaling concept analogous to that used in ballooning, but in the limit that the size of the boundary layer element approaches zero. By taking this limit, a nonlinear first-order differential equation for the coefficient matrix is obtained. The price that is paid is the need to solve the a nonlinear matrix differential equation.

1.3. THE NEW PICTURE FRAME PROCEDURES

In this appendix we develop two new picture frame techniques. However, we limit the shape of the boundary between the picture frame and the open region to be simple; as circle in the cylindrical scattering problems and lines in the waveguide junctions. By using the triangular finite element method to solve the fields interior to the simple shaped picture frame, a simple, efficient and stable algorithm for numerical calculations is produced. We shall call the two new coupling schemes described in this report the "Two-boundary" approach and the "Transfinite elements" approach.

The idea behind the "Two-boundary" approach is derived from the modal analysis technique in which the finite element method and the superposition theorem are used to calculate the fields. First the modal analysis technique is used to get the analytical expressions for the fields in the

region exterior to the picture frame. Second, a number of boundary value problems in the picture frame are set up and solved by the finite element method. In this step, finite element solutions provide an expression for the numerical solutions. Finally, we require that the analytical solution and the numerical solution match along the second boundary. The detailed description of the "Two-boundary" approach will be covered in Section 3. It's application to the waveguide junction problems as well as the results are in Section 4, and its application to open 2-D scattering problems is given in Section 5.

For the "Transfinite elements," we construct basis functions outside the picture frame in such a way so as to convert the integral of the functional for the whole region into a integral over just the picture frame plus a boundary integral. Applying the variational principle then provides a matrix equation to be solved for the scattering solution. Section 6 presents the application of the "Transfinite elements" method to model simple electrostatic problems. The application to the 2-D scattering problems is investigated in Section 7.

SECTION 2 INTRODUCTION TO THE FINITE ELEMENT METHOD

The basic concept of finite element analysis consists of three parts :

1. Interpolation: Distributed physical qualities may be approximated by using linear combination of interpolating functions.
2. Mesh generation: A complicated physical shape may be subdivided into many subregions, and the integrals of distributed functions over the whole region may be broken into summations of the integral over the subregion.
3. Variational principles: For each problem, derive a corresponding functional either by using Galerkin's method or by using the Rayleigh-Ritz method. Then apply the variational procedure to the functional to derive a matrix equation.

2.1. VARIATIONAL PRINCIPLES

The finite element method is based on variational principles developed for the most part in the last century. Variational principles for electromagnetic field problems can be derived from two alternative points of view, namely, the Galerkin's method and the Rayleigh-Ritz method.

Consider the following two dimensional Helmholtz equation

$$\begin{aligned} \nabla^2 \psi + k^2 \psi &= \rho(x,y) && \text{in } \Omega \\ \psi &= 0 && \text{on } \Gamma \end{aligned} \tag{2.1}$$

involving what may be assumed to be a scalar potential variable ψ . The quantity k^2 is a constant invariant with position, whilst ρ is a given forcing function over the problem region Ω , and Γ is the boundary of Ω . For simplicity, we only consider the case of Dirichlet boundary conditions here.

2.1.1. GALERKIN'S METHOD

The steps in Galerkin's method to solve (2.1) are as follows¹⁸:

1. Find a complete function space Λ_u to be called the "trial function space". Any function $u \in \Lambda_u$ must satisfy the Dirichlet boundary conditions on Γ . The trial function space Λ_u will be used to write the numerical approximation of ψ of (2.1) in the form

$$\psi = \sum_{i=1}^N \psi_i \alpha_i(x, y) \quad (2.2)$$

where N is the dimension of Λ_u , the ψ_i 's are the unknown coefficients and $\alpha_i(x, y)$'s are the basis functions of Λ_u .

2. For every trial function u in the trial function space Λ_u , define a residual function $f_u(x, y)$

$$f_u(x, y) = \nabla^2 u(x, y) + k^2 u(x, y) - \rho(x, y) \quad (2.3)$$

3. Construct another function space Λ_v to be called the "testing function space". Any function in Λ_v will be called a testing function and will be used to weight the residual function $f_u(x, y)$ defined in (2.3). Although, Λ_v doesn't have to be the same as Λ_u , often it is convenient to have $\Lambda_u = \Lambda_v$.
4. Assign to each pair (v, u) , $v \in \Lambda_v$ and $u \in \Lambda_u$, a scalar number according to the bilinear form $B(v, u)$

$$B(v, u) = - \int_{\Omega} v(x, y) f_u(x, y) d\Omega \quad (2.4)$$

By Green's theorem $B(v, u)$ can be written as

$$B(v, u) = \int_{\Omega} \nabla v \cdot \nabla u d\Omega - k^2 \int_{\Omega} v u d\Omega + \int_{\Omega} v \rho d\Omega - \int_{\Gamma} v \frac{\partial u}{\partial n} d\Gamma \quad (2.5)$$

Because for any testing function $v \in \Lambda_v$, $v = 0$ on Γ , this simplifies to

$$B(v, u) = \int_{\Omega} \nabla v \cdot \nabla u d\Omega - k^2 \int_{\Omega} v u d\Omega + \int_{\Omega} v \rho d\Omega \quad (2.6)$$

5. The problem of finding the solution of (2.1) is thus converted into the following

$$\begin{aligned} &\text{Find } \psi \in \Lambda_u \text{ such that} \\ &B(v, \psi) = 0 \quad \text{for } \forall v \in \Lambda_v \end{aligned} \quad (2.7)$$

This solution is called a "weak solution" because the solution of (2.7) will be the solution of (2.1) only in an approximate sense.

6. Write

$$\psi = \sum_{i=1}^N \psi_i \alpha_i(x, y) \quad v = \sum_{j=1}^M v_j \beta_j(x, y) \quad (2.8)$$

where M is the dimension of Λ_v , and the $\beta_j(x, y)$'s are basis functions of Λ_v . Then

$$B(v, \psi) = \sum_{j=1}^M \sum_{i=1}^N v_j \left\{ \int_{\Omega} \nabla \beta_j \cdot \nabla \alpha_i - k^2 \beta_j \alpha_i d\Omega \right\} \psi_i + \sum_{j=1}^M v_j \int_{\Omega} \beta_j \rho d\Omega$$

7. Because $B(v, \psi) = 0$ for $\forall v \in \Lambda_v$, we have

$$\sum_{i=1}^N \left\{ \int_{\Omega} (\nabla \beta_j \cdot \nabla \alpha_i - k^2 \beta_j \alpha_i) d\Omega \right\} \psi_i + \int_{\Omega} \beta_j \rho d\Omega = 0 \quad j = 1, \dots, M \quad (2.9)$$

8. Usually, $\Lambda_u = \Lambda_v$, then (2.9) can be written in the matrix form

$$(S - k^2 T) \tilde{\Psi} = \tilde{f} \quad (2.10)$$

where

$\tilde{\Psi}$ is the column vector of the coefficients ψ_i

S, T are matrices with $S_{ij} = \int_{\Omega} \nabla \alpha_j \cdot \nabla \alpha_i d\Omega$

$$T_{ij} = \int_{\Omega} \alpha_j \alpha_i d\Omega$$

and \tilde{f} is a column vector with $f_i = - \int_{\Omega} \alpha_i \rho d\Omega$

Galerkin's method is analyzed in detail in reference¹⁸.

2.1.2. RAYLEIGH-RITZ METHOD

The Rayleigh-Ritz method is more complicated than Galerkin's method because it is not derived directly from the differential equation. Rather, one first forms a functional from the stored energy in the system; minimizing the functional over the set of approximating functions then gives the approximate solution. The concepts embedded in the Rayleigh-Ritz method can be explained in the following steps.

1. The energy functional $F(\psi)$ corresponds to equation (2.1) is

$$\begin{aligned}
 F(\Psi) &= \langle \Psi, \rho \rangle + \langle \rho, \Psi \rangle - \langle \Psi, \nabla^2 \Psi \rangle - k^2 \langle \Psi, \Psi \rangle \\
 &= \int_{\Omega} \Psi \rho \, d\Omega + \int_{\Omega} \rho \Psi \, d\Omega - \int_{\Omega} \Psi \nabla^2 \Psi \, d\Omega - k^2 \int_{\Omega} \Psi \Psi \, d\Omega
 \end{aligned} \tag{2.11}$$

where the inner product $\langle u, v \rangle$ is defined as

$$\langle u, v \rangle = \int_{\Omega} u v \, d\Omega$$

Again, by Green's theorem and applying the same boundary conditions as in the Galerkin's method

$$F(\Psi) = \int_{\Omega} \Psi \rho \, d\Omega + \int_{\Omega} \rho \Psi \, d\Omega + \int_{\Omega} \nabla \Psi \cdot \nabla \Psi \, d\Omega - k^2 \int_{\Omega} \Psi \Psi \, d\Omega \tag{2.12}$$

2. Since we are interested in variations in $F(\Psi)$ about the solution point, we may begin by writing the arbitrary function Ψ as a sum of the true solution ψ and a second arbitrary function ξ multiplied by a scalar ϵ , $\Psi = \psi + \epsilon \xi$. The first variation of $F(\Psi)$ about the solution ψ is given by

$$\delta F(\Psi) |_{\Psi=\psi} = \frac{\partial F}{\partial \epsilon} |_{\epsilon=0}$$

which gives

$$\delta F(\Psi) |_{\Psi=\psi} = 2 \int_{\Omega} \xi \rho \, d\Omega + 2 \int_{\Omega} \nabla \xi \cdot \nabla \psi \, d\Omega - k^2 \int_{\Omega} \xi \psi \, d\Omega$$

by Green's theorem

$$\delta F(\Psi) |_{\Psi=\psi} = -2 \int_{\Omega} \xi (\nabla^2 \psi + k^2 \psi - \rho) \, d\Omega$$

Since ψ is the solution of equation (2.1), the first variation of $F(\Psi)$ about the solution is zero. Thus the energy functional $F(\Psi)$ is stationary about the true solution ψ .

3. If the energy functional $F(\Psi)$ is stationary about a function ϕ , i.e.

$$\Psi = \phi + \epsilon \xi$$

$$\delta F(\Psi) |_{\Psi=\phi} = \frac{\partial F}{\partial \epsilon} |_{\epsilon=0} = 0$$

which gives

$$\delta F(\Psi) |_{\Psi=\phi} = -2 \int_{\Omega} \xi (\nabla^2 \phi + k^2 \phi - \rho) \, d\Omega = 0$$

Since ξ is an arbitrary function, we have $\nabla^2 \phi + k^2 \phi - \rho = 0$. So, the function ϕ will also be the solution of (2.1).

4. Approximating ψ by a linear combination of interpolation functions α .

$$\psi = \sum_{i=1}^N \psi_i \alpha_i(x, y) \quad (2.13)$$

gives the energy functional as

$$F(\psi) = 2 \sum_{i=1}^N \psi_i \int_{\Omega} \alpha_i \rho \, d\Omega + \sum_{i=1}^N \sum_{j=1}^N \psi_i \left\{ \int_{\Omega} \nabla \alpha_i \cdot \nabla \alpha_j - k^2 \alpha_i \alpha_j \, d\Omega \right\} \psi_j$$

5. Setting the first variation of $F(\psi)$ to zero in order to find the stationary point, then results in

$$\sum_{j=1}^N \left\{ \int_{\Omega} \nabla \alpha_i \cdot \nabla \alpha_j - k^2 \alpha_i \alpha_j \right\} d\Omega \psi_j + \int_{\Omega} \alpha_i \rho \, d\Omega = 0$$

$i = 1, \dots, N$

This matrix equation then is the same as the one in (2.10)

The details of the Rayleigh-Ritz method can be found in reference¹⁹.

2.2. MESH GENERATION

The finite element method involves breaking the problem region into mesh of small subregions. Each subregion is called an element.

The mesh can be made in any number of ways. One common method is to use a square or rectangular grid with uniform sized elements. The method that has been used in this thesis employs triangular elements of varying sizes. One advantage of triangular grids is their great flexibility in fitting the geometry of different problems. Also when combined with the Lagrange interpolation polynomials, to be discussed in the next section, the integration over the elements can be performed analytically¹⁹. The algorithm used to generate the triangular mesh is the Delaunay triangulation procedure developed earlier at CMU²⁰. Use of the Delaunay algorithm guarantees that the triangulation has a maximum sum of the smallest angles of the triangles.

2.2.1 DELAUNAY ALGORITHM

For an arbitrary set of points, a geometric structure called Voronoi polygons is defined by the regions where every point within a polygon is closer to that point than to any other. The intersection of three or more Voronoi polygons is called a vertex. This vertex is by definition equidistant from the three or more original points associated with the polygons that formed the vertex. The Delaunay triangulation of the system is formed by forming triangles from the three original points associated with each vertex.

One property of the Delaunay triangulation is that the circumcircle of a Delaunay triangle may not contain a fourth Delaunay vertex. This property is the basis of the swapping algorithm²¹ for Delaunay triangulation which leads itself readily to finite element applications. An arbitrary triangulation is formed from the original points. For each triangle, the neighboring point associated with each of the adjacent triangles is checked. If any of those points is within the circumcircle of the first triangle, the diagonal is swapped. See Figure 2-1.

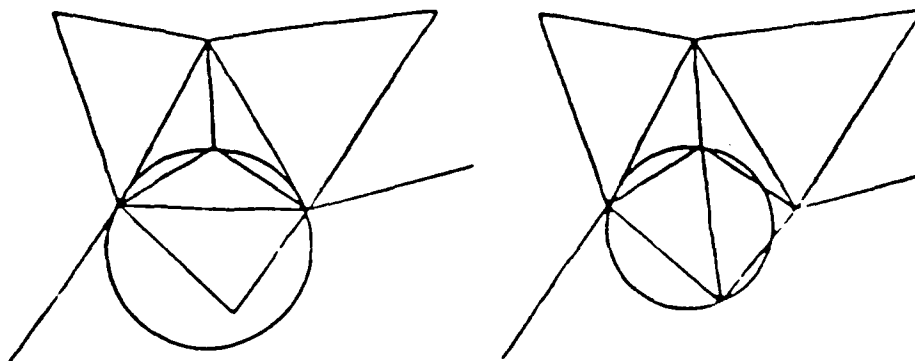


Figure 2-1: Swapping a diagonal

In the event that a diagonal is swapped, it is necessary to check the new triangles again for additional swaps. This procedure is repeated until no more swaps are necessary.

2.3. INTERPOLATION FUNCTIONS

The family of polynomials is one of the simplest class of functions to employ as interpolation functions and were the first to be applied in the finite element method. In this thesis, we only consider the most common interpolation polynomials used in the finite element method, namely the Lagrange interpolation polynomials.

If $\alpha_i(x,y)$ is the Lagrange interpolation polynomial associated with point (x_i, y_i) , then we have by definition

$$\alpha_i(x_j, y_j) = \begin{cases} 0 & \text{if } j \neq i \\ 1 & \text{if } j = i \end{cases} \quad (2.14)$$

Equation (2.14) leads to the following physical interpretation of the coefficients in (2.13)

$$\psi(x_j, y_j) = \sum_{i=1}^N \psi_i \alpha_i(x_j, y_j) = \psi_j$$

so that the coefficient ψ_j is also the function value at node (x_j, y_j) .

In this thesis, we use second order triangular elements. For each triangle, there are six nodes and six quadratic Lagrange interpolation polynomials. Inside each triangle, we interpolate the function ψ by these six interpolation polynomials as

$$\psi(x, y) = \sum_{i=1}^6 \psi_i \alpha_i(x, y)$$

To derive the interpolation polynomials, it is convenient to introduce "homogeneous coordinates" on the triangle.

2.3.1. HOMOGENEOUS COORDINATES

Consider an arbitrary triangle with vertices numbered (1,2,3) and vertex coordinates (x_1, y_1) , (x_2, y_2) , (x_3, y_3) as indicated in Figure 2-2, and let P be a point located within this triangle.

The coordinates (x, y) of the point P may be written in a symmetric form with respect to the triangle (1,2,3) by defining a new type of coordinate system called homogeneous coordinates in the triangle. These homogeneous coordinates are defined as follows: Let d_1 be the distance of the point P from the base 2-3 of the triangle, h_1 be the corresponding altitude, and ζ_1 the ratio

$$\zeta_1 = \frac{d_1}{h_1}$$

The quantity ζ_1 is called a homogeneous coordinate for the point P because its range is from 0 to 1 for any point within the triangle (1,2,3).

In the same way, homogeneous coordinates ζ_2 and ζ_3 ranging from 0 on the other two sides to 1 at vertices 2 and 3 are defined by the equation

$$\zeta_m = \frac{d_m}{h_m}, \quad m = 1, 2, 3$$

In this equation, d_m and h_m are defined analogously to d_1 and h_1 .

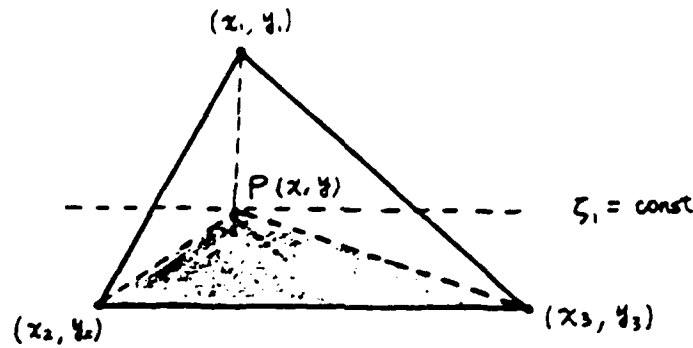


Figure 2-2: A typical triangle with vertices numbered (1,2,3). d_1 is the distance of the point P from the base and h_1 is the triangle altitude. The triangle (1,2,3) is divided into three by the point P.

The homogeneous coordinates ζ_m are also called triangle area coordinates for the following reason: The area of a triangle is one-half its base times its height. Accordingly, the ratio of the area A_{p23} of the triangle (P,2,3) to the area A_{123} of the triangle (1,2,3) is

$$\frac{A_{p23}}{A_{123}} = \frac{d_1}{h_1} = \zeta_1$$

Consequently, the homogeneous coordinate ζ_1 represents not only the ratio of the distance d_1 to the altitude h_1 , but also the ratio of the area of the shaded triangle (P,2,3) in Figure 2-2 to the area of the original triangle (1,2,3).

The three homogeneous coordinates $\zeta_1, \zeta_2, \zeta_3$ cannot be independent, since only two linearly independent coordinates can exist on a plane. The relationship between the $\{\zeta_m\}$ is revealed by examining the properties of the triangles in Figure 2-2 where (1,2,3) represents the original triangle and the remaining three triangles are composed of the lines connecting the point P with vertices 1, 2, and 3. The area A_{123} of the original triangle

$$A_{p23} + A_{1p3} + A_{12p} = A_{123}$$

Dividing both side of this equation by A_{123} yields

$$\zeta_1 + \zeta_2 + \zeta_3 = 1$$

Thus, the sum of the triangle area coordinates is equal to unity.²²

2.3.2. INTERPOLATION ON TRIANGLES

Now, consider the problem of defining quadratic interpolation polynomials on the triangles. Since three point values are required to define a quadratic polynomial, quadratic interpolation polynomials must have three interpolation nodes on each side, see Figure 2-3.

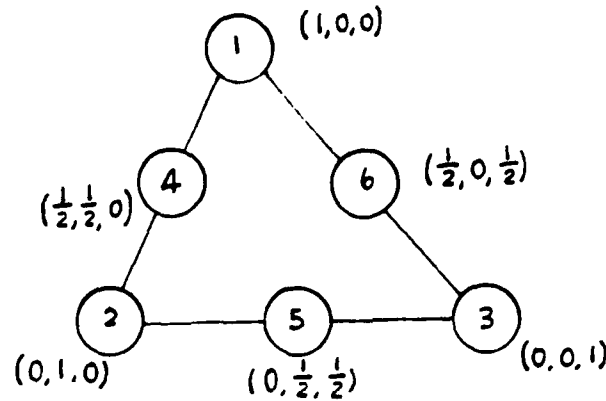


Figure 2-3: Node ordering for a second order triangular element

The polynomial

$$\alpha_1(x,y) = 2\zeta_1(\zeta_1 - \frac{1}{2})$$

$\alpha_1(x,y)$ is zero along the lines $\zeta_1 = 0$ and $\zeta_1 = 1/2$ and it is one at ζ_1 . It follows that $\alpha_1(x,y)$ equals zero at the five points $(\zeta_1, \zeta_2, \zeta_3) = (1/2, 1/2, 0), (1/2, 0, 1/2), (0, 1, 0), (0, 1/2, 1/2), (0, 0, 1)$ and is equal to one at the vertex point number 1. Second-order polynomials which interpolate to 1 at the other two triangle vertices are defined similarly.

To form a polynomial which interpolates to one at the center of side 1-2, we need to define a polynomial which is zero along side 1-3 and 2-3 and has a unit value at the point $(1/2, 1/2, 0)$. The polynomial

$$\alpha_4(x,y) = 4\zeta_1\zeta_2$$

provides these properties. Polynomials which interpolate at the remaining two midside nodes are defined similarly.²²

SECTION 3 THE TWO-BOUNDARY APPROACH

As is implied by the name, two-boundary method for solving open field problems requires two surfaces to be defined in the solution process. Because two boundary surfaces are used, space is divided into three parts by this algorithm. Figure 3-1 shows a portion of the infinite x-y plane in Cartesian coordinates. A bounded region called R_1 is defined so as to contain all sources, inhomogeneities, and anisotropies. The boundary of R_1 is called Γ_1 , and another larger boundary Γ_2 is placed around Γ_1 . The region in between Γ_1 and Γ_2 is called R_2 , and the region exterior to Γ_2 is called R_e . The region enclosed by Γ_2 , i.e. $R_1 \oplus R_2$, will be the region where the finite element method is used, which is then called the "finite element solution region".

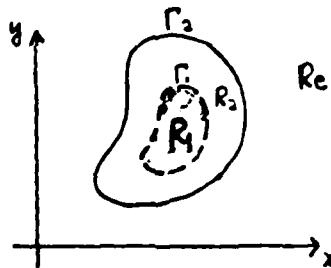


Figure 3-1: Separation of the problem region

3.1. MODAL ANALYSIS

Since the region exterior to R_1 , i.e. $R_2 \oplus R_e$, is homogeneous and source free, homogeneous solutions of the Helmholtz equation can be found by using the method of separation of variables technique. In the region $R_2 \oplus R_e$, the analytical expression for the fields Ψ can be approximated by M modes as

$$\Psi(x,y) = \sum_{i=1}^M a_i \gamma_i(x,y) \quad (3.1)$$

where a_i 's are the coefficients that need to be determined and the $\gamma_i(x,y)$ represent the analytical solution for mode i in the system.

Since equation (3.1) is valid for the region $R_2 \oplus R_e$, it also holds for the fields on the boundary Γ_2 ,

$$\psi|_{\Gamma_2} = \sum_{i=1}^M a_i \gamma_i(x,y)|_{\Gamma_2} \quad (3.2)$$

This leads to the following boundary value problem for the fields in $R_1 \oplus R_2$

$$\begin{aligned} (\nabla^2 + k^2) \psi &= 0 & \text{in } R_1 \oplus R_2 \\ \psi &= \sum_{i=1}^M a_i \gamma_i(x,y)|_{\Gamma_2} & \text{on } \Gamma_2 \end{aligned} \quad (3.3)$$

Equation (3.3) is not a solvable boundary value problem, because the boundary conditions depend on the coefficients a_i 's which are not known yet.

We may use the superposition theorem to decompose equation (3.3) into M boundary value problems corresponding to the modes $\gamma_i(x,y)$. The fields pattern for each mode γ_i is designated λ_i and can be obtained by using the standard finite element method to solve for the fields in region $R_1 \oplus R_2$ with the boundary conditions $\lambda_i(x,y) = \gamma_i(x,y)|_{\Gamma_2}$ on Γ_2 .

Once all the $\lambda_i(x,y)$'s are determined, the fields ψ inside the region $R_1 \oplus R_2$ can be expressed in terms of the unknown coefficients a_i 's

$$\psi(x,y) = \sum_{i=1}^M a_i \lambda_i(x,y) \quad \text{for } (x,y) \in R_1 \oplus R_2 \quad (3.4)$$

3.2. MATCHING

Although, we have not yet solved the fields, the only problem remaining is to determine the M coefficients a_i 's.

Notice that we have two expressions for the solution, one is equation (3.1) which is valid in region $R_2 \oplus R_e$, and the other is equation (3.4) which is valid in region $R_1 \oplus R_2$. It follows that both solutions are valid in the common region R_2 and that they should have same values on the boundary Γ_1 .

Matching the modes obtained from these two solutions on the boundary Γ_1 , either by the

weighted residue method or the least square method, results in a matrix equation which can be solved for the coefficients a_i 's. Once the coefficients a_i 's are known, the fields values at any point can be calculated either by using equation (3.1) or by using equation (3.4). Details of the calculations are presented in Sections 4 and 5.

SECTION 4 TWO BOUNDARY APPROACH IN RECTANGULAR WAVEGUIDE DISCONTINUITIES

4.1. THE NATURE OF THE PROBLEM

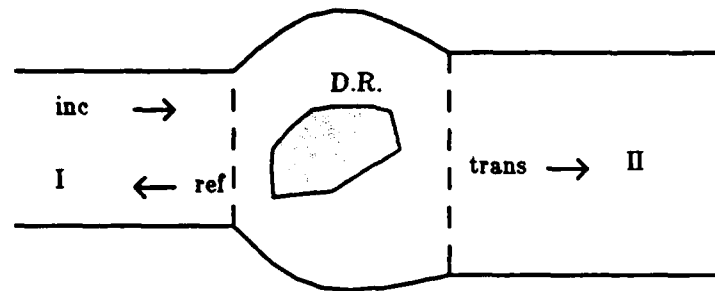


Figure 4-1: A general two-port rectangular waveguide discontinuity

A microwave network with an arbitrary discontinuity and two rectangular waveguide ports is pictured in Figure 4-1. The discontinuity may be an arbitrary discontinuity in a single guide or the coupling between two different guides. Many filters, matching sections, phase-correction units, and other components can be represented by this structure.

Figure 4-1 consists of three parts: rectangular waveguide I on the left, rectangular waveguide II on the right and the region between them called the discontinuity region (D.R.). Note that guides I and II need not be colinear and the discontinuity region can be of arbitrary shape and may contain dielectric objects or even metal objects; however the overall structure must be uniform (ie. have constant cross section) in one direction (either the "broad" or "narrow" transverse direction). This requirement simplifies the resulting boundary value problem to two-dimensions.

If a transverse plane wave is incident from left, then there will be a reflected wave in guide I and a transmitted wave in guide II and evanescent modes in both. The polarization of the waves

in the structure provides two fundamental kinds of waveguide discontinuities: H-plane discontinuities in which the H field is in the plane of the discontinuity and E-plane discontinuities where the E field is in the plane of the discontinuity.

4.2. FORMULATION OF THE TWO BOUNDARY APPROACH

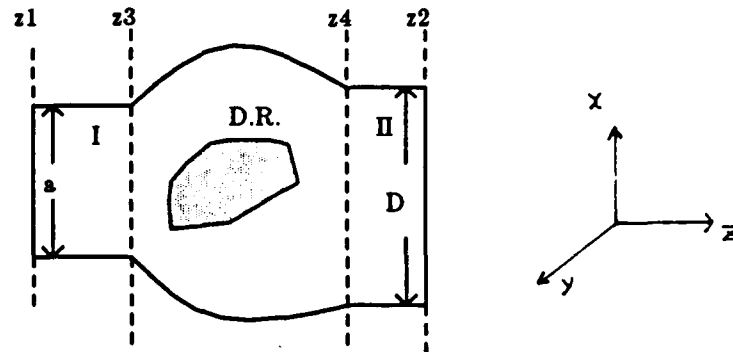


Figure 4-2: Finite Element Solution Region

Assume that the discontinuity in Figure 4-1 is on the x - z plane and that the dimensions of the guides are such that only the dominant mode can propagate in each guide. Because the formulation is similar for H-plane discontinuities and E-plane discontinuities, only the H-plane discontinuity formulation is presented here. In Figure 4-2, we have placed the boundary planes $z=z_1$ and $z=z_2$ to form the "finite element solution region" as discussed in Chapter 3. The finite element solution region must enclose the discontinuity region in the waveguide. Also shown in Figure 4-2 are planes $z=z_3$ and $z=z_4$ which served as the matching boundaries. For an H-plane discontinuity, with an incident wave H_{10} from the left, the incident electric field E_{inc} has only a y component and can be expressed as

$$E_{inc} = \sin\left(\frac{\pi x}{a}\right) \exp(-j\beta^I z), \quad \beta^I = \sqrt{k^2 - \left(\frac{\pi}{a}\right)^2} \quad (4.1)$$

where k is the wavenumber and β^I is the propagation constant in guide I.

The modes for the region exterior to the finite element solution region are:

$$\gamma_i^I(x, z) = \sin\left(\frac{i\pi x}{a}\right) \cdot \exp(\alpha_i^I z) \quad \text{in guide I.}$$

$$\gamma_i^{II}(x, z) = \sin\left(\frac{i\pi x}{D}\right) \cdot \exp(\alpha_i^{II} z) \quad \text{in guide II.}$$

where

$$\alpha_i^I = \left\{ \left(\frac{i\pi}{a}\right)^2 - k^2 \right\}^{1/2} \quad \text{and} \quad \alpha_i^{II} = \left\{ \left(\frac{i\pi}{D}\right)^2 - k^2 \right\}^{1/2} \quad (4.2)$$

$$i = 1, \dots$$

The modes γ_i^I represent the reflected wave modes in the waveguide I, and γ_i^{II} are the transmitted wave modes in waveguide II. Set

$$\begin{aligned} \psi_i^I(x) &= \sin\left(\frac{i\pi x}{a}\right) & \psi_i^I(z) &= \exp(\alpha_i^I z) \\ \text{and} \\ \psi_i^{II}(x) &= \sin\left(\frac{i\pi x}{D}\right) & \psi_i^{II}(z) &= \exp(\alpha_i^{II} z) \end{aligned} \quad (4.3)$$

Then the modes can be written as the product of two functions, one depends only on x and the other depends only on z .

$$\begin{aligned} \gamma_i^I(x, z) &= \psi_i^I(x) \cdot \psi_i^I(z) \\ \text{and} \\ \gamma_i^{II}(x, z) &= \psi_i^{II}(x) \cdot \psi_i^{II}(z) \end{aligned} \quad (4.4)$$

Combining equations (4.1) – (4.3) gives the analytical expression for the fields inside guides I and II as

$$\begin{aligned} E^I(x, z) &= \psi_1^I(x) \cdot \left\{ \exp(-j\beta^I z) + R_1 \psi_1^I(z) \right\} + \sum_{i=2}^N R_i \psi_i^I(x) \psi_i^I(z) \quad z \leq z_3 \\ \text{and} \\ E^{II}(x, z) &= \sum_{i=1}^M T_i \psi_i^{II}(x) \psi_i^{II}(z) \quad z \geq z_4 \end{aligned} \quad (4.5)$$

Here the R_i and T_i are the reflection and transmission coefficients for each mode, N is the number of modes used in guide I and M is the number of modes used in guide II.

From the discussion in Chapter 3, two set of fields patterns λ_i^I and λ_i^{II} within the finite element solution region are obtained. Both solve the Helmholtz equation in the finite element solution region, but with different boundary conditions on planes $z = z_1$, $z = z_2$. The boundary conditions for λ_i^I are $\lambda_i^I(x, z_1) = \psi_i^I(x)$ and $\lambda_i^I(x, z_2) = 0$, and for λ_i^{II} , $\lambda_i^{II}(x, z_1) = 0$ and $\lambda_i^{II}(x, z_2) = \psi_i^{II}(x)$. It follows that the numerical solution in the finite element solution region may be written as

$$\tilde{E} = \{ \exp(-j\beta^I z_1) + R_1 \psi_1^I(z_1) \} \lambda_1^I + \sum_{i=2}^N R_i \psi_i^I(z_1) \lambda_i^I + \sum_{i=1}^M T_i \psi_i^{II}(z_2) \lambda_i^{II} \quad (4.6)$$

Now, we introduce two inner products for complex valued functions one on the plane $z = z_3$, the other on the plane $z = z_4$, as

$$\begin{aligned} \langle u(x), v(x) \rangle_I &= \int_0^a v^*(x) u(x) dx \\ \text{and} \\ \langle u(x), v(x) \rangle_{II} &= \int_0^D v^*(x) u(x) dx \end{aligned} \quad (4.7)$$

where $*$ represents the complex conjugate. Since both equations (4.5) and (4.6) hold in the region $z_3 \geq z \geq z_1$ and $z_2 \geq z \geq z_4$, which then give the following equations need to be solved for the coefficients R_i and T_i .

$$\begin{aligned} \langle \tilde{E}(x, z_3), \psi_i^I(x) \rangle_I &= \langle E^I(x, z_3), \psi_i^I(x) \rangle_I \quad i = 1 \dots N \\ \text{and} \\ \langle \tilde{E}(x, z_4), \psi_i^{II}(x) \rangle_{II} &= \langle E^{II}(x, z_4), \psi_i^{II}(x) \rangle_{II} \quad i = 1 \dots M \end{aligned} \quad (4.8)$$

Finally, substitute equation (4.5) and (4.6) into (4.8) results in the $(N+M)$ times $(N+M)$ complex matrix equation

$$\left\{ \begin{bmatrix} A_{11} & \dots & A_{1N} & B_{11} & \dots & B_{1M} \\ \vdots & & \vdots & \vdots & & \vdots \\ A_{N1} & \dots & A_{NN} & B_{N1} & \dots & B_{NM} \\ \vdots & & \vdots & \vdots & & \vdots \\ C_{11} & \dots & C_{1N} & D_{11} & \dots & D_{1M} \\ \vdots & & \vdots & \vdots & & \vdots \\ C_{M1} & \dots & C_{MN} & D_{M1} & \dots & D_{MM} \end{bmatrix} \begin{bmatrix} \psi_1^I(z_2) & 0 & & 0 \\ 0 & \psi_N^I(z_1) & & 0 \\ \vdots & \vdots & \ddots & \vdots \\ 0 & 0 & & \psi_M^{II}(z_4) \end{bmatrix} \begin{bmatrix} \psi_1^I(z_1) \frac{a}{2} & 0 & & 0 \\ 0 & \psi_N^I(z_1) \frac{a}{2} & & 0 \\ \vdots & \vdots & \ddots & \vdots \\ 0 & 0 & & \psi_M^{II}(z_2) \frac{D}{2} \end{bmatrix} \begin{bmatrix} R_1 \\ \vdots \\ R_N \\ T_1 \\ \vdots \\ T_M \end{bmatrix} = \begin{bmatrix} -\exp(-j\beta^I z_3) A_{11} \\ + \exp(-j\beta^I z_1) \frac{a}{2} \\ \vdots \\ -\exp(-j\beta^I z_3) A_{M1} \\ -\exp(-j\beta^I z_3) C_{11} \\ \vdots \\ -\exp(-j\beta^I z_3) C_{M1} \end{bmatrix} \quad (4.9)$$

where

$$\begin{aligned} A_{ji} &= \langle \lambda_i^I(x, z_3), \psi_j^I(x) \rangle_I & B_{ji} &= \langle \lambda_i^{II}(x, z_3), \psi_j^I(x) \rangle_I \\ C_{ji} &= \langle \lambda_i^I(x, z_4), \psi_j^{II}(x) \rangle_{II} & D_{ji} &= \langle \lambda_i^{II}(x, z_4), \psi_j^{II}(x) \rangle_{II} \end{aligned}$$

4.3. NUMERICAL RESULTS AND COMPARISON

A number of waveguide discontinuity problems have been studied and the results from this analysis will be compared with that obtained from other theories and from experimental data. The results here employ three modes on both sides for matching. Our experience indicates that evanescent modes die out very quickly so that even if a small finite element solution region is used "three modes matching" still provides good results.

4.3.1. H-PLANE STEP AND E-PLANE STEP

Figure 4-3 shows a rectangular waveguide of width " a " joined symmetrically with a guide of width " D ". The discontinuity in this problem occurs in the H-plane. Figure 4-3 provides a comparison of our results with the approximate analytical solution of Lewin²³. For the discontinuity in the E-plane, the results from present method as well as those from Marcuvitz²⁴ are given in Figure 4-4.

4.3.2. THICK IRISES

Here we consider two types of irises in rectangular waveguides. Figure 4-5(a) and Figure 4-5(b) show the magnitude and phase angles of the reflection coefficient due to square inductive irises of various sizes. The agreement between the results computed here and that obtained by Davies⁵ is within a few percent. Figure 4-6(a) and Figure 4-6(b) show the real and imaginary parts of the E field contour lines for $\delta/a = 0.2$, $a/\lambda = 0.7$.

Figure 4-7 compares the VSWR ratio calculated from present method with the analytic solutions from Kerns²⁵ for the single half-round inductive obstacle for $r/a = 0.2$.

4.3.3. WAVEGUIDE BENDINGS

The method we have developed may also be used to calculate the scattering of waves by waveguide bends. The structure of the waveguide bends we are considering is shown in Figure 4-8. In this figure, the planes " t " are reference planes for the parameters R and T . Table 4-1 gives a comparison of present theory and experimental data from Marcuvitz²⁴ for different bending angles.

4.3.4. DIELECTRIC LOADED WAVEGUIDE

Figure 4-9 presents a dielectric loaded waveguide problem. We have solved this problem and compared our results with the approximate solutions of Marcuvitz²⁴, who estimated the error in his approximation to be less than a few percent. This comparison is presented in Table 4-2.

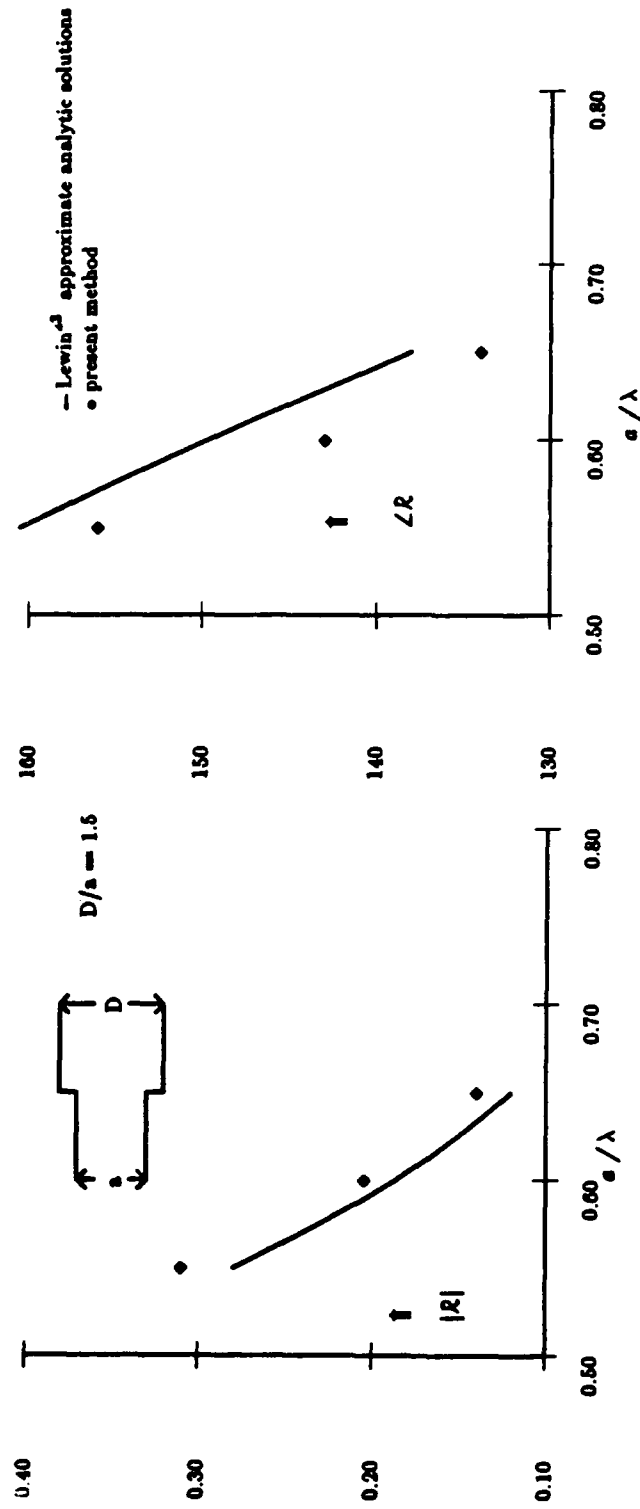


Figure 4-3: Magnitude and phase of reflection coefficient of H-plane step discontinuity

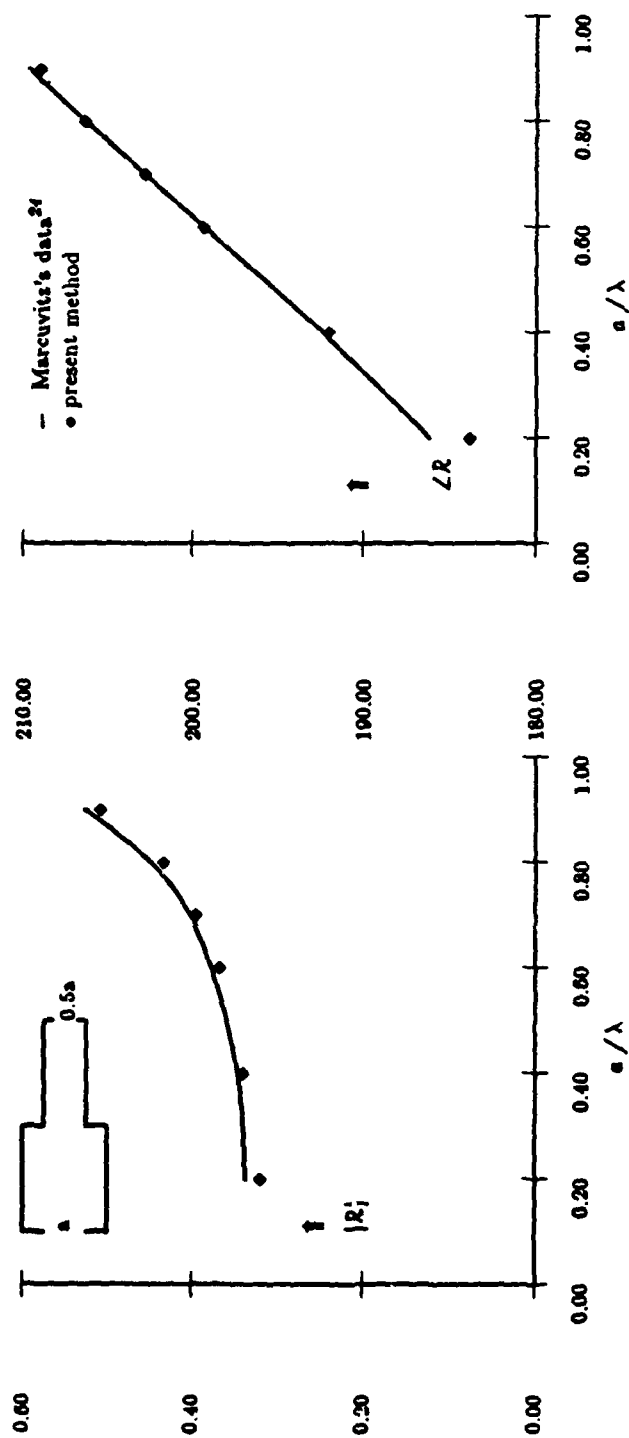


Figure 4-4: Magnitude and phase of reflection coefficient of E-plane step discontinuity

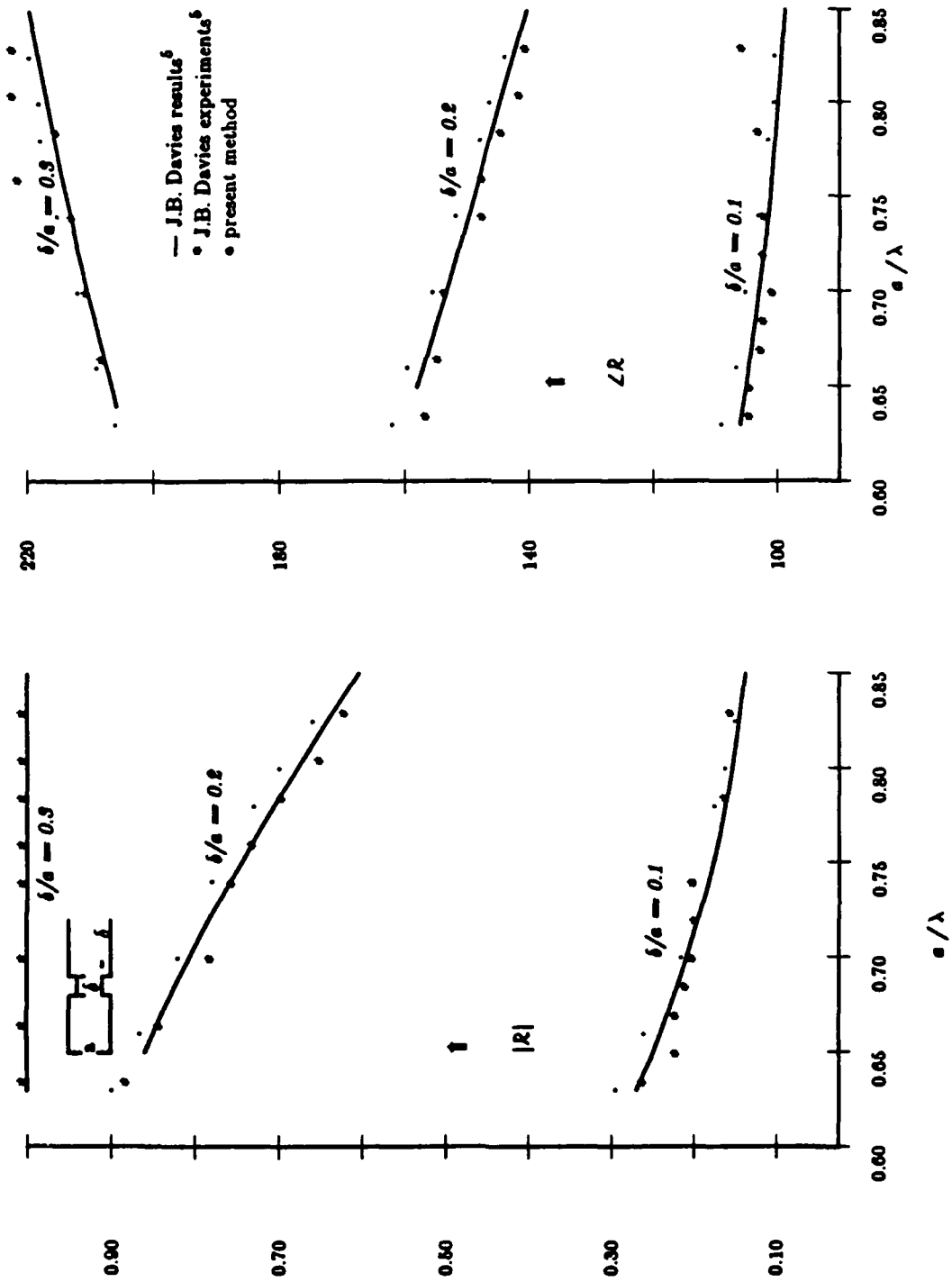
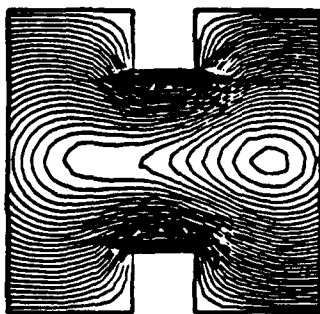
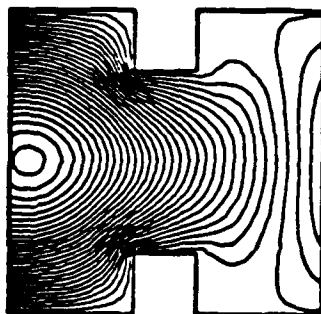


Figure 4-5: Magnitude and phase of reflection coefficient of square inductive irises (H-plane discontinuity)



(a) Real Part



(b) Imaginary part

Figure 4-6: (a) Real and (b) Imaginary parts of the E field contour lines for $\delta/a = 0.2$, $a/\lambda = 0.7$

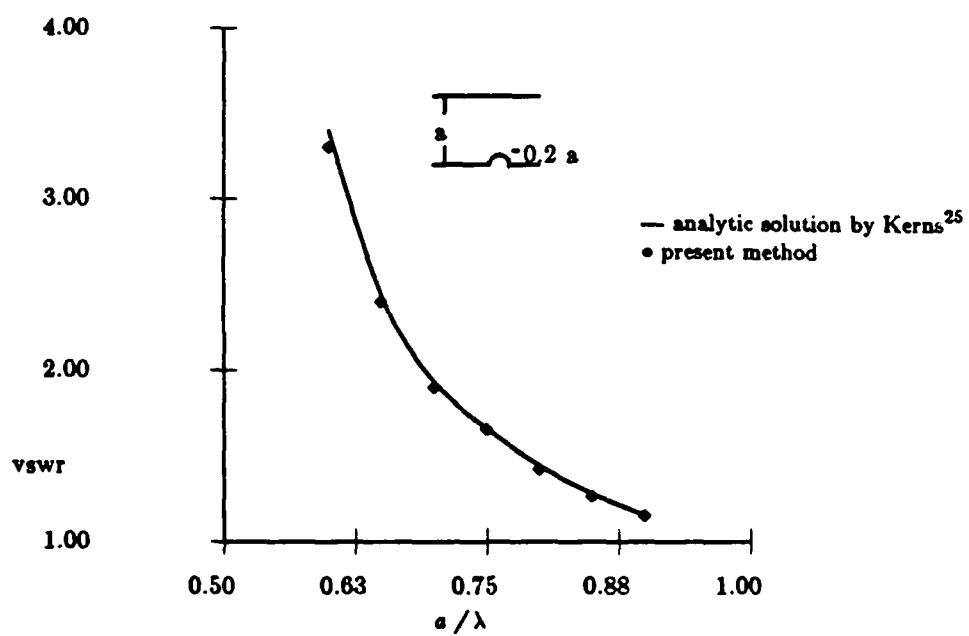


Figure 4-7: Single half-round inductive obstacle

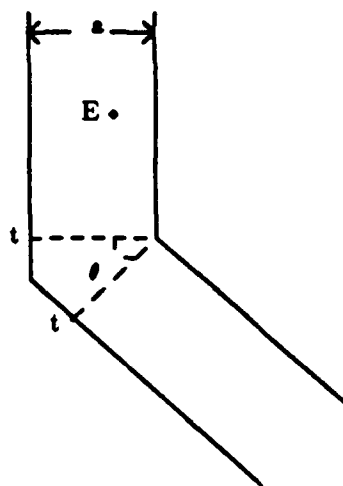


Figure 4-8: Waveguide bending

Table 4-1: The reflection and transmission coefficients R and T , relative to the reference planes t , were calculated by present method for H-plane corners with $\theta = 30^\circ$, $\theta = 60^\circ$, $\theta = 90^\circ$ and compared with experimental data from Marcuvitz²⁴.

| $\frac{\lambda}{a}$ | $\theta = 30$ | | $\theta = 60$ | | $\theta = 90$ | |
|---------------------|-----------------------|-----------------------|-----------------------|-----------------------|-----------------------|-----------------------|
| | experimental data | present method | experimental data | present method | experimental data | present method |
| 0.762 | $R = -0.028 - j0.02$ | $R = -0.029 - j0.022$ | $R = -0.139 + j0.057$ | $R = -0.144 + j0.054$ | $R = -0.053 + j0.417$ | $R = 0.041 + j0.430$ |
| | $T = 0.581 - j0.813$ | $T = 0.596 - j0.803$ | $T = -0.373 - j0.916$ | $T = -0.350 - j0.924$ | $T = -0.900 + j0.114$ | $T = -0.898 + j0.084$ |
| 0.7144 | $R = -0.030 - j0.027$ | $R = -0.028 - j0.026$ | $R = -0.154 + j0.024$ | $R = -0.153 + j0.021$ | $R = -0.115 + j0.365$ | $R = -0.128 + j0.366$ |
| | $T = 0.670 - j0.741$ | $T = 0.676 - j0.737$ | $T = -0.152 - j0.976$ | $T = -0.137 - j0.979$ | $T = -0.881 - j0.278$ | $T = -0.870 - j0.303$ |
| 0.6724 | $R = -0.028 - j0.031$ | $R = -0.027 - j0.030$ | $R = -0.161 - j0.006$ | $R = -0.161 - j0.009$ | $R = -0.226 + j0.296$ | $R = -0.236 + j0.292$ |
| | $T = 0.737 - j0.675$ | $T = 0.742 - j0.669$ | $T = 0.038 - j0.986$ | $T = 0.053 - j0.986$ | $T = -0.738 - j0.563$ | $T = -0.722 - j0.581$ |

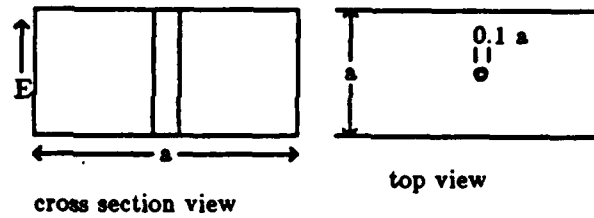


Figure 4-9: Dielectric post waveguide

Table 4-2: Dielectric post in rectangular guide (H_{10} mode) our results compared with the approximate analytic solutions calculated from the formula in Marcuvitz²⁴ for different dielectric constants. ($\lambda/a \approx 1.4$)

| ϵ_r | Approximate Analytic solution | Present method | |
|--------------|-------------------------------------|---------------------------|---------------------------|
| | | mesh 1 matrix size 146 | mesh 2 matrix size 269 |
| 4.0 | $R = -0.025 - j0.155$ | $R = -0.021 - j0.142$ | $R = -0.022 - j0.148$ |
| | $T = 0.974 - j0.157$ | $T = 0.982 - j0.130$ | $T = 0.977 - j0.149$ |
| 9.0 | $R = -0.191 - j0.391$ | $R = -0.172 - j0.379$ | $R = -0.175 - j0.378$ |
| | $T = 0.809 - j0.396$ | $T = 0.832 - j0.371$ | $T = 0.824 - j0.382$ |
| 16.0 | $R = -0.569 - j0.490$ | $R = -0.528 - j0.500$ | $R = -0.534 - j0.494$ |
| | $T = 0.431 - j0.501$ | $T = 0.474 - j0.498$ | $T = 0.466 - j0.503$ |
| 25.0 | $R = -0.882 - j0.313$ | $R = -0.851 - j0.354$ | $R = -0.859 - j0.339$ |
| | $T = 0.117 - j0.331$ | $T = 0.150 - j0.360$ | $T = 0.140 - j0.356$ |

SECTION 5 THE TWO-BOUNDARY APPROACH FOR OPEN SCATTERING PROBLEMS

5.1. INTRODUCTION

An important practical application of electromagnetic field theory is the prediction of the radar cross-sections of bodies that lie in unbounded space and are illuminated by an electromagnetic wave. Radar cross-sections provide a measure of the amount of energy scattered by a body in a given direction and may be calculated if the electric field around the body is known.

In the waveguide junction problem of Section 4, the governing equation is the Helmholtz equation and the geometry extends to infinity only one dimension. Using the same governing equation but extending to infinity in two dimensions, open cylindrical scattering problems can be treated as a modification of waveguide junction problems. The discontinuities in the waveguide which cause the perturbation of the fields is replaced by scatterers in free space that deflect the incident wave. Further, the reflected and transmitted waves we computed in Section 4 are now the scattered fields from the structure.

The cross section of a cylinder with refraction index η is shown in Figure 5-1. Define the incident field E^i and H^i as the field with the cylinder absent and the scattered field E^s and H^s as the difference between the total field with the cylinder present (E^t, H^t) and the incident field, that is,

$$E^s = E^t - E^i \quad H^s = H^t - H^i$$

By assuming that the cylinder is infinitely long and that the incident wave propagates in the plane of the figure, the scattering problem is reduced to two dimensions. When the length of the cylinder is very large compared to the wavelength, this assumption will not contribute too much error in the analysis. However if the length of the cylinder is of the same order as the wavelength then a three dimensional analysis is needed.

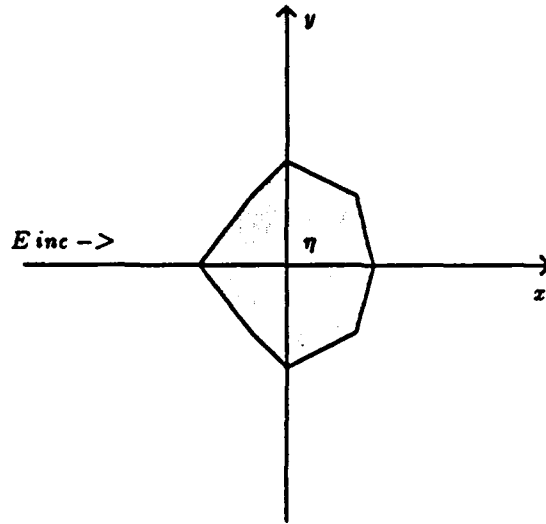


Figure 5-1: The cross section of a scatterer

In this Section, we treat only the case of a TE plane incident wave having the electric field in the z direction. For the other cases, such as incident TM waves or cylindrical wave, the analysis follows in much the same way. From Maxwell equations, the total electric field with the cylinder present must satisfy the Helmholtz equation in all space

$$(\nabla^2 + k_0^2 \eta) E^t = 0$$

k_0 is the wavenumber in free space and η is the refractive index of the material. Furthermore, the scattered field will die out as we go away from the cylinder, the boundary conditions at infinity is $E^t = E^i$. Finally we will adopt the polar coordinates (r, θ) system to analyze open scattering problems since here two dimensions extend to infinity.

5.2. FORMULATION AND APPLICATION OF TWO-BOUNDARY APPROACH

5.2.1. MODAL ANALYSIS

For simplicity, assume that the incident wave is a TE plane wave that propagates in the x direction and that the geometry of the scatterer is symmetric with respect to the x axis. We define a circle Γ_1 with radius r_1 to serve as the boundary of the finite element solution region, and call it the "picture frame circle". A second circle Γ_2 with smaller radius r_2 is defined to be the mode matching boundary and is called the "matching circle", as shown in Figure 5-2.

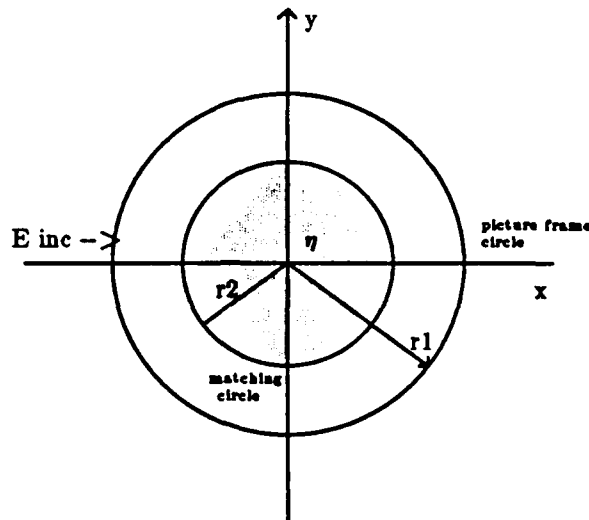


Figure 5-2: The picture frame circle and the matching circle

The reasons for choosing circles as the picture frame and matching boundaries are:

1. The circle is the simplest shape to be used as a boundary in polar coordinates.
2. The analytical solution for the exterior region is given by Hankel functions in the r direction. Computing the Hankel functions is an expensive task compared to other numerical procedures. By using circles for the picture frame and matching boundaries we only need to compute the Hankel function once at each radius.
3. Since Hankel functions oscillate and change many orders of magnitude, the numerical solutions would be unstable if the boundaries involved radii of different magnitudes. For a circular boundary, only one radius is involved and this leads to stable numerical procedures.

The analytical solution for the scattered field in the region $r \geq r_2$ can be found by using the method of separation of variables¹. The result is

$$\gamma_i(r, \theta) = H_i(k_0 r) \cos(i\theta) \quad (5.1)$$

due to the symmetry, only the cos terms are introduced in (5.1). k_0 is the wavenumber in the free space, and H_i is the Hankel function of second kind of the order i . If we use $(M+1)$ modes to approximate the scattered electric field, then, together with the incident electric field, the analytical expression for the total field in the region $r \geq r_2$ is

$$E^t(r, \theta) = \exp(-jk_0 r \cos \theta) + \sum_{i=0}^M a_i \gamma_i(r, \theta) \quad r \geq r_2 \quad (5.2)$$

where $\exp(-jk_0 r \cos \theta)$ is the incident electric field and a_i 's are the coefficients that need to be determined. Note that, in general, the coefficients a_i are complex since all the functions are complex valued in (5.1).

Since equation (5.2) holds for $r \geq r_2$, it gives the electric field at the boundary Γ_1 as

$$E^t(r_1, \theta) = \exp(-jk_0 r_1 \cos \theta) + \sum_{i=0}^M a_i \gamma_i(r_1, \theta) \quad (5.3)$$

We may approximate the term $\exp(-jk_0 r_1 \cos \theta)$ by its $(M+1)$ Fourier components as

$$\exp(-jk_0 r_1 \cos \theta) = c_0 + \sum_{i=1}^M c_i \cos(i\theta)$$

where

$$c_0 = \frac{1}{2\pi} \int_0^{2\pi} \exp(-jk_0 r_1 \cos(\theta)) d\theta$$

$$c_i = \frac{1}{\pi} \int_0^{2\pi} \exp(-jk_0 r_1 \cos(\theta)) \cos(i\theta) d\theta$$

Thus, equation (5.3) can be written as

$$E^t(r_1, \theta) = \{a_0 H_0(k_0 r_1) + c_0\} + \sum_{i=1}^M \{a_i H_i(k_0 r_1) + c_i\} \cos(i\theta) \quad (5.4)$$

From equation (5.4), we set up $(M+1)$ boundary value problems for the field patterns $\lambda_i(r, \theta)$ inside the finite element solution region. $\lambda_i(r, \theta)$ is obtained by using the finite element method to solve the Helmholtz equation with the boundary conditions $\lambda_i(r_1, \theta) = \cos(i\theta)$ on the boundary Γ_1 within the finite element solution region. Once the $(M+1)$ field patterns are known, by using the superposition theorem, the total field in the finite element solution region can be expressed as follows

$$\tilde{E}^t(r, \theta) = \{a_0 H_0(k_0 r_1) + c_0\} \lambda_0(r, \theta) + \sum_{i=1}^M \{a_i H_i(k_0 r_1) + c_i\} \lambda_i(r, \theta) \quad (5.5)$$

Again, both equations (5.2) and (5.5) are valid in the region $r_2 \leq r \leq r_1$, so that we have two solutions for the field on the matching circle Γ_2

$$E^t(r_2, \theta) = \exp(-jk_0 r_2 \cos \theta) + \sum_{i=0}^M a_i \gamma_i(r_2, \theta) \quad (5.6)$$

and

$$\tilde{E}^t(r_2, \theta) = \sum_{i=0}^M \{a_i H_i(k_0 r_1) + c_i\} \lambda_i(r_2, \theta) \quad (5.7)$$

The last step is to match these two solutions on the circle Γ_2 , from which the complex coefficients a_i 's can be solved.

5.2.2. MATCHING FORMULATION

Matching the two solutions is performed by minimizing the square of the difference between (5.6) and (5.7) on the matching circle. From (5.6) and (5.7) we construct an L_2 norm of the difference between the numerical solution and the analytical solution on the matching circle

$$L_2^2 = \int_0^{2\pi} |\tilde{E}^t(r_2, \theta) - E^t(r_2, \theta)|^2 d\theta$$

and

$$|\tilde{E}^t(r_2, \theta) - E^t(r_2, \theta)|^2 = \left\{ K(\theta) + \sum_{i=0}^M a_i Q_i(\theta) \right\} \cdot \left\{ K^*(\theta) + \sum_{i=0}^M a_i^* Q_i^*(\theta) \right\}$$

where

$$K(\theta) = \exp(-jk_0 r_2 \cos \theta) - \sum_{i=0}^M c_i \lambda_i(r_2, \theta)$$

$$Q_i(\theta) = H_i(k_0 r_2) \cos(i\theta) - H_i(k_0 r_1) \lambda_i(r_2, \theta)$$

where the superscript $*$ represents the complex conjugate. By writing $a_i = x_i + j y_i$ and minimizing L_2^2 with respect to x_i 's and y_i 's, the following equations are obtained

$$\sum_{i=0}^M x_i \int_0^{2\pi} \operatorname{Re}\{Q_l Q_i^*\} d\theta + \sum_{i=0}^M y_i \int_0^{2\pi} \operatorname{Im}\{Q_l Q_i^*\} d\theta = - \int_0^{2\pi} \operatorname{Re}\{K^* Q_l\} d\theta$$

$$\sum_{i=0}^M x_i \int_0^{2\pi} \operatorname{Im}\{Q_l Q_i^*\} d\theta + \sum_{i=0}^M y_i \int_0^{2\pi} \operatorname{Re}\{Q_l Q_i^*\} d\theta = \int_0^{2\pi} \operatorname{Im}\{K^* Q_l\} d\theta$$

$$l = 0 \dots M \quad (5.8)$$

Finally from (5.8) we can solve for x_i 's and y_i 's and obtain the coefficients a_i 's.

5.2.3. FAR FIELD PATTERN

Once the complex coefficients a_i 's are known, the scattered field in the exterior region is obtained as

$$E^s(r, \theta) = \sum_{i=0}^M a_i \gamma_i(r, \theta) \quad r \geq r_2 \quad (5.9)$$

At large distances ($r \gg \text{wavelength}$), the scattered field in terms of (5.9) can be written as

$$E^e = \left(\frac{2j}{\pi k_0 r}\right)^{1/2} \exp(-jk_0 r) \cdot \left\{a_0 + \sum_{i=1}^N j^i a_i \cos(i\theta)\right\}$$

It is customary to define the far field scattering pattern by the equation

$$g(\theta) = a_0 + \sum_{i=1}^N j^i a_i \cos(i\theta)$$

5.3. NUMERICAL RESULTS

Shown in Figure 5-3 is the geometry of two parallel circular cylinders with radii 0.2 wavelength and 0.1 wavelength separated by 0.4 wavelength. The refraction indexes are 2.0 for both cylinders. This problem has been analyzed by Mei¹¹. The radius of the picture frame circle is 0.6 wavelength as also shown in the figure. Figure 5-4 shows two different meshes used to solve this problem: Figure 5-4 (a) contains 165 unknowns and Figure 5-4 (b) contains 287 unknowns.

5.3.1. INCIDENT ANGLE $\theta_{inc} = 0^\circ$

When a plane wave is incident with angle $\theta_{inc} = 0^\circ$ from the x axis, the solution should be symmetric with respect to the x axis. Figure 5-5 presents a plot of lines of equal values of E_z at time phase 0° , calculated by using $N = 4$ and $r_2 = 0.4$ wavelength in the program. The jagged lines in this figure are a result of imperfections in the plotter and do not represent discontinuities in the solutions which were smooth. The resultant amplitude of the far field pattern from the program compared with solutions obtained by Mei¹¹ are shown in Figure 5-6 for the two meshes (a) and (b).

5.3.2. INCIDENT ANGLE $\theta_{inc} = 90^\circ$

Shown in Figure 5-7 are the plots of equal values of E_z for an incident angle of $\theta_{inc} = 90^\circ$. The parameters used in the program are : $N = 4$, $r_2 = 0.4$ wavelength, and the mesh used is the same as Figure 5-4(b). Figure 5-8 is a comparison of the amplitude and phase of the far field pattern obtained by the present method and that obtained by Mei¹¹.

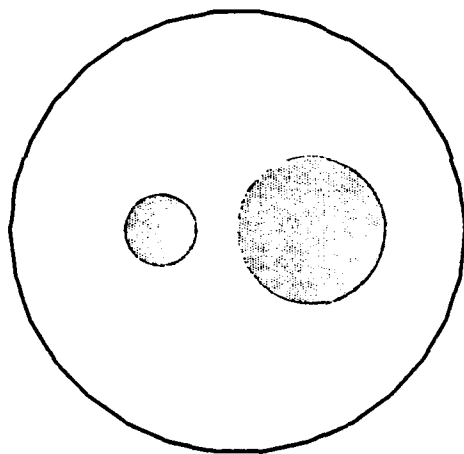
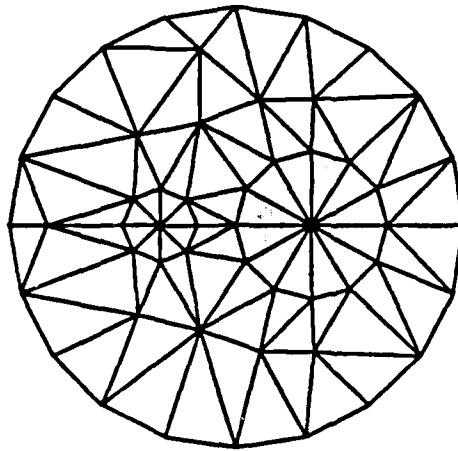
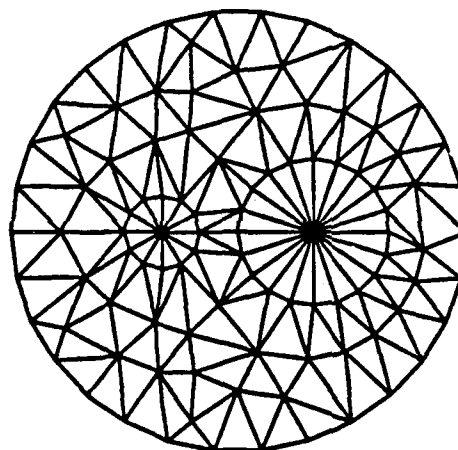


Figure 5-3: Two parallel circular cylinders with radii
0.2 wavelength and 0.1 wavelength
separated by 0.4 wavelength

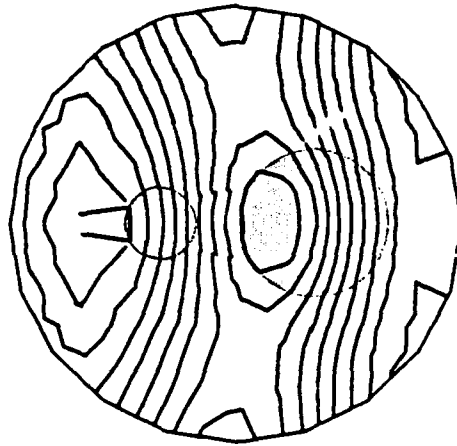


(a)



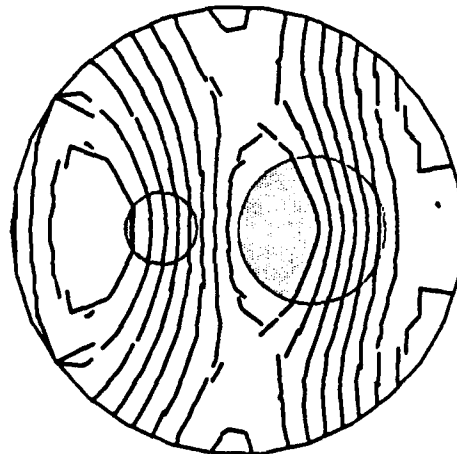
(b)

Figure 5-4: Finite element meshes for the problem in Figure 5-3
(a) 165 unknowns (b) 287 unknowns



← inc

(a)



← inc

(b)

Figure 5-5: Plots of equal values of E_z with time phase 0°

(a) for the mesh in Figure 5-4 (a)

(b) for the mesh in Figure 5-4 (b)

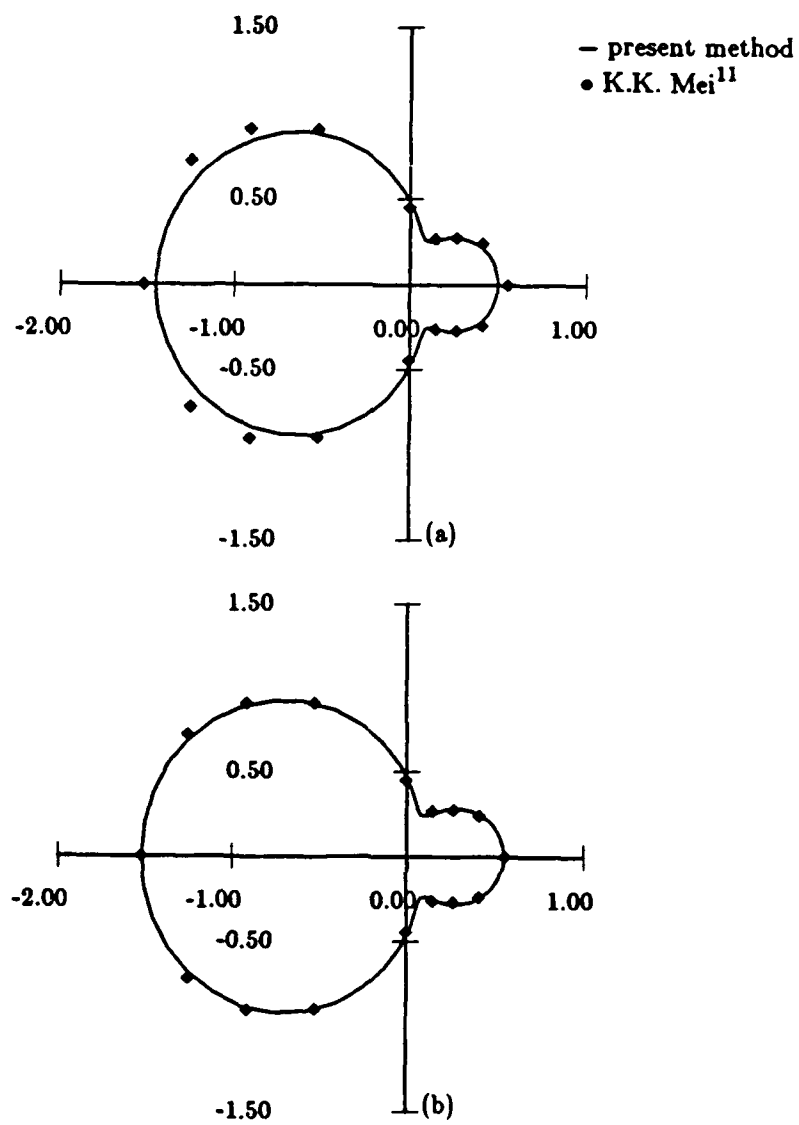
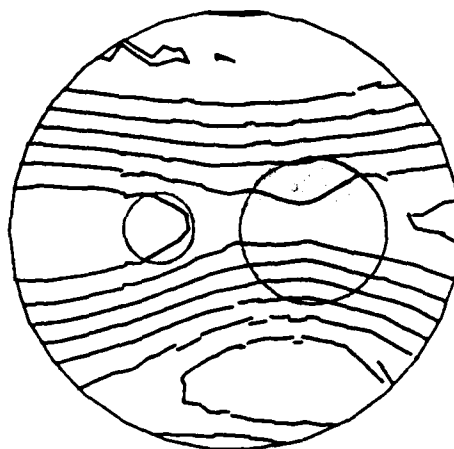


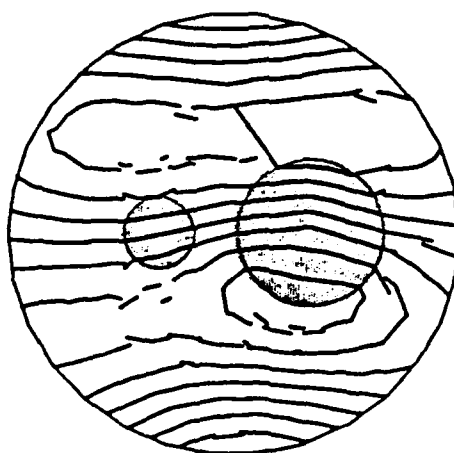
Figure 5-6: Amplitude of the far field pattern for $\theta_{\text{inc}} = 0^\circ$

inc
↓



(a) time phase = 0

inc
↓



(b) time phase = 90

Figure 5-7: Plots of equal E_z lines for $\theta_{inc} = 90^\circ$

(a) time phase = 0°

(b) time phase = 90°

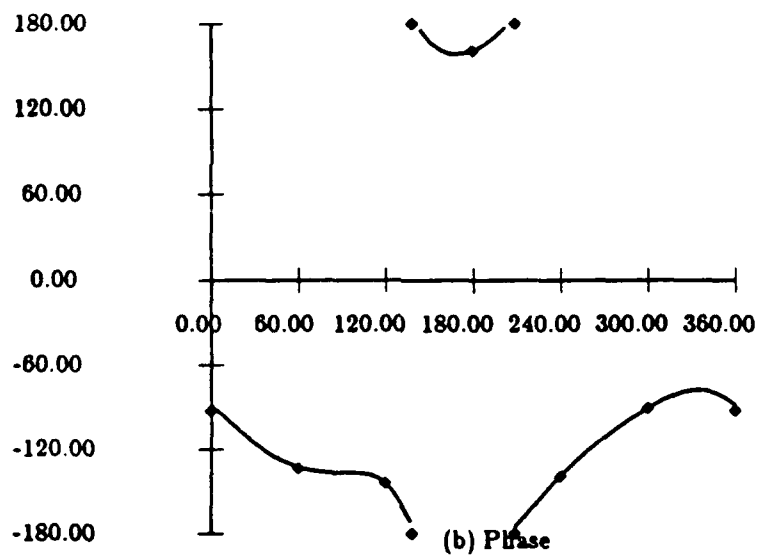
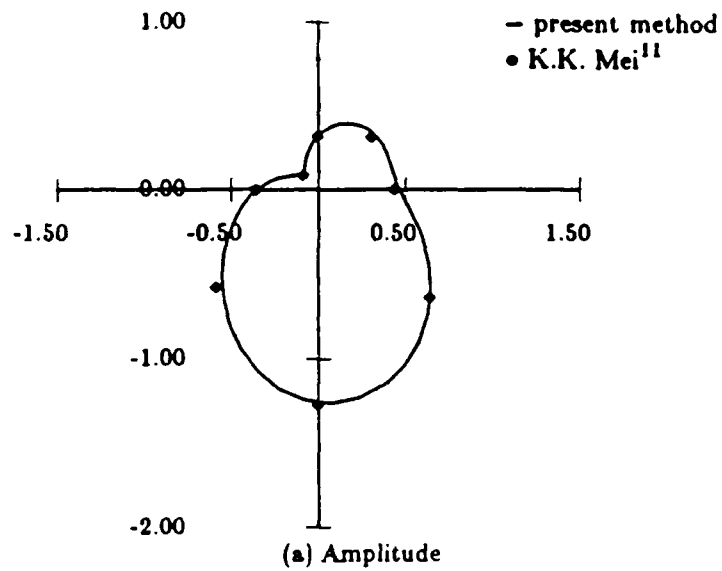


Figure 5-8: Far field pattern (a) amplitude (b) phase

SECTION 6 THE TRANSFINITE ELEMENT METHOD FOR ELECTROSTATIC PROBLEMS

Described in this chapter and in Section 7 is a novel coupling scheme for the open problems called the "transfinite element method". The purpose of this name is to denote the fact that analytical basis functions are employed in the infinite exterior region. In this chapter, we take the electrostatics as a simple case to develop the theory. In Section 7, we return to the open scattering problems but using the transfinite element method.

6.1. GENERAL DESCRIPTION OF THE TRANSFINITE ELEMENTS METHOD

The solution procedure for applying the transfinite elements method is

1. Derive a functional either by using the Rayleigh-Ritz method or by using Galerkin's method for the problem being solved. The functional derived will be an integral over the entire problem region.
2. Create a picture frame that separates the problem region into two parts Ω_i and Ω_e . The region interior to the picture frame is Ω_i and the region exterior to the picture frame is Ω_e . Let Γ be the boundary between them. The finite element method is used in the interior region, so the picture frame must enclose all inhomogeneities and other quantities that must be modeled by the finite element method. The functional integral over the entire region is thus separated into two parts: one integral over the interior region Ω_i and the other over the exterior region Ω_e .
3. Because the exterior region Ω_e is homogeneous, we can create a complete function space A_e for all of the functions that satisfy the boundary value problem in the exterior region Ω_e by using the superposition theorem and the method of separation of variables. The basis functions in A_e thus found will be exact solution of the problem in the exterior region. It follows that the integral of the functional over Ω_e is zero and that only the integral over the interior region Ω_i must be computed.
4. Apply the standard finite element method in the interior region. The basis functions employed can be the conventional Lagrange interpolation polynomials. The function space A_i constructed from these polynomials represent the the basis vectors for the function space for the numerical solution in the interior region.

5. Impose continuity conditions of the solution between the function space A_i and the function space A_e along the boundary Γ . This may be accomplished simply by setting the values from both solutions equal at the boundary nodes. Note that usually, the number of unknowns used to approximate the solution in the exterior region Ω_e is less than the number of nodes on the boundary Γ . The final function space A for the numerical solutions in the whole region will be the union of the function space A_i and A_e restricted by the continuity conditions imposed on the boundary Γ .
6. Finally, apply the stationarity property of the functional on the function space A to obtain a matrix equation to be solved for the coefficients in the approximation.

6.2. FORMULATION OF TRANSFFINITE ELEMENTS IN THE ELECTROSTATIC PROBLEMS

6.2.1. FUNCTIONAL

The particular problem with which we will be concerned here is the solution of the Poisson equation

$$-\nabla \cdot \epsilon_r \nabla \psi = g \quad \text{in } \Omega_\infty$$

subject to the boundary condition

$$\psi = 0 \quad \text{at } \infty \quad (6.1)$$

The problem region Ω_∞ for (6.1) is of course unbounded.

According to the Rayleigh-Ritz method, the solution of (6.1) may be obtained by minimizing the following functional

$$F(\psi) = \int_{\Omega_\infty} \epsilon_r \nabla \psi \cdot \nabla \psi \, d\Omega - 2 \int_{\Omega_\infty} g \psi \, d\Omega \quad (6.2)$$

By using a circle Γ with radius r_1 to enclose all inhomogenities and sources, we separate Ω_∞ into two regions: an interior region Ω_i and the exterior region Ω_e , as shown in Figure 6-1.

The integral in (6.2) can be integrated separately over Ω_i and Ω_e as follows

$$F(\psi) = \int_{\Omega_i} \epsilon_r \nabla \psi \cdot \nabla \psi \, d\Omega - 2 \int_{\Omega_i} g \psi \, d\Omega + \int_{\Omega_e} \nabla \psi \cdot \nabla \psi \, d\Omega \quad (6.3)$$

By Green's theorem we may rewrite this as

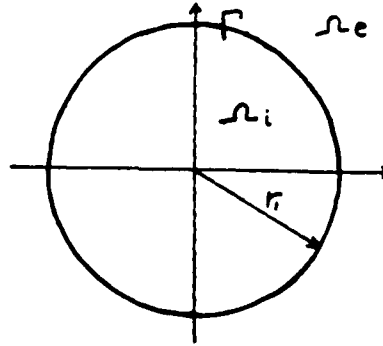


Figure 6-1: The separation of the problem region
interior region Ω_i , exterior region Ω_e and the boundary Γ

$$F(\psi) = \int_{\Omega_i} \epsilon_r \nabla \psi \cdot \nabla \psi d\Omega - 2 \int_{\Omega_i} g\psi d\Omega - \int_{\Gamma} \psi \frac{\partial \psi}{\partial r} d\Gamma - \int_{\Omega_e} \psi \nabla^2 \psi d\Omega \quad (6.4)$$

The reason for converting the functional from (6.3) to (6.4) will become clear in the following section.

6.2.2. THE FUNCTION SPACE

Note that the exterior region Ω_e now is homogeneous and source free. If the net charge contained in the interior region Ω_i is zero, the function space Λ_e obtained by using the method of separation of variables is

$$\Lambda_e = \left\{ \psi^e \mid \psi^e = \sum_{i=1}^M \frac{1}{r^i} \cdot (a_i \cos(i\theta) + b_i \sin(i\theta)) \quad r \geq r_1 \right\} \quad (6.5)$$

where M is the number of terms used to approximate the solution in the region Ω_e , and a_i and b_i are scalar numbers. If the net charge in Ω_i is not zero, a logarithmic term that vanishes at a certain reference point must be included in the expansion.

We subdivide the interior region Ω_i into second order triangular finite elements and use Lagrange polynomials as the interpolation functions. The function space Λ_i for the solution in the Ω_i is

$$\Lambda_i = \left\{ \psi^i \mid \psi^i = \sum_{i=1}^N \psi_i^I \alpha_i^I + \sum_{i=1}^P \psi_i^F \alpha_i^F \quad r \leq r_1 \right\} \quad (6.6)$$

where we have separated the interpolation polynomials into α_i^I for the nodes in Ω_i but not on the boundary Γ and α_i^F for the nodes on the boundary Γ . Corresponding to α_i^I and α_i^F are the solution values ψ_i^I and ψ_i^F , respectively. This subdivision will help in imposing continuity conditions in the procedure.

The combined function space $\Lambda = \Lambda_i \cup \Lambda_e$ as discussed in section 6.1 form the new function space Λ

$$\Lambda = \left\{ \psi \mid \psi = \begin{cases} \psi^i & \text{in } \Omega_i \\ \psi^e & \text{in } \Omega_e \end{cases}, \psi \in C^0 \right\} \quad (6.7)$$

Continuity of the field is imposed by setting

$$\begin{bmatrix} \psi_1^F \\ \psi_2^F \\ \vdots \\ \psi_p^F \end{bmatrix} = \begin{bmatrix} \cos \theta_1 \dots \cos (M\theta_1) \sin (M\theta_1) \\ \cos \theta_2 \dots \cos (M\theta_2) \sin (M\theta_2) \\ \vdots \\ \cos \theta_p \sin \theta_p \dots \cos (M\theta_p) \sin (M\theta_p) \end{bmatrix} \cdot \begin{bmatrix} \frac{1}{r_1} & 0 \\ & \frac{1}{r_1} \\ & \vdots \\ 0 & \frac{1}{r_1^M} \\ & \frac{1}{r_1^M} \end{bmatrix} \begin{bmatrix} a_1 \\ b_1 \\ \vdots \\ a_M \\ b_M \end{bmatrix} \quad (6.8)$$

= $\theta \quad R \quad \tilde{A}$

where (r_1, θ_i) is the polar coordinates for the boundary point ψ_i^F , and

$$\Theta = \begin{bmatrix} \cos \theta_1 \dots \cos M\theta_1 \sin M\theta_1 \\ \cos \theta_2 \dots \cos M\theta_2 \sin M\theta_2 \\ \vdots \\ \cos \theta_p \dots \cos M\theta_p \sin M\theta_p \end{bmatrix} \quad R = \begin{bmatrix} \frac{1}{r_1} & 0 \\ & \frac{1}{r_1} \\ & \vdots \\ 0 & \frac{1}{r_1^M} \\ & \frac{1}{r_1^M} \end{bmatrix} \quad \tilde{A} = \begin{bmatrix} a_1 \\ b_1 \\ \vdots \\ a_M \\ b_M \end{bmatrix}$$

6.2.3. THE BOUNDARY INTEGRAL

Since the functions in A are analytical solutions of the Laplace equation, the integral over Ω_e in the functional (6.4) is zero for any choice of the coefficients a_i and b_i . Thus the functional reduces to the following form

$$F(\psi) = \int_{\Omega_i} \epsilon_r \nabla \psi^i \cdot \nabla \psi^i d\Omega - 2 \int_{\Omega_i} g \psi^i d\Omega - \int_{\Gamma} \psi^e \frac{\partial \psi^e}{\partial r} d\Gamma \quad (6.9)$$

Thus by a judicious choice for the function space A , the functional $F(\psi)$ is reduced from integrals over the entire unbounded region into integrals over the interior region plus a boundary integral term. This reduction has also been exploited by Silvester and Hsieh⁹, although their procedure for modeling the exterior region was quite different.

The boundary integral term

$$B = \int_{\Gamma} \psi^e \frac{\partial \psi^e}{\partial r} d\Gamma$$

in (6.9) is evaluated simply by analytical integration. From (6.5), we have

$$\frac{\partial \psi^e}{\partial r} = - \sum_{i=1}^M \frac{i}{r^{i+1}} \{ a_i \cos(i\theta) + b_i \sin(i\theta) \} \quad (6.10)$$

Substituting (6.10) and (6.5) into B gives the result

$$\int_{\Gamma} \psi^e \frac{\partial \psi^e}{\partial r} d\Gamma = [a_1 b_1 \dots a_M b_M] \begin{bmatrix} \frac{\pi}{r^2} & & & & & \\ & \frac{\pi}{r^2} & & & & \\ & & \ddots & & & \\ & & & \frac{M\pi}{r^{2M}} & & \\ & & & & \frac{M\pi}{r^{2M}} & \\ & & & & & \end{bmatrix} \begin{bmatrix} a_1 \\ b_1 \\ \vdots \\ a_M \\ b_M \end{bmatrix}$$

$$= \tilde{A} D \tilde{A} \quad (6.11)$$

where

$$\underset{\sim}{A} = \underset{\sim}{A}^T \quad D = \begin{bmatrix} \frac{\pi}{r^2} & & & \\ & \frac{\pi}{r^2} & & \\ & & \ddots & \\ & & & \frac{M\pi}{r^{2M}} \\ & & & & \frac{M\pi}{r^{2M}} \end{bmatrix}$$

6.2.4. THE RESULTING MATRIX EQUATION

From equation (6.8), the nodal values ψ^i can be written as a connection matrix times a column vector

$$\begin{bmatrix} \psi_1^I \\ \vdots \\ \psi_N^I \\ \vdots \\ \psi_P^I \end{bmatrix} = \begin{bmatrix} I^N & 0 \\ 0 & \Theta R \end{bmatrix} \begin{bmatrix} \psi_1^I \\ \vdots \\ \psi_N^I \\ a_1 \\ b_1 \\ \vdots \\ a_M \\ b_M \end{bmatrix} = \underset{\sim}{C} \underset{\sim}{X} \quad (6.12)$$

where I^N is an N by N identity matrix, and

$$\underset{\sim}{C} = \begin{bmatrix} I^N & 0 \\ 0 & \Theta R \end{bmatrix} \quad \underset{\sim}{X} = \begin{bmatrix} \psi_1^I \\ \vdots \\ \psi_N^I \\ a_1 \\ b_1 \\ \vdots \\ a_m \\ b_m \end{bmatrix} \quad (6.13)$$

Substituting (6.11) and (6.12) into the functional (6.9) results in

$$F(\underset{\sim}{x}) = \underset{\sim}{x}^T \underset{\sim}{C}^T \underset{\sim}{S} \underset{\sim}{C} \underset{\sim}{x} - 2 \underset{\sim}{q}^T \underset{\sim}{C} \underset{\sim}{x} + \underset{\sim}{A}^T D \underset{\sim}{A}$$

where

$$S = \int_{\Omega_i} \nabla \underset{\sim}{\alpha} \cdot \nabla \underset{\sim}{\alpha} \, d\Omega \quad q = \int_{\Omega_i} g \underset{\sim}{\alpha} \, d\Omega$$

where the $\underset{\sim}{}$ below a variable indicates a row vector, and T represents the transpose of a matrix.

Finally minimizing the functional $F(x)$ with respect to the variables x gives the resulting matrix equation

$$\begin{bmatrix} S_{II} & S_{I\Gamma} & \theta R \\ & R\theta^T S_{\Gamma\Gamma} \theta R & \\ R\theta^T S_{\Gamma I} & + & D \end{bmatrix} \widetilde{x} = \widetilde{g} \quad (6.14)$$

Notice that the matrix on the left-hand-side is real, symmetric and positive definite and can therefore be solved very efficiently using the incomplete Choleski pre-conditioned conjugate Gradient Method²⁶. Also note that if the number of coefficients for the exterior region is less than the number of nodes on the boundary Γ , as is often the case, that the total number of unknowns is reduced by applying the transfinite element procedure.

6.3. NUMERICAL RESULTS

6.3.1. PARALLEL-PLATE CAPACITOR

The problem of a square, parallel-plate capacitor was chosen as an example to illustrate the method. A cross-section of the geometry is shown in Figure 6-2 and represents two infinitely long, thin conducting plates. This problem is of particular interest since it contains a singularity at the edge of the capacitor plate. The mesh used for this problem is shown in Figure 6-3 and a plot of the equal potential lines is shown in Figure 6-4. As is evident from the plot, the behaviors of the solution inside the picture frame is the same as one would expect if all space were modeled.

6.3.2. CIRCULAR CONDUCTORS

The second example is two infinitely long circular conductors both with radius A and separated by distance D , the ratio A/D is equal to 0.25. The exact value of the capacitance per unit length of this system is given by the formula²⁷

$$C = \frac{\pi \epsilon_0}{\cosh^{-1}(D/2A)}$$

In this case the value of $C = 2.3855 \epsilon_0$. Due to the symmetry of the problem, we used only one half of the problem region. The geometry of the problem and the semi-circle which served as the boundary Γ is shown in Figure 6-5; the mesh and the resulting equi-potential line plot are in Figure 6-6 and Figure 6-7, respectively. The capacitance we obtained is $2.3783 \epsilon_0$, an error of 0.3%.

6.3.3. FOUR LAYERS CAPACITOR

The last electrostatics example is two infinitely long rectangular cylinders filled with four different dielectrics. The relative dielectric constants are 2.0, 3.0, 4.0, 5.0 for layer I, II, III, IV; as shown in Figure 6-8. A simple approximation which treat these four capacitors in series gives the $C = 3.97351 \epsilon_0$ per unit length. Analysis by the transfinite element method gives a value $5.044 \epsilon_0$. Based on the appearance of potential plot in Figure 6-10, we expect that the transfinite element analysis provides the better result.

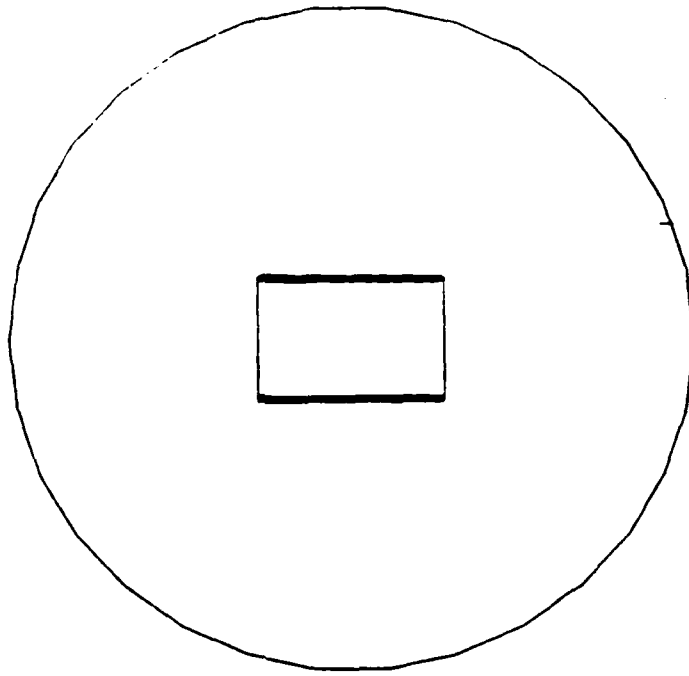


Figure 6-2: The cross-section of the parallel-plate capacitor

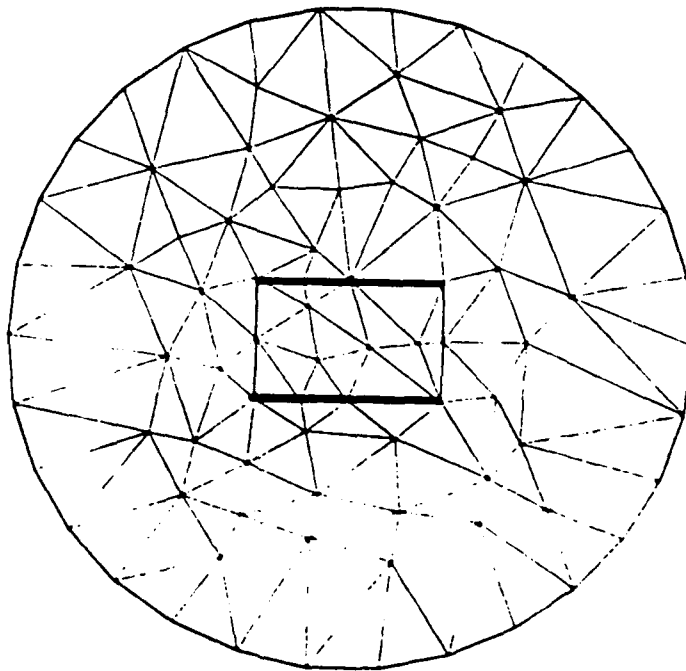


Figure 6-3: Mesh for the parallel-plate capacitor

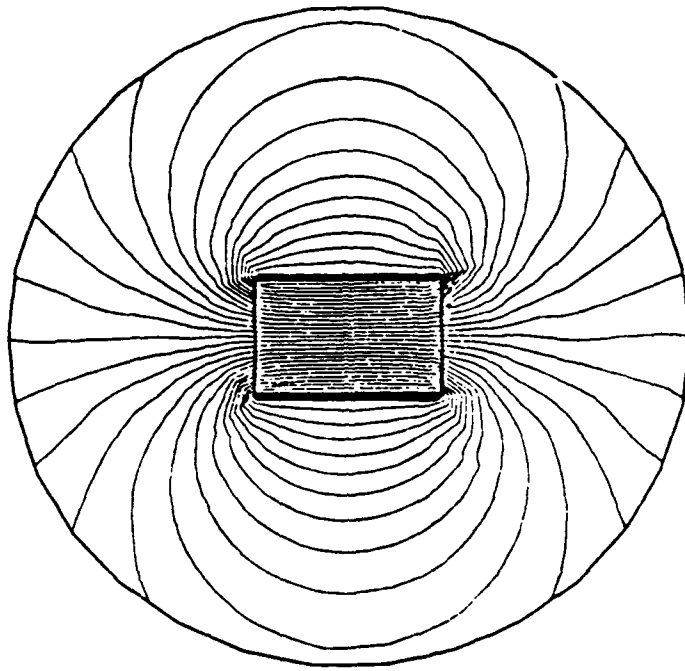


Figure 6-4: The equal potential lines plot. The potential on the top conductor is +1 volt and the potential on the bottom conductor -1 volt

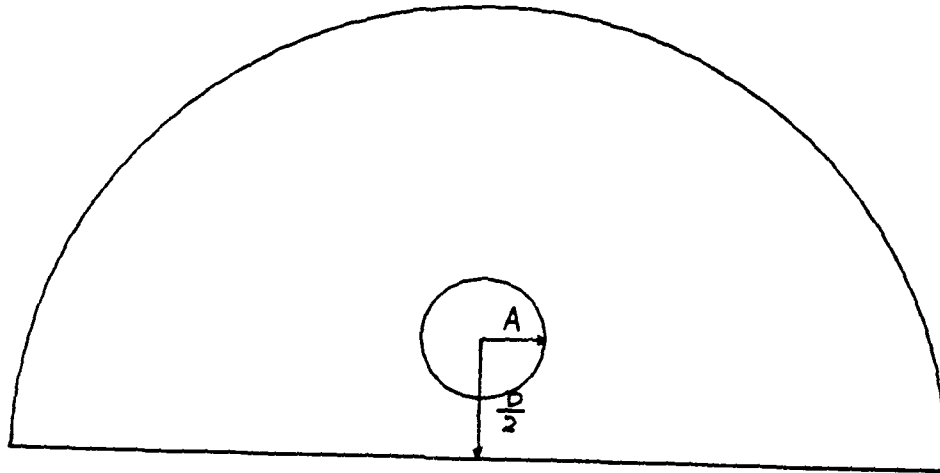


Figure 6-5: Circular cylinders with $D = 4 A$

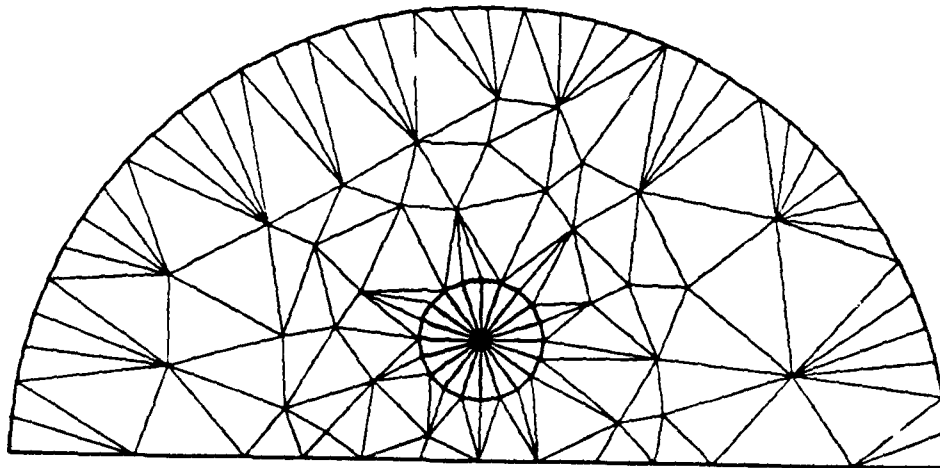


Figure 6-6: Mesh for example 2

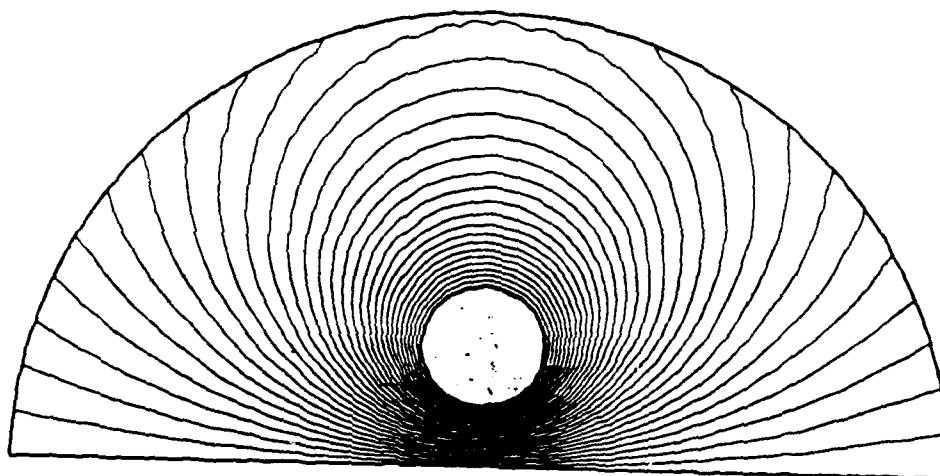


Figure 6-7: The equal potential lines plot for example 2. The potential on the circular conductor is 1 volt and the potential on the ground plane is 0 volt

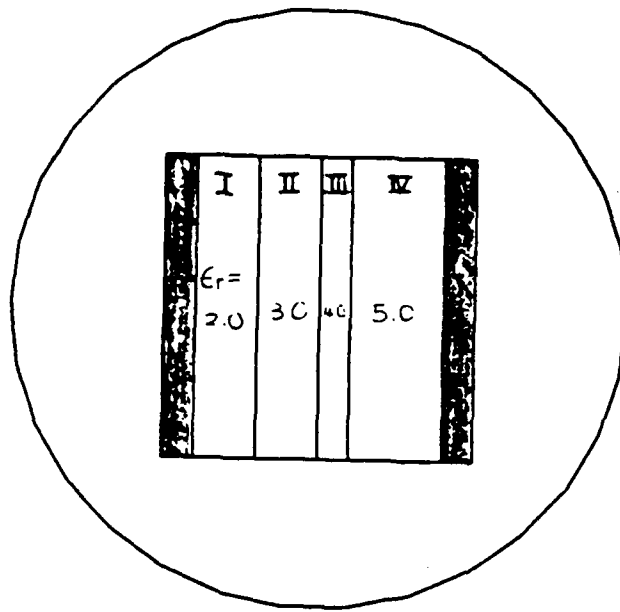


Figure 6-8: The geometry of four layers capacitor, with relative dielectric constants 2.0, 3.0, 4.0, 5.0

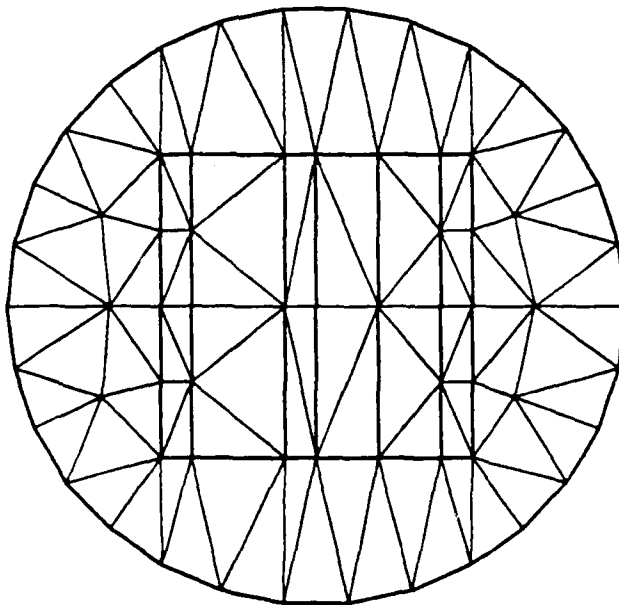


Figure 6-9: The mesh for the four layers capacitor

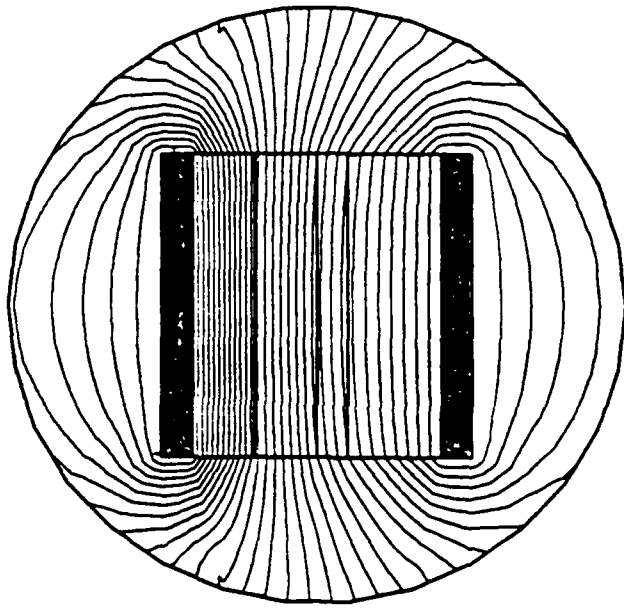


Figure 6-10: The equal potential lines plot

SECTION 7 THE TRANSFINITE ELEMENTS METHOD FOR OPEN SCATTERING PROBLEMS

7.1. FORMULATION IN TERMS OF THE TRANSFINITE ELEMENTS METHOD

7.1.1. WEAK FORMULATION OF GALERKIN'S METHOD

As mentioned in Section 2, variational principles can be obtained either by using Galerkin's method or by using the Rayleigh-Ritz method. It worth pointing out that Galerkin's method is more general than Rayleigh-Ritz method since it allows non-self adjoint operators to be modelled.

By applying Galerkin's method as discussed in Section 2, the following bilinear form is obtained

$$B(v, u) = \int_{\Omega_{\infty}} v^* (\nabla^2 u + k_0^2 \eta u) d\Omega \quad (7.1)$$

where Ω_{∞} is the problem region and $*$ represents the complex conjugate. As shown in Figure 6-1, the circle Γ with radius r_1 separates the problem into Ω_i and Ω_e . From the Green's theorem, the bilinear form $B(v, u)$ in (7.1) can be written as

$$B(v, u) = \int_{\Omega_i} (\nabla v^* \cdot \nabla u - v^* k_0^2 \eta u) d\Omega - \int_{\Gamma} v^* \frac{\partial u}{\partial n} d\Gamma - \int_{\Omega_e} v^* (\nabla^2 u + k_0^2 u) d\Omega \quad (7.2)$$

7.1.2. THE FUNCTION SPACES

The trial function space for u and the testing function space for v are set equal in the analysis here. The scattered field E^s in the region Ω_e can be approximated by

$$E^s = a_0 H_0(k_0 r) + \sum_{i=1}^M H_i(k_0 r) \{a_i \cos(i\theta) + b_i \sin(i\theta)\} \quad (7.3)$$

Combining this with the incident electric field $\exp(-jk_0 r \cos\theta)$ gives the function space A_e

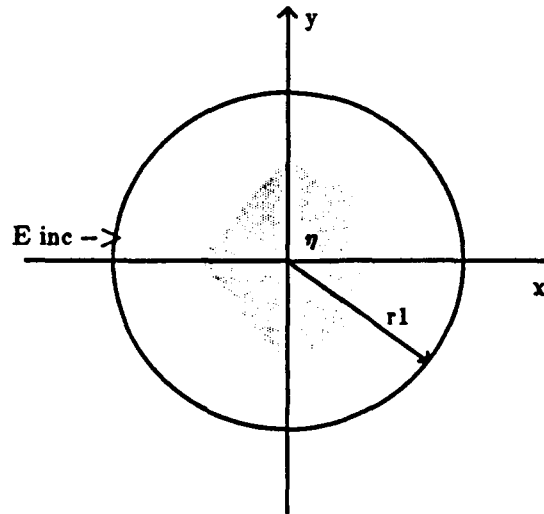


Figure 7-1: Interior region Ω_i , Exterior region Ω_e
and the boundary Γ

$$\Lambda_e = \left\{ \psi^e \mid \psi^e = \exp(-jk_0 r \cos \theta) + a_0 H_0(k_0 r) + \sum_{i=1}^M H_i(k_0 r) \cdot \{a_i \cos(i\theta) + b_i \sin(i\theta)\} \right\} \quad (7.4)$$

The function space Λ_i in the interior region Ω_i is

$$\Lambda_i = \left\{ \psi^i \mid \psi^i = \sum_{i=1}^N \psi_i^I \alpha_i^I + \sum_{i=1}^P \psi_i^R \alpha_i^R \right\}$$

Where the same notation is used here as in Chapter 6. Continuity of fields at the boundary Γ results in the conditions

$$\begin{bmatrix} \psi_1^\Gamma \\ \psi_2^\Gamma \\ \vdots \\ \psi_p^\Gamma \end{bmatrix} = \begin{bmatrix} \exp(-jk_0 r_1 \cos \theta_1) \\ \exp(-jk_0 r_2 \cos \theta_2) \\ \vdots \\ \exp(-jk_0 r_p \cos \theta_p) \end{bmatrix} + \begin{bmatrix} 1 \cos \theta_1 \sin \theta_1 \dots \cos M \theta_1 \sin M \theta_1 \\ 1 \cos \theta_2 \sin \theta_2 \dots \cos M \theta_2 \sin M \theta_2 \\ \vdots \\ 1 \cos \theta_p \sin \theta_p \dots \cos M \theta_p \sin M \theta_p \end{bmatrix} \begin{bmatrix} H_0 & & & \\ & H_1 & & 0 \\ & & \ddots & \\ 0 & & & H_M \end{bmatrix} \begin{bmatrix} a_0 \\ a_1 \\ b_1 \\ \vdots \\ a_M \\ b_M \end{bmatrix}$$

$$= \widehat{E}^{\text{inc}} + \Theta H \widehat{A}$$

(7.5)

Note that the matrix H is diagonal. The function space Λ is the union of Λ_e and Λ_i restricted with the continuity conditions (7.5).

Since u and v are both in the function space Λ they must satisfy the Helmholtz equation in the exterior region exactly, then the bilinear form $B(v, u)$ simplifies to

$$B(v, u) = \int_{\Omega_i} (\nabla v \cdot \nabla u - v \nabla^2 u) \, d\Omega - \int_{\Gamma} v \frac{\partial u}{\partial n} \, d\Gamma \quad (7.6)$$

The functions u and v can be expressed as

$$u = \begin{cases} \sum_{i=1}^N \alpha_i^I u_i^I + \sum_{i=1}^P \alpha_i^F u_i^F & \text{in } \Omega_i \\ E^{inc} + a_0 H_0(k_0 r) + \sum_{n=1}^M H_n(k_0 r) (a_n \cos(n\theta) + b_n \sin(n\theta)) & \text{in } \Omega_e \end{cases}$$

$$v = \begin{cases} \sum_{i=1}^N \alpha_i^I v_i^I + \sum_{i=1}^P \alpha_i^F v_i^F & \text{in } \Omega_i \\ E^{inc} + c_0 H_0(k_0 r) + \sum_{n=1}^M H_n(k_0 r) (c_n \cos(n\theta) + d_n \sin(n\theta)) & \text{in } \Omega_e \end{cases} \quad (7.7)$$

7.1.3. BOUNDARY INTEGRAL TERM

Note that since Γ is a circle with radius r_1 , the boundary integral term simplifies to

$$I = \int_{\Gamma} v^* \frac{\partial u}{\partial n} d\Gamma = r_1 \int_0^{2\pi} v^*(r_1, \theta) \frac{\partial u}{\partial r}(r_1, \theta) d\theta \quad (7.8)$$

From equation (7.7), we have that

$$v^*(r_1, \theta) = E^{inc*}(r_1, \theta) + c_0^* H_0^*(k_0 r_1) + \sum_{n=1}^M H_n^*(k_0 r_1) (c_n^* \cos(n\theta) + d_n^* \sin(n\theta))$$

and

$$\frac{\partial u}{\partial r}(r_1, \theta) = \frac{\partial E^{inc}}{\partial r}(r_1, \theta) + a_0 H_0(k_0 r_1) + \sum_{n=1}^M h_n(k_0 r_1) (a_n \cos(n\theta) + b_n \sin(n\theta)) \quad (7.9)$$

where $h_i(k_0 r_1) = \frac{dH_i(k_0 r)}{dr} \big|_{k_0 r_1}$. Approximating E^{inc} and $\frac{\partial E^{inc}}{\partial r}$ by $(2M+1)$ Fourier components gives

$$E^{inc}(r_1, \theta) \sim e_0 + \sum_{n=1}^M \{ e_n \cos(n\theta) + f_n \sin(n\theta) \}$$

$$\frac{\partial E^{inc}}{\partial r}(r_1, \theta) \sim g_0 + \sum_{n=1}^M \{ g_n \cos(n\theta) + l_n \sin(n\theta) \}$$

Thus substituting (7.9) into (7.8), integrating, and using the orthogonality property of trigonometric functions, the boundary integral (7.8) assumes the matrix form

$$I = [c_0 c_1 d_1 \dots c_M d_M]^* \cdot \left\{ \pi r_1 \begin{bmatrix} 2H_0^* h_0 & & 0 \\ H_1^* h_1 & & \\ & H_1^* h_1 & \\ & & \ddots \\ 0 & & & H_M^* h_M \\ & & & & H_M^* h_M \end{bmatrix} \begin{bmatrix} a_0 \\ a_1 \\ b_1 \\ \vdots \\ a_M \\ b_M \end{bmatrix} + \pi r_1 \begin{bmatrix} 2H_0^* g_0 \\ H_1^* g_1 \\ H_1^* l_1 \\ \vdots \\ H_M^* g_M \\ H_M^* l_M \end{bmatrix} \right\}$$

$$= \underline{\epsilon}^* Q \tilde{A} + \underline{\epsilon}^* \tilde{R}$$

where

$$c^* = [c_0 \ c_1 \ d_1 \ \dots \ c_M \ d_M]^*$$

$$Q = \pi r_1$$

$$\begin{bmatrix} 2H_0^* h_0 & & 0 \\ H_1^* h_1 & & \\ & H_1^* h_1 & \\ & & \ddots \\ 0 & & & H_M^* h_M \\ & & & & H_M^* h_M \end{bmatrix}$$

and

$$\tilde{A} = \begin{bmatrix} a_0 \\ a_1 \\ b_1 \\ \vdots \\ a_M \\ b_M \end{bmatrix}$$

$$\tilde{R} = \begin{bmatrix} 2H_0^* g_0 \\ H_1^* g_1 \\ H_1^* l_1 \\ \vdots \\ H_M^* g_M \\ H_M^* l_M \end{bmatrix}$$

(7.10)

Note that the matrix Q is also diagonal.

7.1.4. A MATRIX EQUATION FOR SCATTERING

From equations (7.5) and (7.10), we see that the functional $B(v,u)$ can be expressed in the matrix form

$$B(v,u) = \left[\underline{v}^I \ \underline{E}^{inc} + \underline{\epsilon} H \underline{\theta}^T \right]^* \cdot \begin{bmatrix} S_{II} & S_{I\Gamma} \\ S_{\Gamma I} & S_{\Gamma\Gamma} \end{bmatrix} \cdot \begin{bmatrix} \underline{\psi}^I \\ \underline{E}^{inc} + \underline{\theta} H \tilde{A} \end{bmatrix} - \underline{\epsilon}^* Q \tilde{A} - \underline{\epsilon}^* \tilde{R}$$

(7.11)

where

$$S_{ij} = \int_{\Omega_i} (\nabla \alpha_i \cdot \nabla \alpha_j - \alpha_i k_0^2 \eta \alpha_j) d\Omega$$

To obtain a weak solution for $u = \psi$, $B(v, \psi) = 0$ for $\forall v \in \Lambda$. This condition results in the following complex matrix equation to be solved for the coefficients $\tilde{\psi}^I$ and $\tilde{\lambda}$

$$\begin{bmatrix} S_{II} & S_{I\Gamma^{\Theta H}} \\ H^{\star \Theta T} S_{\Gamma I} & H^{\star \Theta T} S_{\Gamma\Gamma^{\Theta H}} - Q \end{bmatrix} \begin{bmatrix} \tilde{\psi}^I \\ \tilde{\lambda} \end{bmatrix} = - \begin{bmatrix} H^{\star \Theta T} S_I \tilde{E}^{inc} \\ H^{\star \Theta T} S_{\Gamma\Gamma} \tilde{E}^{inc} \end{bmatrix} + \begin{bmatrix} 0 \\ \tilde{R} \end{bmatrix}$$

(7.12)

Equation (7.12) can be simplified to give the final results

$$\begin{bmatrix} S_{II} & S_{I\Gamma^{\Theta}} \\ \Theta^T S_{\Gamma I} & \Theta^T S_{\Gamma\Gamma^{\Theta}} - Q(H \cdot H^{\star})^{-1} \end{bmatrix} \begin{bmatrix} \tilde{\psi}^I \\ H \tilde{\lambda} \end{bmatrix} = \begin{bmatrix} -H^{\star \Theta T} S_{I\Gamma} \tilde{E}^{inc} \\ (H^{\star})^{-1} \tilde{R} - \Theta^T S_{\Gamma\Gamma} \tilde{E}^{inc} \end{bmatrix}$$

(7.13)

7.2. NUMERICAL RESULTS

The validity and versatility of the techniques presented here are demonstrated by the following examples.

7.2.1. A CIRCULAR CYLINDER WITH ITS CENTER OFFSET FROM THE ORIGIN

Numerical solutions are generated by the transfinite element method with the center of the boundary circle Γ at the origin, while the center of the scatterer, which has radius 0.3λ , is offset by 0.2λ from the origin, as shown in Figure 7-2. Figure 7-3 is the mesh used in the program, which corresponds to 187 unknowns. Placing it off-center in this analysis provides a good test of the validity of the method.

I. Figure 7-4 is the far field pattern $|g(\psi)|$ for the refraction index of the scatterer equals to 2.0, excellent agreement between numerical and exact solution exists. The exact solutions in Figure 7-4 are obtained by using the method of separation of variables¹¹. The equal electric field plots for different time phases are shown in Figure 7-5. The elements outside the circle in Figure 7-3 are used to interpolate the field values in the exterior region. The electric field outside the boundary circle Γ has been evaluated by using equation (7.4).

II. Shown in Figure 7-6 are the intensity plots and the far field patterns $|g(\psi)|$ for refraction indices of $2.0+j2.0$, $2.0+j20.0$ and $2.0+j200.0$. The strange curves within the shaded area are due to the fact that the field intensities are almost zero there. Unfortunately, analytic solution for these lossy cases do not exist for comparison.

7.2.2. PLANE WAVE SCATTERING BY A ELLIPTIC CYLINDER

Figure 7-8 presents the far field pattern $|g(\psi)|$ for the elliptic cylinder scatterer in Figure 7-7 with a refraction index of 2.0. The results calculated here are compared with solutions from Marin⁷ and again verify the accuracy of the transfinite element approach. Propagation patterns at different time phases are shown in Figure 7-9.

7.2.3. SCATTERER WITH NONCONVEX NONSYMMETRIC CROSS-SECTION

The cross-section of a kidney-shaped scatterer is shown in Figure 7-10(a) where the dimension of the maximum object radius is 0.32λ . The incident radiation is a plane wave with wavelength 1 cm, and the direction of the incident wave is 45° from the positive x-axis. Three different materials with refraction indexes 7, $6+j 200$ and $j 20000$ are investigated, which are correspond approximately to glass, salt, and carbon.^{28,29}

Figure 7-10(b) provides the finite element mesh used in the program. The results of these calculations are shown in Figure 7-11 and are arranged in order top to bottom of increasing conductivity. The graphs on the left side of Figure 7-11 are plots of the intensity of the total wave. The graphs on the right side of Figure 7-11 display $|g(\psi)|$ versus ψ for these three materials along with a comparison with the results of Marin⁷.

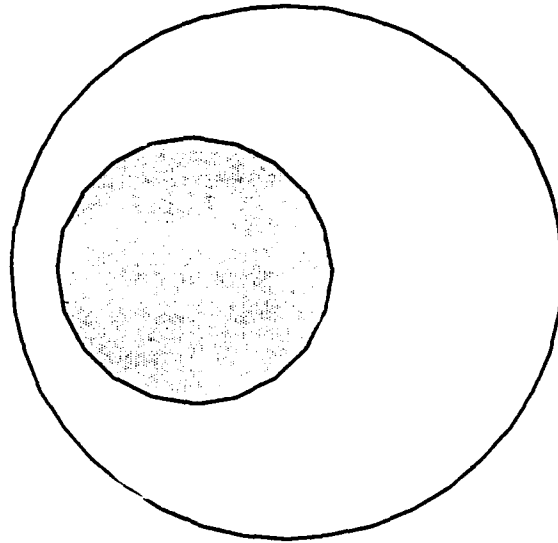


Figure 7-2: Off-center Circular Cylinder Scatterer

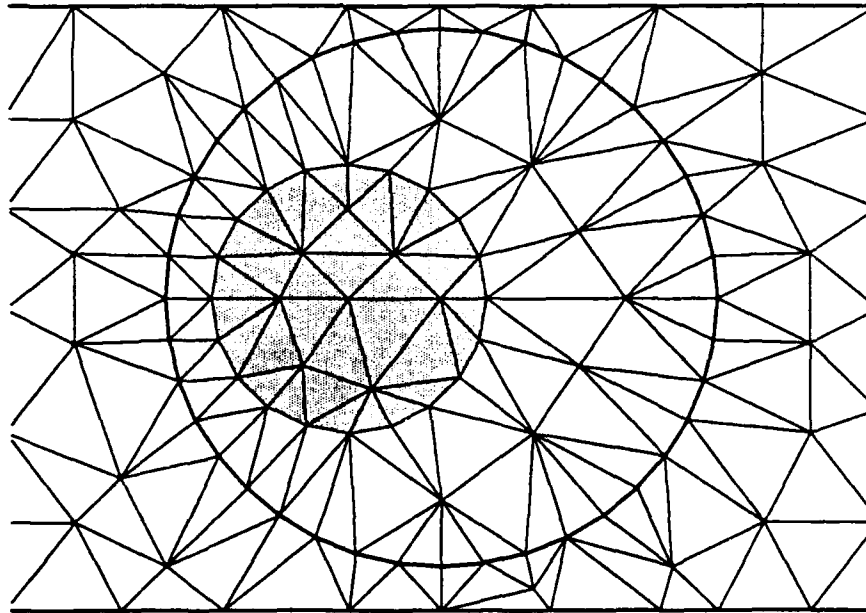


Figure 7-3: Mesh size 187 unknowns

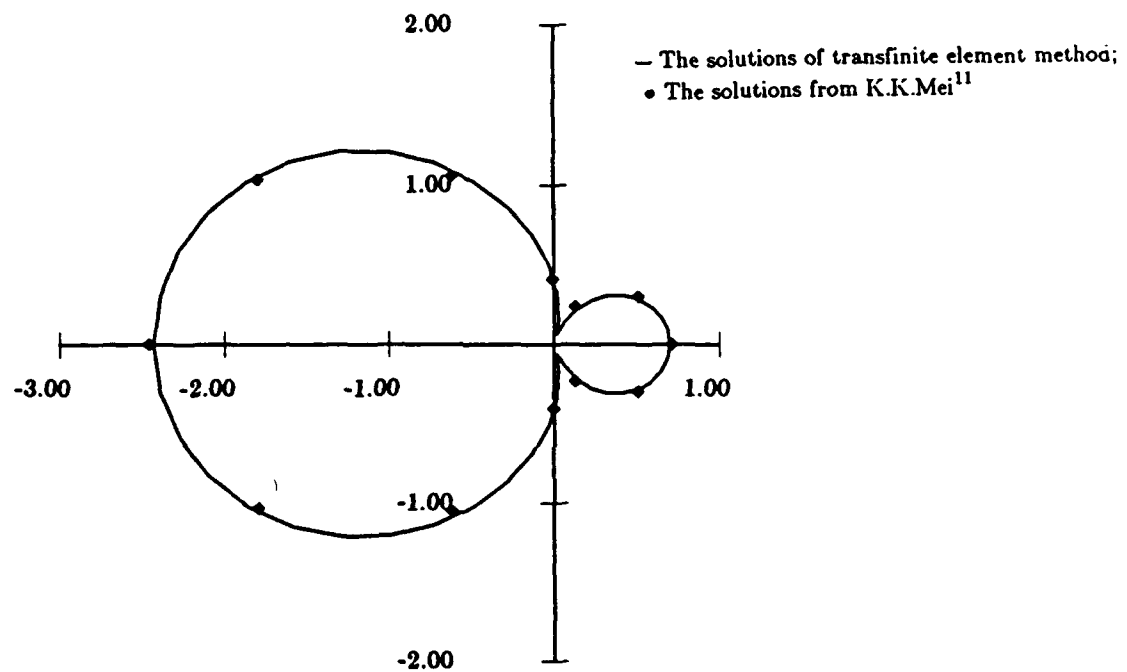
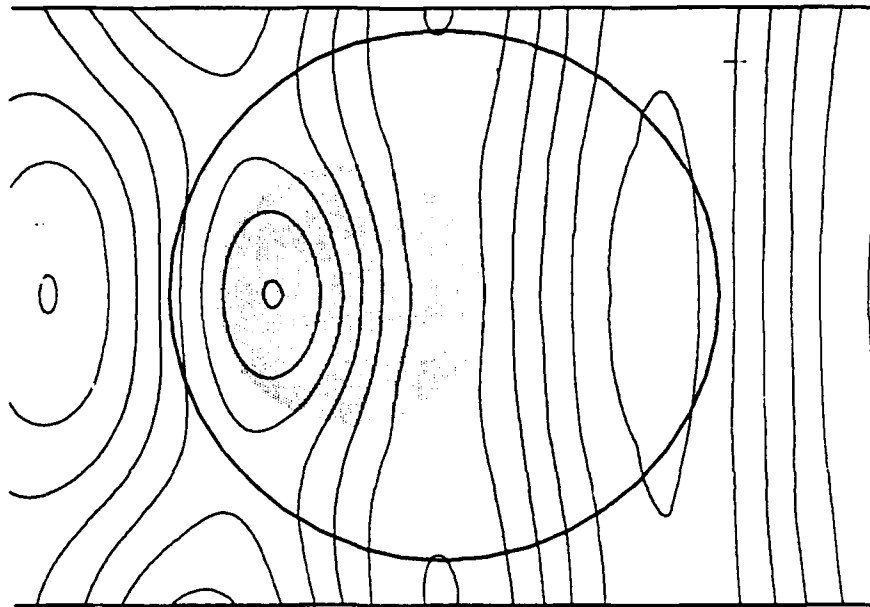
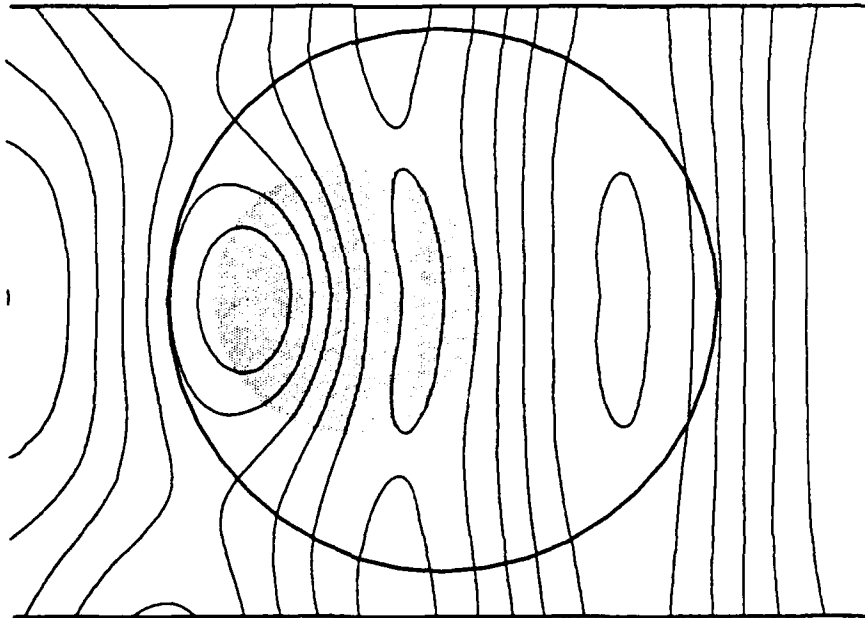


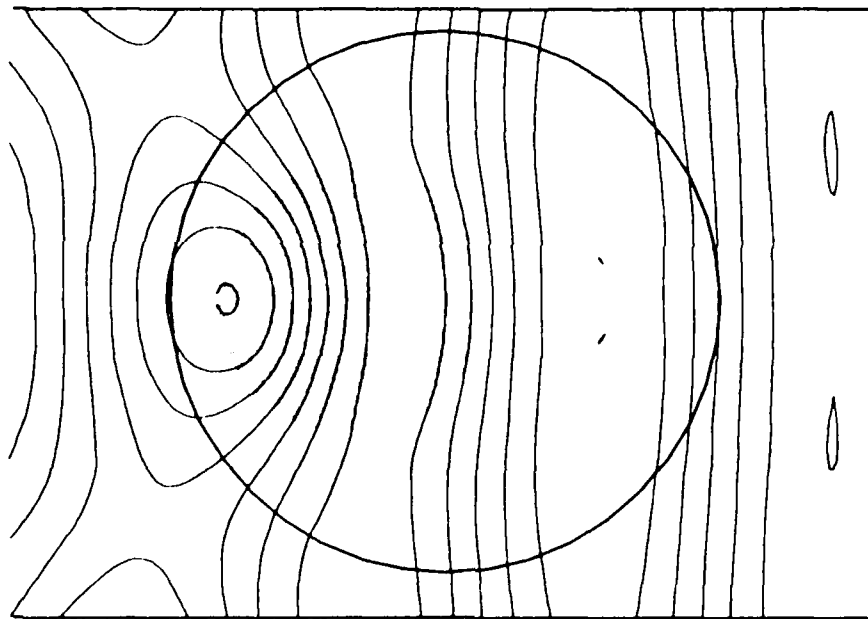
Figure 7-4: The far field pattern for refractive index = 2.0



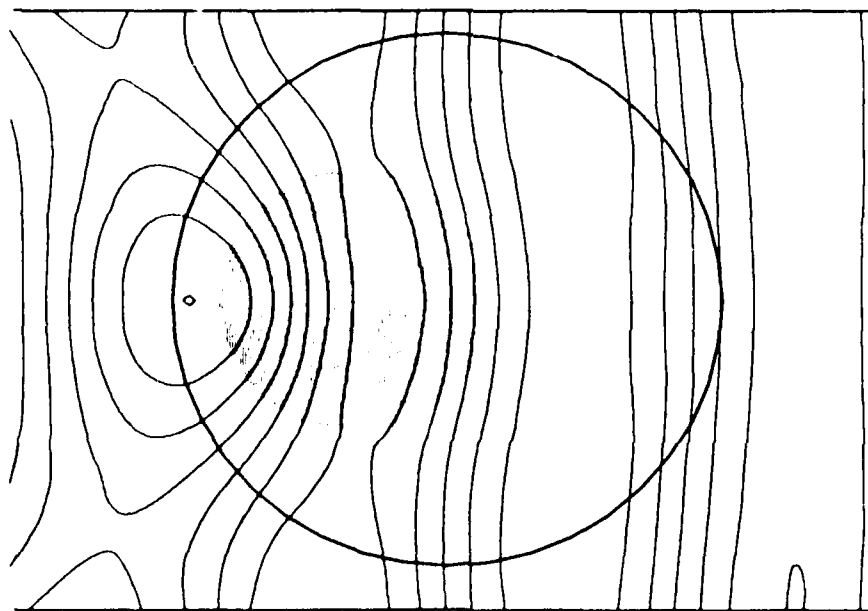
(a) time phase 0



(b) time phase 30

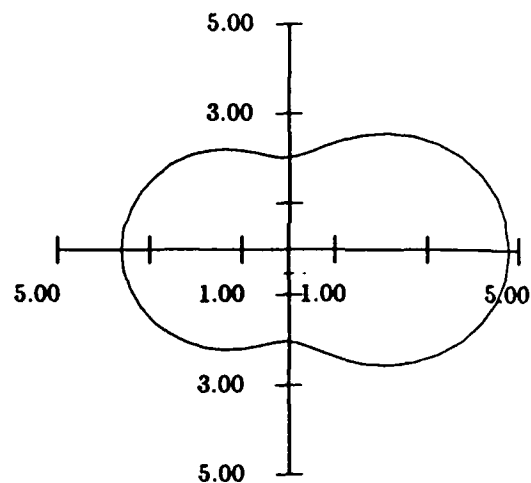
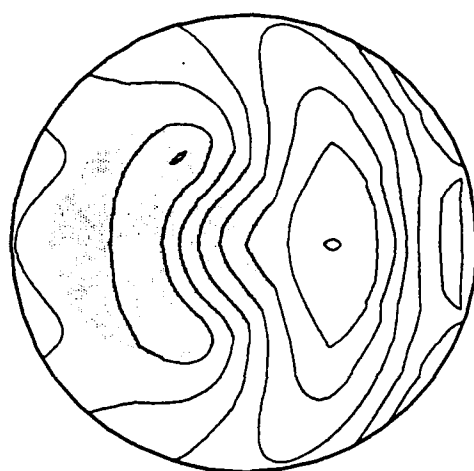


(c) time phase 60

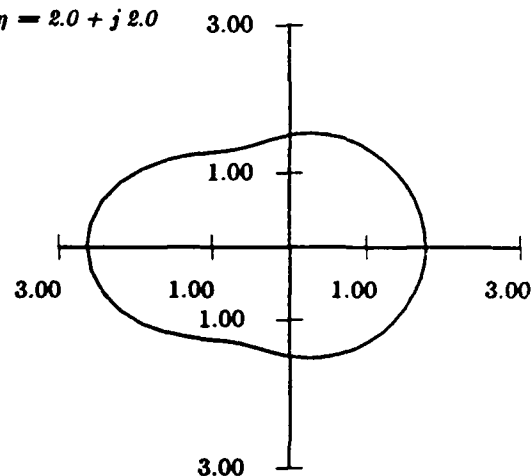
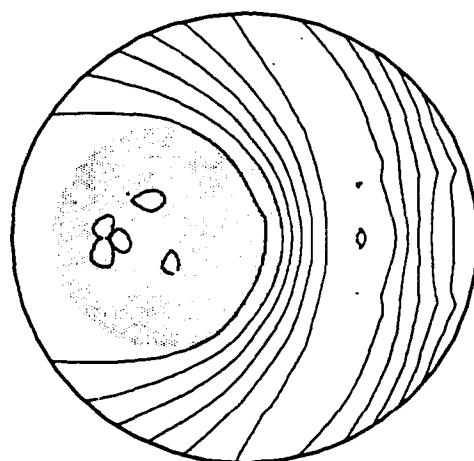


(d) time phase 90

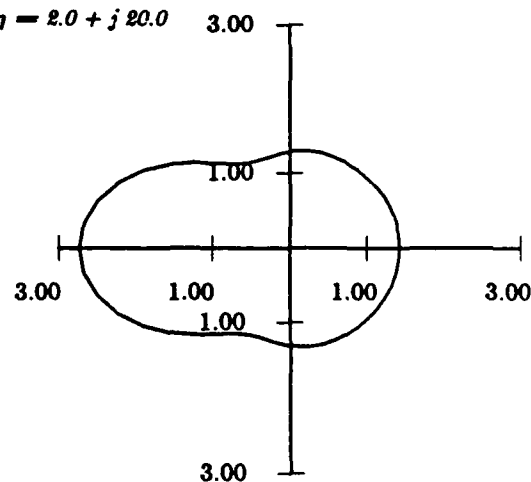
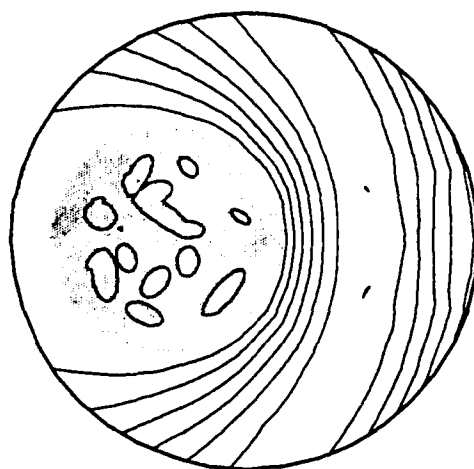
Figure 7-5: Equal line plots of E field for different time phases
(a) time phase 0° (b) time phase 30°
(c) time phase 60° (d) time phase 90°



(a) $\eta = 2.0 + j 2.0$

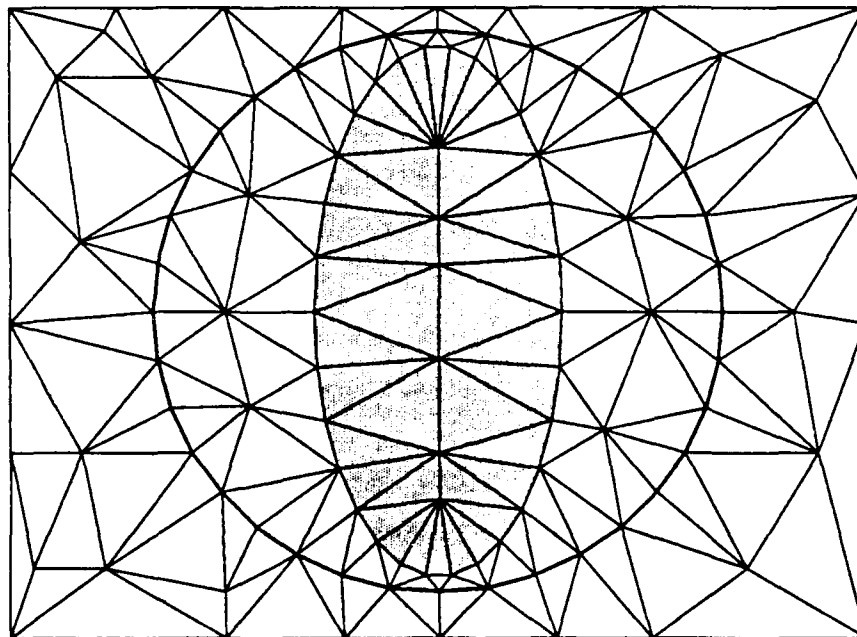
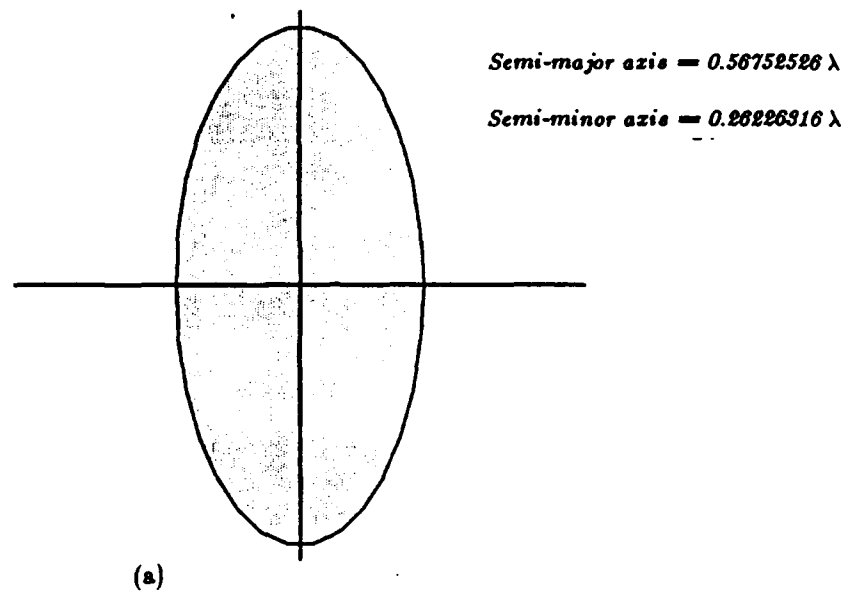


(b) $\eta = 2.0 + j 20.0$



(c) $\eta = 2.0 + j 200.0$

Figure 7-6: The intensity plots and the far field pattern plots for various refraction indexes.
(a) $2 + j 2$. (b) $2 + j 20$. (c) $2 + j 200$.



(b) Matrix size 214

Figure 7-7: Dielectric elliptic cylinder and the corresponding mesh

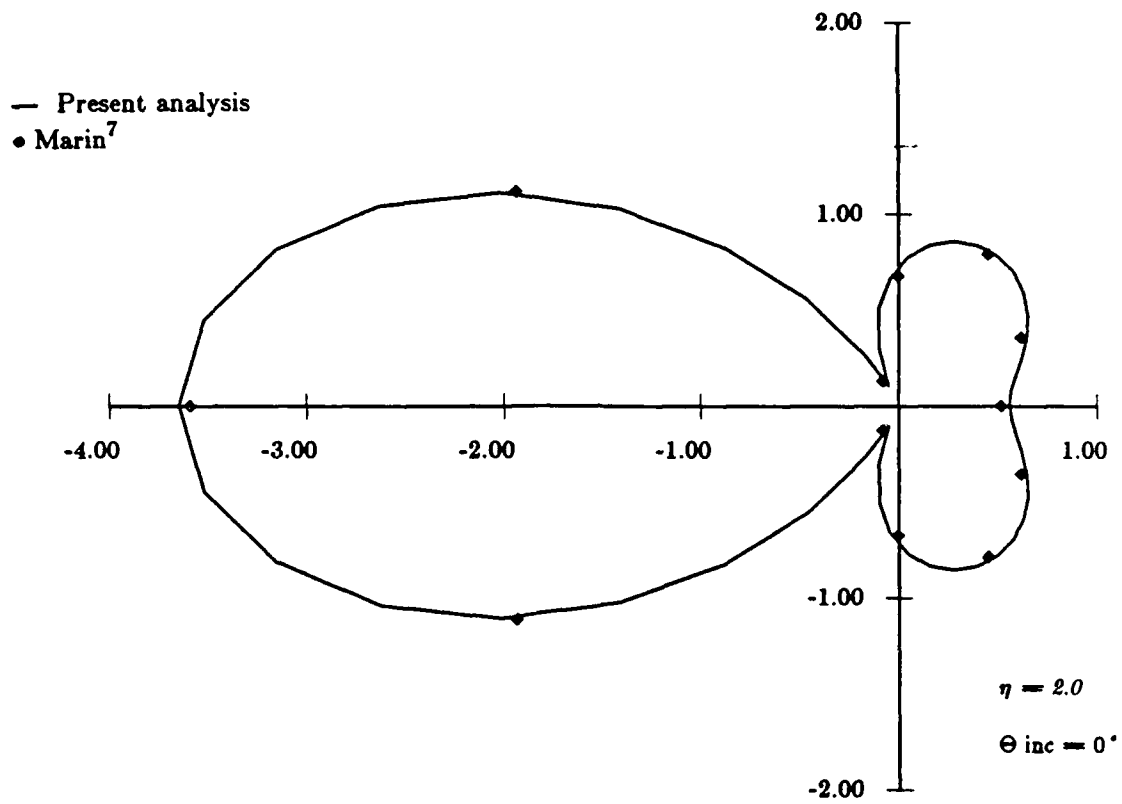
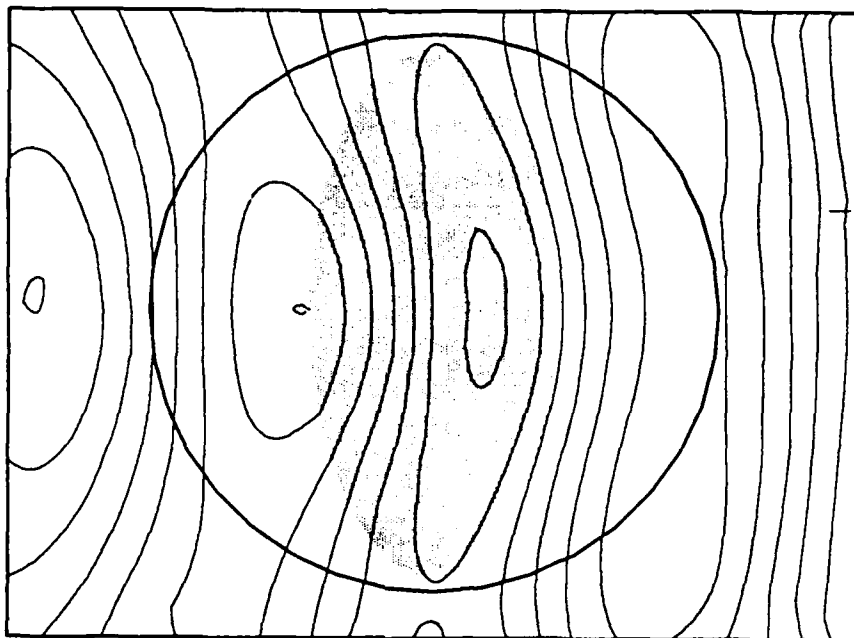
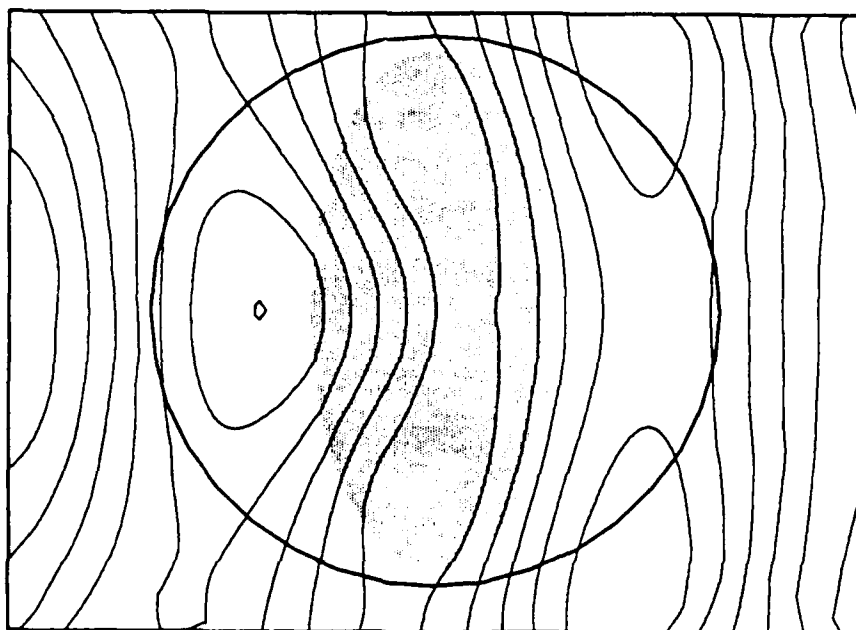
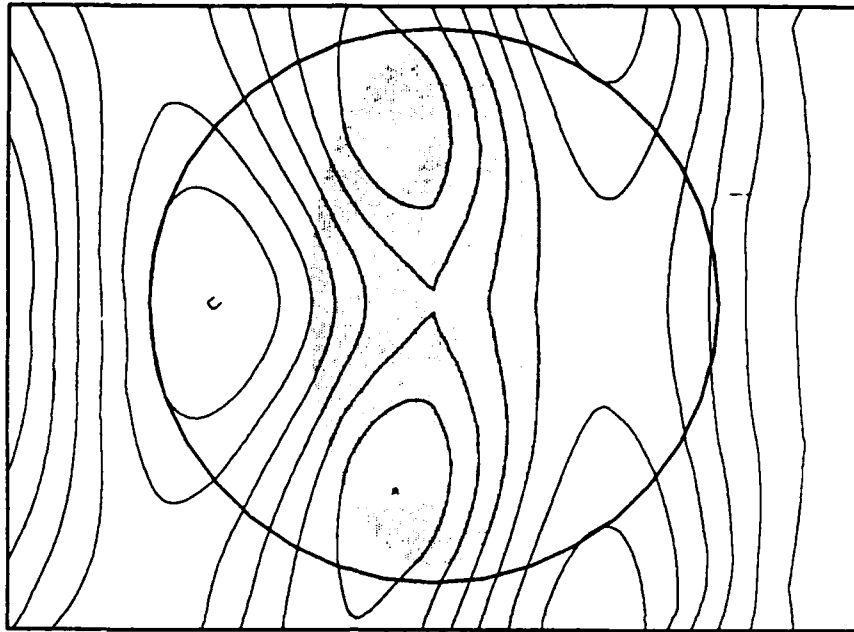
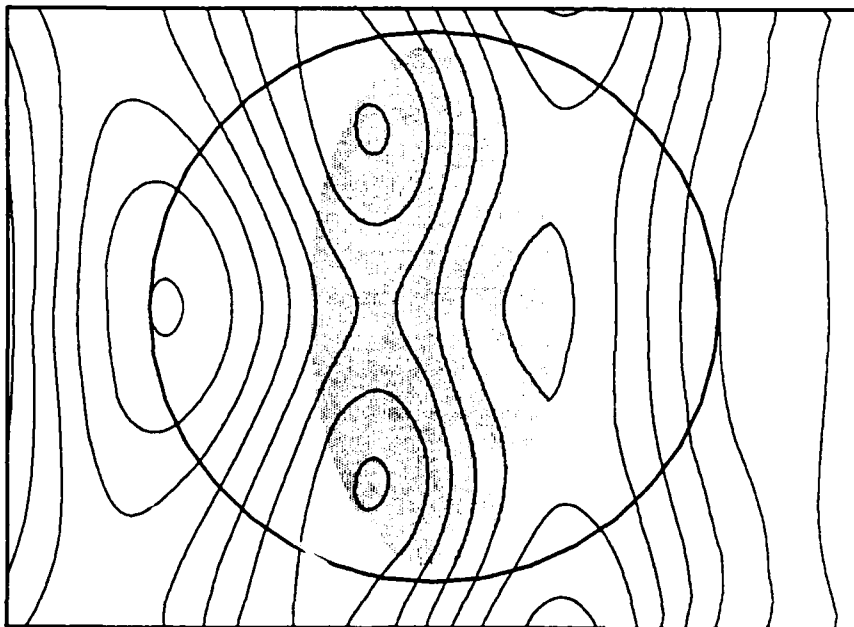


Figure 7-8: The far field pattern of plane wave scattered by the dielectric elliptic cylinder in Figure 7-7

(a) time phase 0° (b) time phase 30°

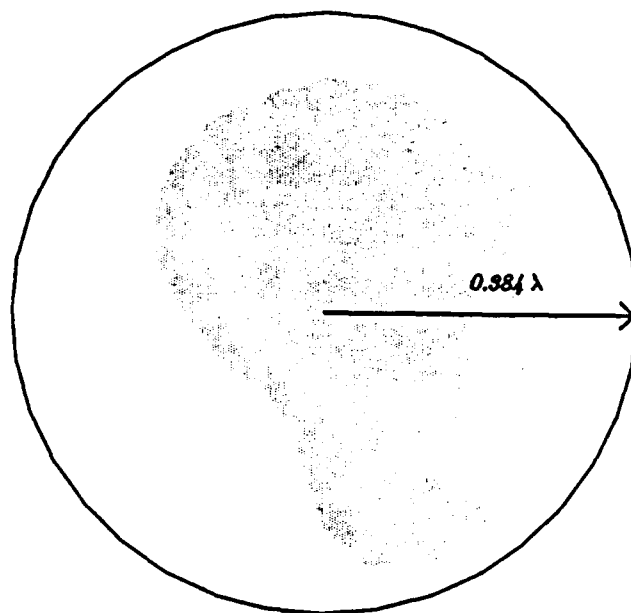


(c) time phase 60°

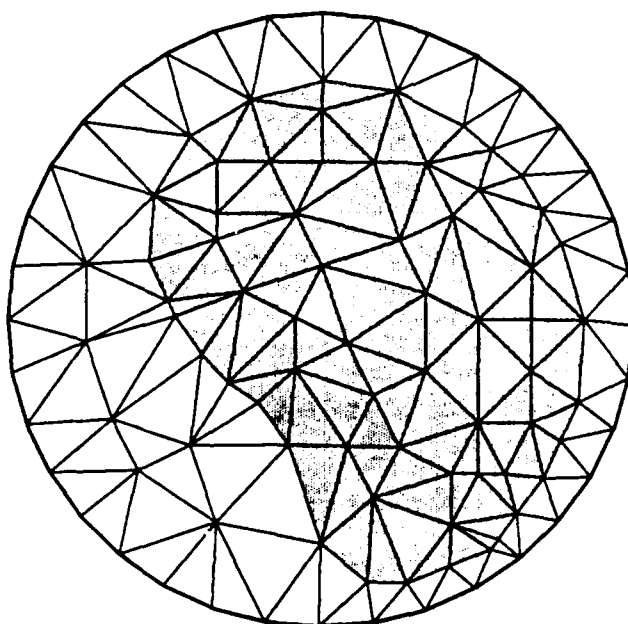


(d) time phase 90°

Figure 7-9: The equal line plots of electric field for different time phases



(a)



(b) mesh -- Matrix size 314

Figure 7-10: The geometry (a) and mesh (b) for a kidney-shaped scatterer

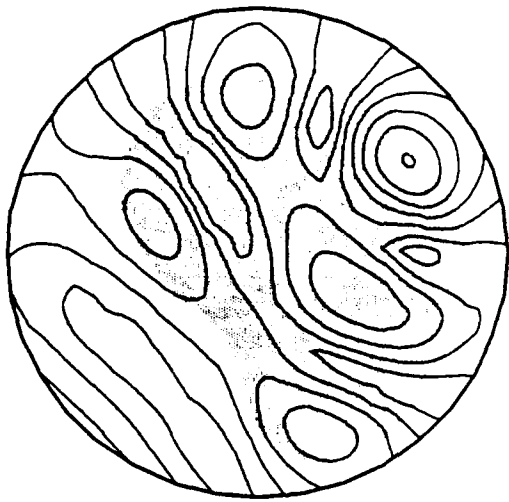
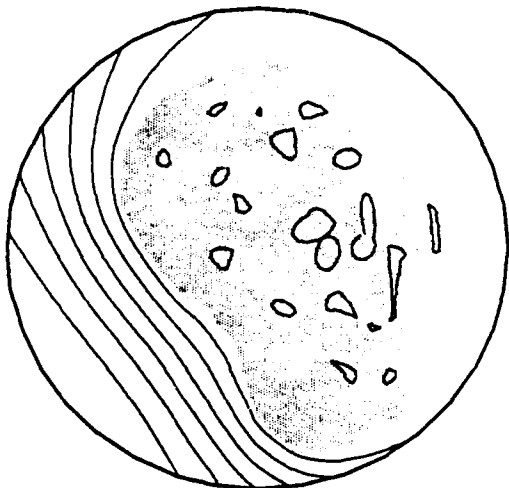
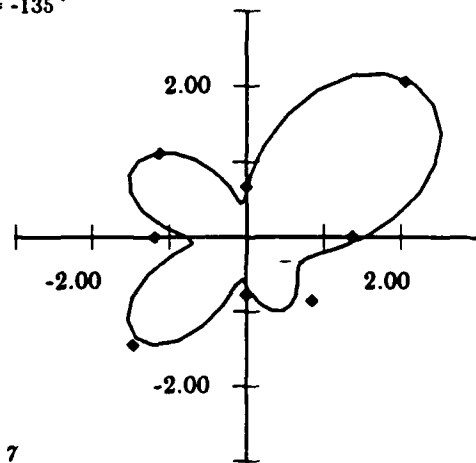
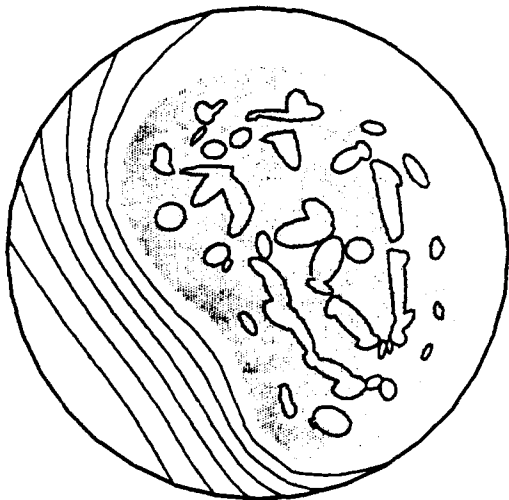
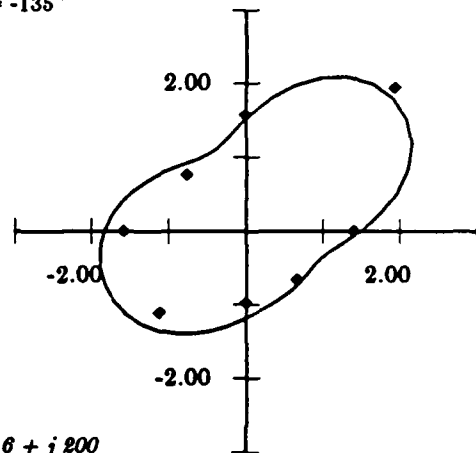
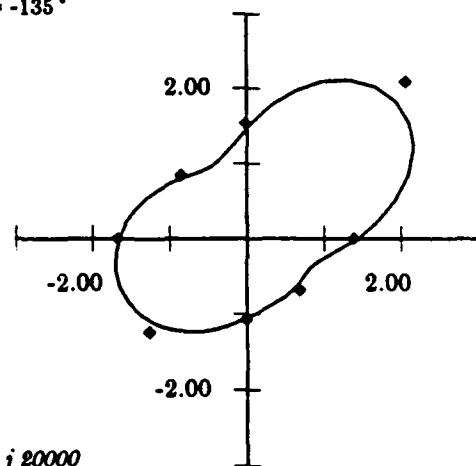
$\Theta_{inc} = -135^\circ$ (a) $\eta = 7$ $\Theta_{inc} = -135^\circ$ (b) $\eta = 6 + j 200$ $\Theta_{inc} = -135^\circ$ (c) $\eta = j 20000$ 

Figure 7-11: Intensity plots and far field pattern plots for different refraction indexes

REFERENCES

1. R. F. Harrington, *Fields Computation by Moment Methods*, The Macmillan Co., 1968.
2. P.J.B. Clarricoats and K.R. Slinn, "Numerical solutions of waveguide-discontinuity problems", *Proc. Inst. Elec. Eng.* 1967, pp. 878-887.
3. A. Wexler, "Solution of waveguide discontinuities by modal analysis", *IEEE Trans.*, Sept. 1967, pp. 508-516.
4. W.J. Cole, E.R. Nagelberg and C.M. Nagel, "Iterative solution of waveguide discontinuity problems", *Bell Syst. Tech. J.* 1967, pp. 649-722.
5. C.A. Muilwyk and J.B. Davies, "The numerical solution of rectangular waveguide junctions and discontinuities of arbitrary cross section", *IEEE Trans.*, Aug. 1967, pp. 450-454.
6. C.G. Montgomery, R.H. Dicke and E.M. Purcell, *Principles of Microwave Circuits*, McGraw-Hill, New York, 1948.
7. Samuel P. Marin, "Computing Scattering Amplitudes for Arbitrary Cylinders Under Incident Plane Waves", *IEEE Trans.*, Nov. 1982, pp. 1045-1049.
8. M. Koshiha, K. Hayota and M. Suzuki, "Improved Finite-Element Formulation in Terms of the Magnetic Field Vector for Dielectric Waveguides", *IEEE Trans.*, Vol. MTT-33, Mar. 1985, pp. 227-233.
9. P. Silvester and M.S. Hsieh, "Finite-element solution of 2-dimensional exterior field problems", *Proc. Inst. Elec. Eng.*, Dec. 1971, pp. 1743-1747.
10. B. H. McDonald and A. Wexler, "Finite-Element Solution of Unbounded Field Problems", *IEEE Trans.*, Dec. 1972, pp. 841-847.
11. She-Kong Chang and K.K. Mei, "Application of the Unimoment Method to Electromagnetic Scattering of Dielectric Cylinders", *IEEE Trans.*, Jan. 1976, pp. 35-42.
12. Peter Bettess, "Infinite Element", *International Journal for Numerical Methods in Engineering*, 1977, pp. 53-63.
13. P.P. Silvester, D.A. Lowther, C.J. Carpenter, "Exterior finite elements for two dimensional field problems with open boundaries", *Proc IEE*, 1977, pp. 1267-1270.
14. G. Dasgupta, "Computation of Exterior Potential Fields by Infinite Substructuring", *Computer Methods in Applied Mechanics and Engineering*, 1984, pp. 295-305.
15. H. Hurwitz, Jr., "Tests of a nonlinear matrix equation formulation of infinitesimal scaling", *General Electric Corporate Research and Development Report 89CRD084*, May 1983.
16. H. Hurwitz, "Application of infinitesimal scaling to finite element analysis", *General Electric Corporate Research and Development Report 89CRD085*, May 1983.
17. H. Hurwitz, Jr., "Infinitesimal Scaling - A new Procedure for Modeling Exterior Field problems", *IEEE Trans. Magnetics*, Sep. 1984, pp. 1918-1923.
18. G. Strang and G.J. Fix, *An Analysis of the Finite Element Method*, Prentice-Hall, NJ., 1973.

19. P.P. Silvester and R.L. Ferrari, *Finite Elements for Electrical Engineers*, Cambridge, London, 1983.
20. Z. J. Cendes, D. N. Shenton and H. Shahnasser, "Magnetic Field Computation Using Delaunay Triangulation and Complementary Finite Element Methods", *IEEE Transaction*, 1983, pp. 2551-2554.
21. C.L. Lawson, *Software for C1 Surface Interpolation*, Academic press, New York, 1977.
22. Z.J. Cendes, "Solution of Dielectric Loaded Waveguides By Finite Element Methods", Master's thesis, McGill University, March 1970.
23. L. Lewin, *Advanced Theory of Waveguides*, Iliffe and Sons, London, 1951.
24. N. Marcuvitz, *Waveguide Handbook*, McGraw-Hill, New York, 1951.
25. D. M. Kerns, "Half-round inductive obstacles in rectangular waveguide", *J. Research NBS*, April-June 1960, pp. 113-130.
26. G. H. Golub and C. F. Van Loan, *MATRIX Computation*, , .
27. E. C. Jordan and K. G. Balmain, *Electromagnetic Waves and Radiating Systems*, Prentice-Hall, 1968.
28. W. T. Scott, *The Physics of Electricity and Magnetism*, Wiley, New York, 1966.
29. R. C. Weast, *Handbook of Chemistry and Physics*, The Chemical Rubber Co., 48th ed. Cleveland OH, 1967.

APPENDIX F - AN ADAPTIVE SPECTRAL RESPONSE MODELING PROCEDURE FOR ELECTROMAGNETIC SCATTERING

ABSTRACT

An adaptive scheme is proposed to generate the spectral response of waveguide junctions in minimum computation time. The procedure uses the newly developed transfinite element method to determine the fields in junctions at a few adaptively selected frequencies and then employs these solutions to generate the spectral response throughout the frequency range of interest. In typical problems, the method converges in five or six iterations to the full spectral response evaluated at one hundred points. We show by solving example problems that the new procedure is orders of magnitude faster than the alternatives.

INTRODUCTION

Microwave circuits in use today often employ planar geometries that may be represented mathematically as an N -port microwave junction. An N -port microwave junction is, in general, defined as a structure that consists of an arbitrarily shaped cavity, with or without dielectrics, and has N rectangular ports coupling in and out of the cavity. A number of studies have been made of microwave junction problems^{1,2,3,4}. However, the classical analyses have been largely confined to networks of simple shape or of geometry that lends itself to analytical or semi-analytical methods of solution.

The highly complex geometries used in microwave circuits today makes it necessary to use numerical methods for analysis. Multi-port microwave junctions are solved numerically in the literature by using one of two approaches: the eigensolution method^{5,6} and the deterministic method^{7,8,9}. In the eigensolution method, either the finite element method or the finite difference method is used to compute the eigenvalues and the eigenvectors of the normal modes of the junction, and then circuit theory is used to determine the circuit parameters¹⁰. In the deterministic method, the field solution is computed at a single specified frequency and scattering parameters computed at that frequency only; the entire process must be repeated to determine the solution at other frequencies.

While the eigensolution method is mathematically elegant, it has the disadvantage of requiring the solution of large matrix eigenvalue equations. Since the solution of matrix eigenvalue problems is expensive, recent work has focused on the deterministic approach that requires the solution of deterministic

matrix equations only^{7,8}. Recently, Webb⁸ has used finite element method for the analysis of *H*-plane rectangular waveguide problems. In his procedure, a set of boundary value problems is solved in order to get the field solution at a single frequency point. Two similar procedures have been developed by Konshiba. In Reference 7, the boundary element is combined with modal analysis to solve waveguide discontinuity problems and the finite element method is combined with modal analysis to solve for fields in an *H*-plane waveguide circulator in Reference 9. Unfortunately, however, both of these procedures result in non-symmetric matrix equations that are expensive to solve.

In this paper, we introduce a new, highly efficient procedure for modeling *N*-port waveguide junctions. The basis of the procedure is the transfinite element method^{11,12} in which modal basis functions are combined with finite element basis functions to provide solutions for open boundary problems. This procedure results in symmetric sparse matrix equations that can be solved very efficiently by using the preconditioned bi-conjugate gradient algorithm. Further, we develop a spectral response estimation procedure by which solutions at a few adaptively selected frequencies are used to generate the full solution in the frequency range of interest.

Numerical results are given for a *T*-junction, a screen filter containing *E*-plane metal inserts and a dielectric filter to show the validity of the present procedure. A comparison of the computation times required by the adaptive procedure and by the direct deterministic procedure for the *T*-junction problem is also presented.

FORMULATION

THE TRANSFINITE ELEMENT METHOD

The structure to be analysed consists of a cavity coupled with *N* rectangular waveguides. The shape of the cavity and the dimensions of the waveguides are arbitrary, but the overall structure must be uniform so that the problem can be approximated by two-dimensional analysis. To simplify the formulation, we assume that the junction is in the *H*-plane: problems involving *E*-plane junctions can be treated in much the same way. Microwave planar circuit problems differ only in that the electric field is taken to be a constant perpendicular to the plane of the circuit and that regions of different dielectric constant are seldom used.

Consider exciting port 1 by the dominant TE_{10} mode. The field over the cavity region Ω_1 and the port regions extending to infinity must satisfy the Helmholtz equation:

$$\begin{aligned} \nabla^2 E + k^2 \epsilon_r E &= 0 \\ k^2 &= \omega^2 \epsilon_0 \mu_0 \end{aligned} \quad (1)$$

where ω is the angular frequency of the excitation, ϵ_0 and μ_0 are the permittivity and the permeability of the free space, respectively, and ϵ_r is the relative dielectric constant of the material.

In the transfinite element method^{11,12}, the problem region is divided into two parts. An interior region Ω_i of finite extent and an exterior region Ω_e that is homogeneous and unbounded. Within Ω_i finite element basis functions are used to approximate the field; in Ω_e analytical solutions of the Helmholtz equation provide a basis set for the field. Employing both sets of basis functions in a variational procedure and requiring continuity along the boundary between Ω_i and Ω_e gives a symmetric matrix equation that is solved for the field.

The application of the transfinite element method to multi-port microwave circuits is presented in Reference 12. In this procedure, Equation (1) is converted into the matrix equation

$$([\hat{S}] - k^2 [\hat{T}] + [\hat{\gamma}]) \tilde{\psi} = -\tilde{f} + k^2 \tilde{g} \quad (2)$$

where $[\hat{S}]$ and $[\hat{T}]$ are complex symmetric matrices, $[\hat{\gamma}]$ is a diagonal matrix, $\tilde{\psi}$ is the solution vector, k is the wavenumber, and \tilde{f} and \tilde{g} are known vectors.

With respect to spectral modeling, we note that the matrices $[\hat{S}]$ and $[\hat{T}]$ and the vectors \tilde{f} and \tilde{g} are frequency independent and can be computed once and stored for any problem geometry. Only the wavenumber k and the matrix $[\hat{\gamma}]$ depend on frequency. However, since $[\hat{\gamma}]$ is a diagonal matrix with only N times M non-zero entries, where N is the number of ports in the circuit and M is the number of basis functions used to approximate the fields in each port, it requires very little work to compute $[\hat{\gamma}]$.

Figure 1 provides the transfinite element solution of a microwave T-junction at 3 GHz.

SPECTRUM MODELING

In designing microwave components, the frequency response over a given frequency range is often required. With the deterministic approach in which Equation (1) is solved at a given frequency, Equation (2) must be solved L times to get L points on the spectrum. For problems where the response changes very quickly, the number of points L used to generate the spectrum must be large in order to get satisfactory answers. The adaptive scheme proposed here for modeling the spectral response is best explained by referring to Figure 2. Instead of solving Equation (2) L times, we solve the matrix equation at a few adaptively selected optimal frequencies and then use these solutions as basis functions to generate the entire spectral response.

A preliminary illustration of the procedure is as follows: In Figure 2(a), the three-port junction of Figure 1 is solved by using the transfinite element method at the two limiting frequencies indicated by the dots near the horizontal axis. These two solutions are then used as basis functions to generate a crude spectral response curve throughout the region of interest. This is plotted as solid lines in Figure 2(a). Next, we compute the error in the solution throughout the frequency range by substituting the crude solution values into the governing equations for the system and by evaluating the residual. As explained below, this may be done very efficiently. We then solve the system once again using the transfinite element algorithm at the frequency that gave the maximum residual on the last pass. The new dot in Figure 2(b) shows the location of this solution as well as the new spectral response curve computed by using the three transfinite element solutions as basis functions. This process is repeated for six iterations in Figure 2 until the error in the entire spectral response curve is within acceptable limits. As is evident from Figure 2(f), the procedure converges to the solution given in Reference 4, but as shown below, in much less computer time.

THE ADAPTIVE ALGORITHM

To develop the adaptive spectral response modeling algorithm, first approximate the solution $\tilde{\Psi}$ of Equation (2) at an arbitrary frequency ω by a linear combination of the basis functions $\tilde{\Psi}_i$,

$$\tilde{\Psi}(\omega) = \sum_{i=1}^n a_i(\omega) \tilde{\Psi}_i \quad (3)$$

where n is the number of basis functions and a_i are unknown coefficients. The basis functions $\tilde{\Psi}_i$ are taken to be the solutions of (2) at n specified frequencies ω_i . Substituting Equation (3) into (2) gives

$$([\hat{S}] - k^2[\hat{T}] + [\hat{\gamma}]) \cdot \sum_{i=1}^n a_i(\omega) \tilde{\psi}_i = -\tilde{f} + k^2 \tilde{g} \quad (4)$$

Since $[\hat{S}]$, $[\hat{T}]$, \tilde{f} , and \tilde{g} are frequency independent, we can rewrite Equation (4) as

$$\sum_{i=1}^n a_i(\omega) (\tilde{\phi}_i - k^2 \tilde{\phi}_i + [\hat{\gamma}] \cdot \tilde{\psi}_i) = \tilde{f} - k^2 \tilde{g} \quad (5)$$

where

$$\begin{aligned} \tilde{\phi}_i &= [\hat{S}] \cdot \tilde{\psi}_i \\ \tilde{\phi}_i &= [\hat{T}] \cdot \tilde{\psi}_i \end{aligned} \quad (6)$$

Now applying the method of least-squares to Equation (5) leads to the following matrix equation for the coefficients a_i

$$([A] - k^2[B] + k^4[C] + [D]) \tilde{a} = \tilde{F} - k^2 \tilde{G} + k^4 \tilde{H} + \tilde{\gamma} \quad (7)$$

where

$$\begin{aligned}
A_{ij} &= \phi_i^* \phi_j \\
B_{ij} &= \phi_i^* \phi_j + \phi_i^* \phi_j \\
C_{ij} &= \phi_i^* \phi_j \\
D_{ij} &= \phi_i^* [\hat{\gamma}] \phi_j - \phi_i^* [\hat{\gamma}]^* \phi_j - k^2 (\phi_i^* [\hat{\gamma}] \phi_j + \phi_i^* [\hat{\gamma}]^* \phi_j) + \phi_i^* [\hat{\gamma}] [\hat{\gamma}] \phi_j \\
F_i &= \phi_i^* \tilde{f} \\
G_i &= \phi_i^* \tilde{f} + \phi_i^* \tilde{g} \\
H_i &= \phi_i^* \tilde{g} \\
d_i &= \phi_i^* [\hat{\gamma}]^* \tilde{f} - k^2 \phi_i^* [\hat{\gamma}]^* \tilde{g}
\end{aligned}$$

(8)

Notice that in (8), only the matrix $[D]$ and the vector \tilde{d} depend on the frequency ω . The computation time for evaluating $[D]$ and \tilde{d} for each frequency is negligible because $[\hat{\gamma}]$ is a diagonal matrix. Matrix Equation (7) is therefore trivial to set up and it is inexpensive to solve since it is only of order n .

The residual associated with the frequency ω after solving for the coefficients $a_i(\omega)$ is evaluated as follows

$$\tilde{r} = \tilde{f} - k^2 \tilde{g} - \sum_{i=1}^n a_i(\omega) (\phi_i^* - k^2 \phi_i^* + [\hat{\gamma}] \psi_i)$$

(9)

The norm of the residual is given by

$$|r(\omega)| = (\tilde{r}^* \cdot \tilde{r})^{1/2}$$

(10)

The entire adaptive solution process is presented in the flowchart in Figure 3. First, input the desired frequency limits ω_p , ω_g and L , the number of equal divisions in the frequency range to be used. Next solve (2) at the two limiting frequencies to generate the basis functions $\tilde{\psi}_1$, $\tilde{\psi}_2$ and the auxiliary functions $\tilde{\phi}_1$, $\tilde{\phi}_2$, $\tilde{\phi}_1$, $\tilde{\phi}_2$. From the basis functions and the auxiliary functions, compute the components of matrices $[A]$, $[B]$, $[C]$ and of vectors \tilde{F} , \tilde{G} , \tilde{H} . Then generate L approximate solutions at the intermediate frequencies and compute the residue at each frequency to indicate the corresponding error. At the maximum residual, solve Equation (2) again and add the new solution to the basis set for generating the spectrum. Repeat the process until the maximum residual is smaller than the prescribed error tolerance η .

NUMERICAL RESULTS

Figures 4-5 provide examples of spectrum response obtained by using the new adaptive spectrum modeling procedure. The number of modes used in each port to generate the results is 3 for all of the problems shown. Solutions of Equation (2) are obtained in the computer program by using the preconditioned bi-conjugate gradient method and have relative residual L_2 norms smaller than $1.0e-5$. The error tolerance η employed is $1.0e-4$.

Figure 2 shows the convergence of the procedure for modeling the T-junction in Figure 1 throughout the frequency range of dominant mode propagation. The number of frequency points L used was 50, and the frequencies that are solved for and used as the basis functions in the procedure are indicated by dots on the axis. As shown in Figure 2, the procedure converges when $n = 6$. Comparing the final adaptivity produced spectral response with the boundary element deterministic solution of Reference 7 shows excellent agreement.

The analysis presented here is not limited to dominant mode propagation. Figure 4 shows the spectral response computed by the adaptive spectrum modeling procedure for the E-plane metal insert filter shown in Figure 4(f) from 30 GHz to 60 GHz. The number of frequency points used was 100 for the plots in Figure 4(a) - 4(e), and the procedure terminates in six iterations. A comparison of the final spectrum response with that obtained by the field expansion calculation in Reference 13 is given in Figure 4(e).

Figure 5(a) presents the adaptive solution of a waveguide dielectric filter modeled by Koshiba and Suzuki⁷. Here we used $L = 100$ spectral points; the total number of solved frequency points was only 5.

Figure 6 shows a comparison of the computer time required by the new procedure and that of the deterministic approach. The time for the deterministic approach is based on the total time needed to solve Equation (2). The times reported are for the T-junction problem using a DEC VAX 11/780 computer; the matrix size was 500 by 500.

CONCLUSIONS

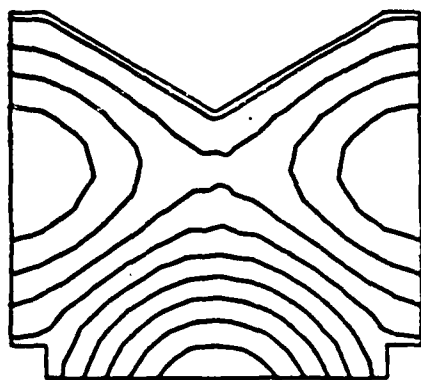
A very efficient procedure for determining the spectral response of microwave circuits has been developed. The procedure may be applied to waveguide junctions involving either E -plane or H -plane discontinuities or to microwave planar circuits. The spectral response evaluation procedure employs the transfinite element method to solve for the field at a few adaptively selected frequencies and then constructs the solution at any frequency by using the computed solutions as basis functions. In typical problems, only five or six transfinite element solutions are required to converge to the full spectral response evaluated at 100 points throughout the frequency range of interest.

In the past, there were two basic alternatives to computing the spectral response of microwave circuits: One could employ the eigensolution approach that required expensive eigenvalue problems to be solved but gave solutions at in-between frequencies very economically, or one could employ the existing deterministic approach that provided solutions at a specified frequency relatively efficiently but had to be reapplied at every frequency of interest. The new spectral response modeling procedure combines the advantages of both approaches and gives the full spectral response in orders of magnitude less computing time than the alternatives.

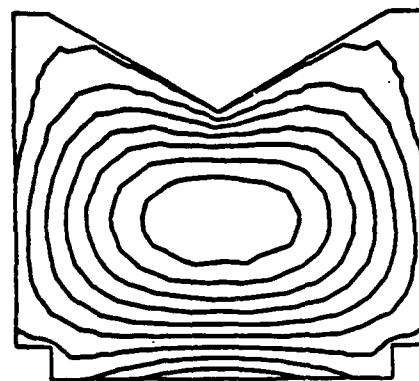
REFERENCES

1. C. G. Montgomery, R. H. Dicke and E. M. Purcell, *Principles of Microwave Circuits*, McGraw-Hill, New York, 1948.
2. N. Marcuvitz, *Waveguide Handbook*, McGraw-Hill, New York, 1951.
3. D. M. Kerns, "Half-Round Inductive Obstacles in Rectangular Waveguide", *J. Research NBS*, April-June 1960, pp. 113-130.
4. H. Schmiedel and F. Arndt, "Field Theory Design of Rectangular Waveguide Multiple-Slot Narrow-Wall Couplers", *IEEE Trans. Microwave Theory Tech.*, Vol. MTT-34, July 1986, pp. 791-797.
5. P. Silvester, "Finite Element Analysis of Planar Microwave Networks", *IEEE Trans. Microwave Theory Tech.*, Vol. MTT-221, February 1973, pp. 104-108.

6. G. D'Inzeo, F. Giannini, C. M. Sodi, and R. Sorrentino, "Method of Analysis and Filtering Properties of Microwave Planar Networks", *IEEE Trans. Microwave Theory Tech.*, Vol. *MTT-26*, July 1987, pp. 462-471.
7. M. Koshiha and M. Suzuki, "Application of the Boundary-Element Method to Waveguide Discontinuities", *IEEE Trans. Microwave Tech.*, Vol. *MTT-34*, February 1986, pp. 301-307.
8. J. P. Webb and S. Parihar, "Finite Element Analysis of H-Plane Rectangular Waveguide Problems", *IEEE Proceedings*, Vol. *133*, Pt. H, April 1986, pp. 91-94.
9. M. Koshiha and M. Suzuki, "Finite-Element Analysis of H-Plane Waveguide Junction with Arbitrarily Shaped Ferrite Post", *IEEE Trans. Microwave Theory Tech.*, Vol. *MTT-34*, January 1986, pp. 103-109.
10. P. P. Civalleri and S. Ridella, "Impedance and Admittance Matrices of Distributed Three-Layer N-Ports", *IEEE Trans. Circuit Theory*, Vol. *CT-17*, August 1970, pp. 392-398.
11. J. F. Lee and Z. J. Cendes, "Transfinite Elements - A Highly Efficient Procedure for Modeling Open Field Problems", *J. of Applied Physics*, accepted for publication.
12. J. F. Lee and Z. J. Cendes, "Transfinite Element Analysis of Multi-Port Microwave Networks", *IEEE Trans. on Microwave Theory Tech.*, submitted.
13. F. Arndt, J. Beike, D. Grauerholz, C. Lingemann and J. Bornemann, "E-Plane Integrated Parallel-Strip Screen Waveguide Filters", *IEEE Trans. Microwave Theory Tech.*, Vol. *MTT-33*, July 1985, pp. 654-659.



(a)



(b)

Figure 1: Transfinite Element Solution of a Microwave T-Junction at (a) Real Part of the Constant E Field, (b) Imaginary Part.

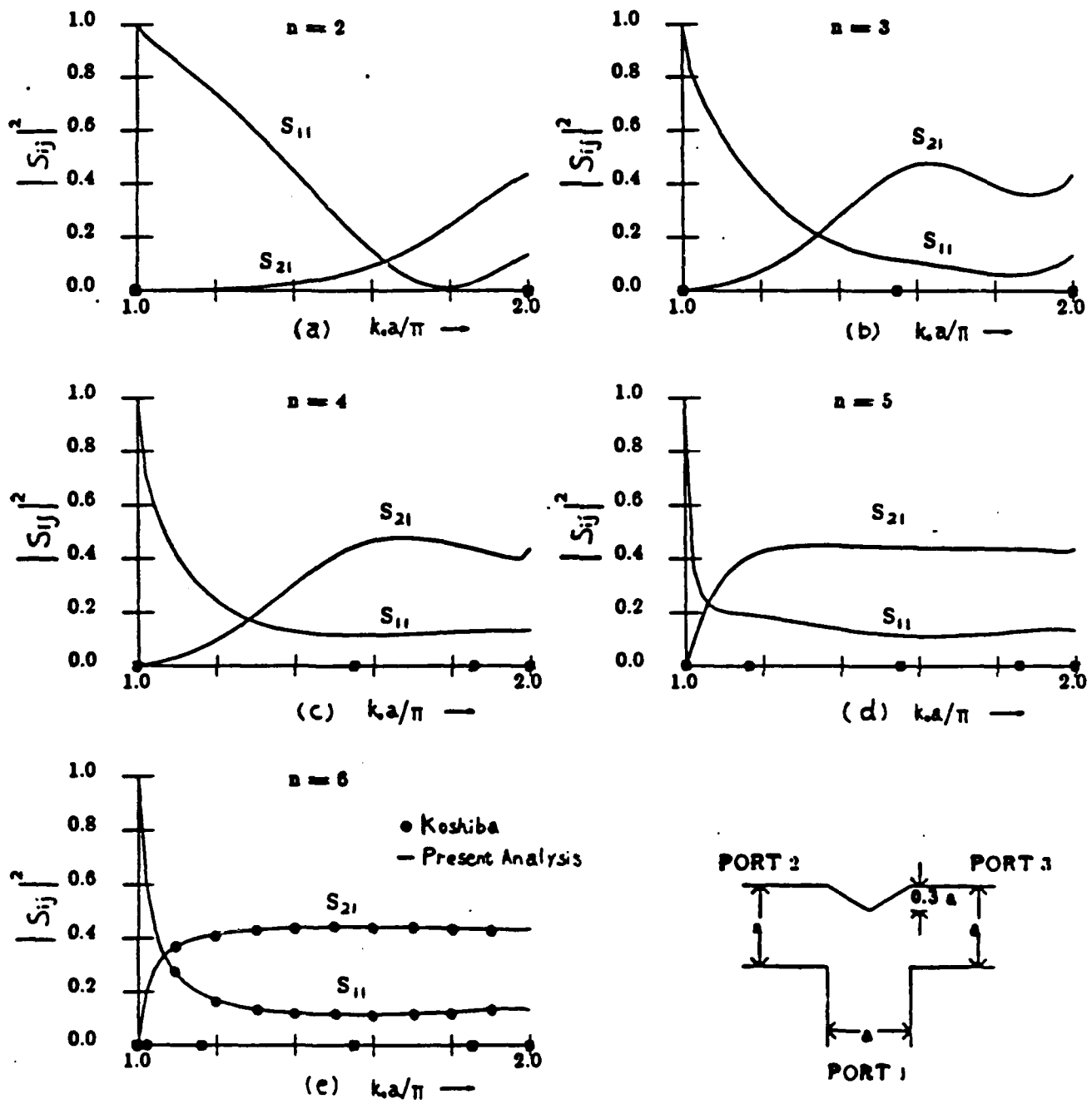


Figure 2: Power Reflection and Transmission Coefficients of the T-Junction in Figure 1.

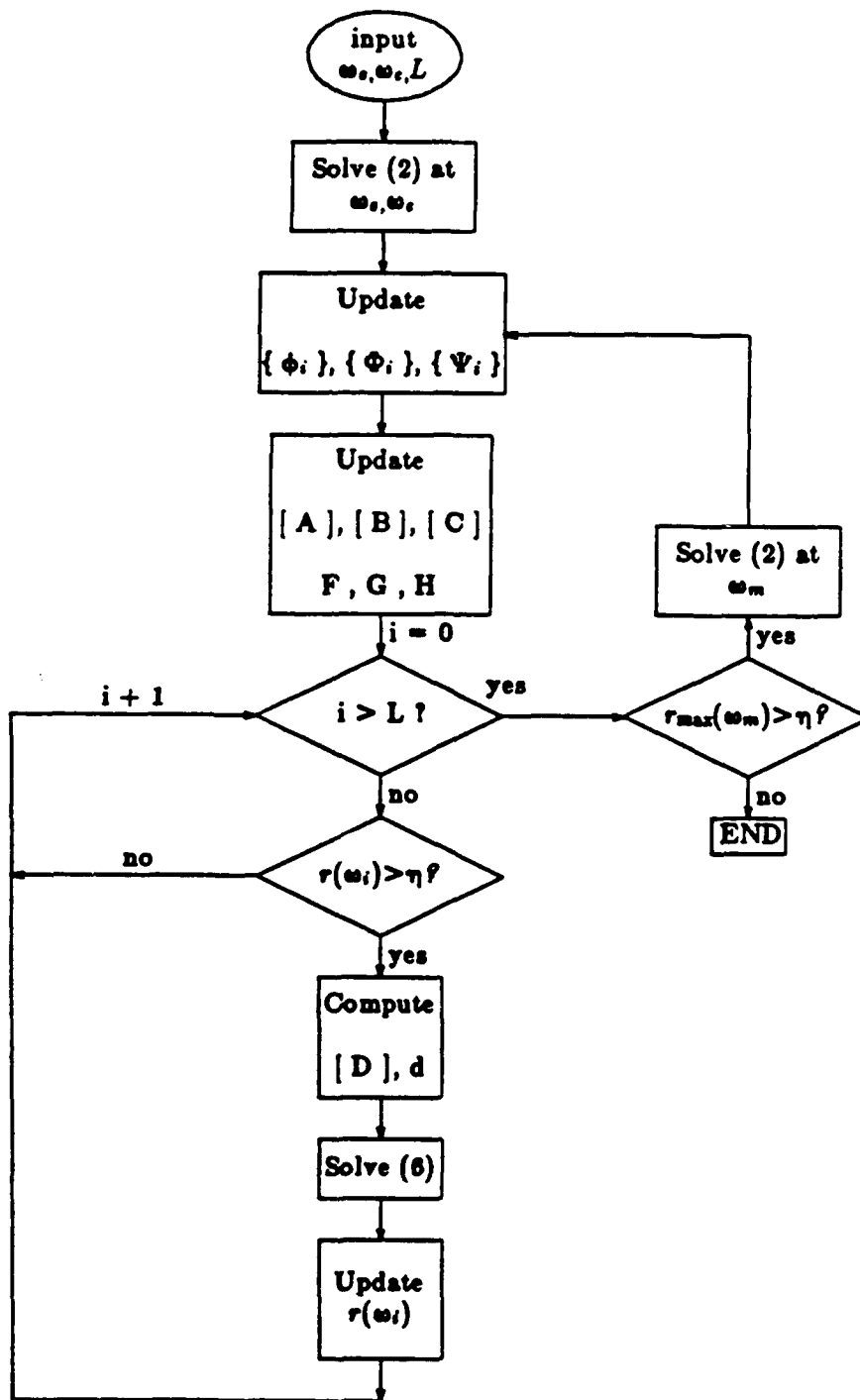


Figure 3: Flow Chart of the Adaptive Spectrum Modeling Procedure.

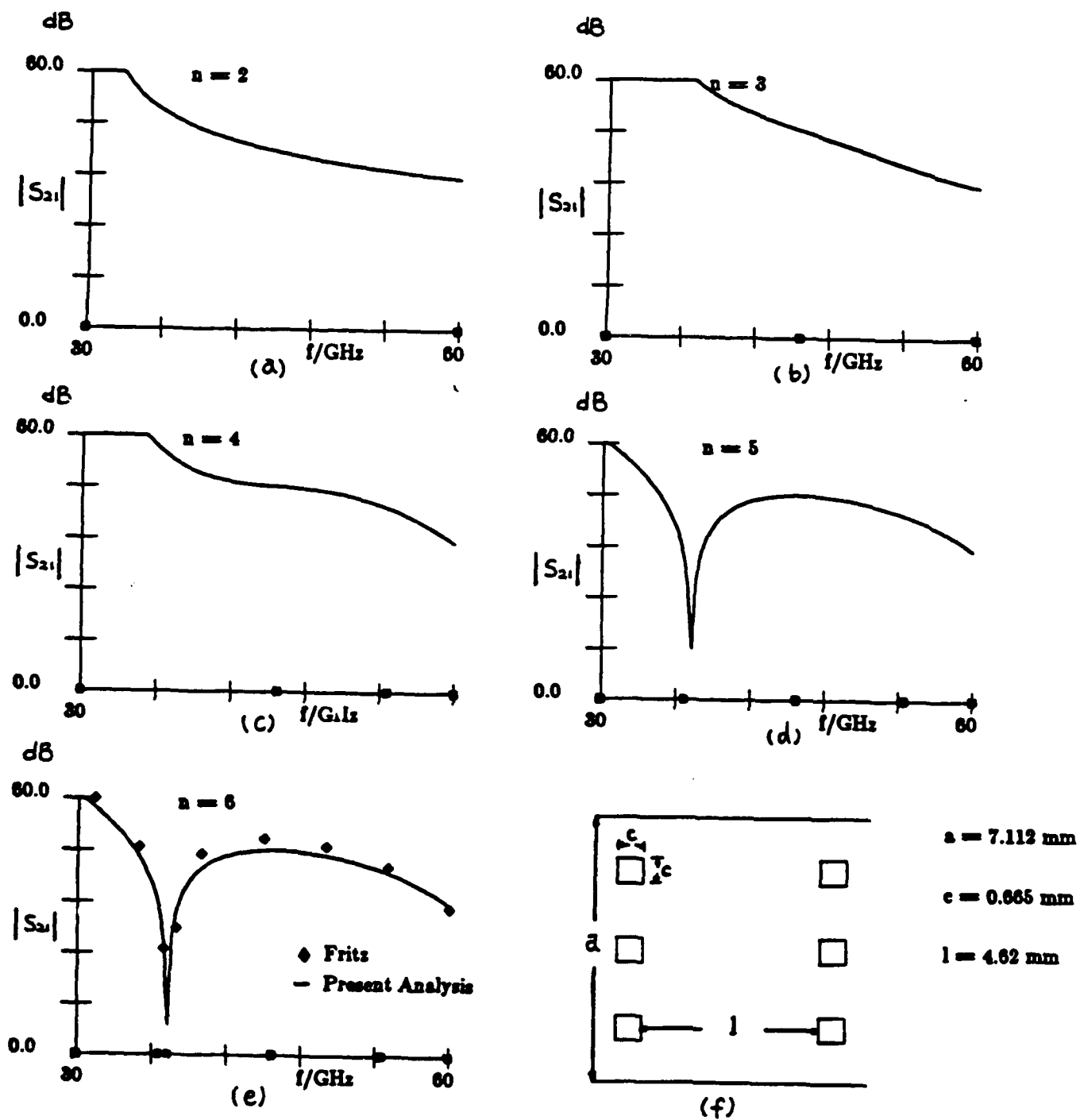


Figure 4: Power Transmission Coefficient of an *E*-Plane Integrated Screen Filter.

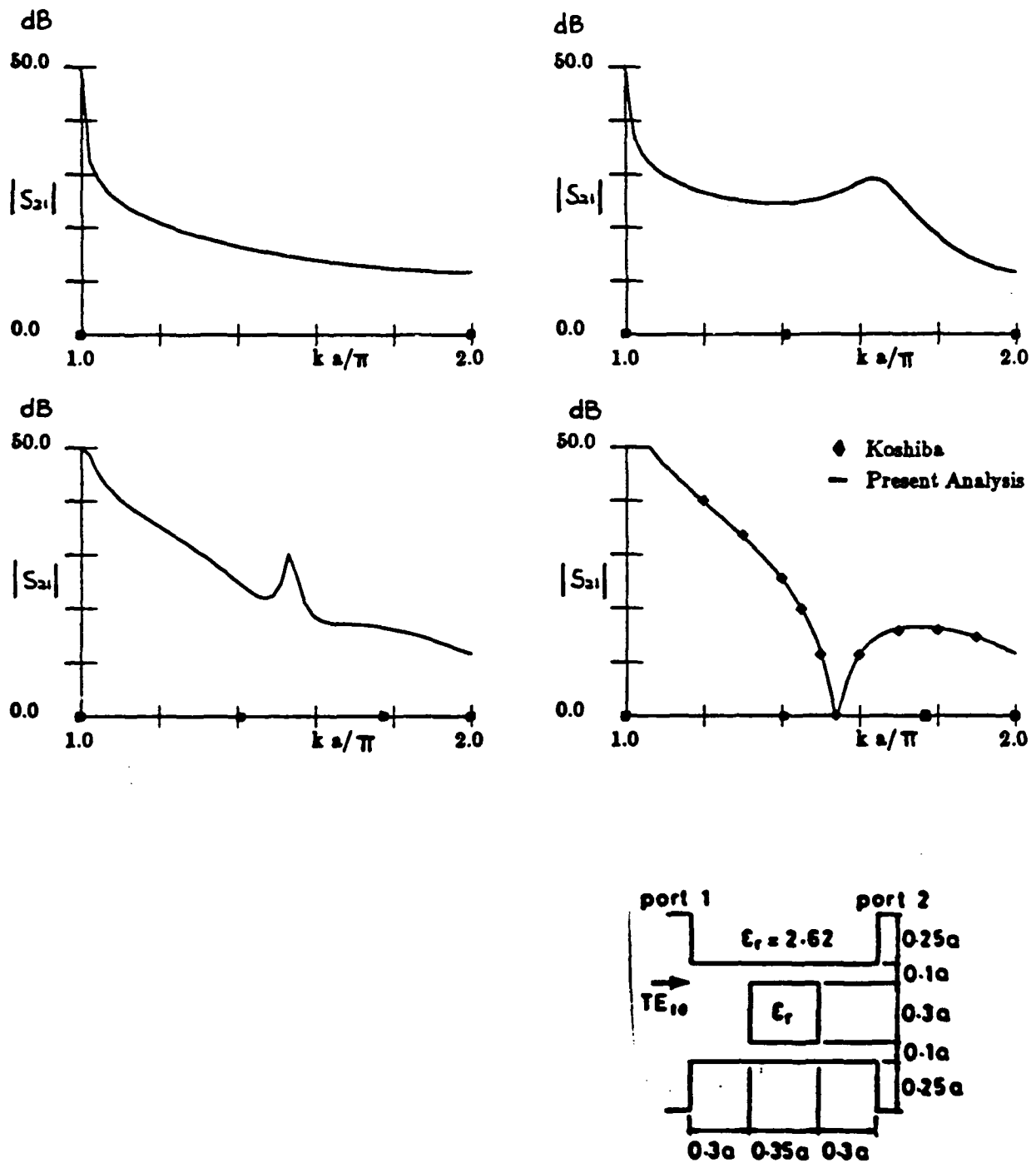


Figure 5 : Power Transmission Coefficient of a Waveguide Dielectric Filter.

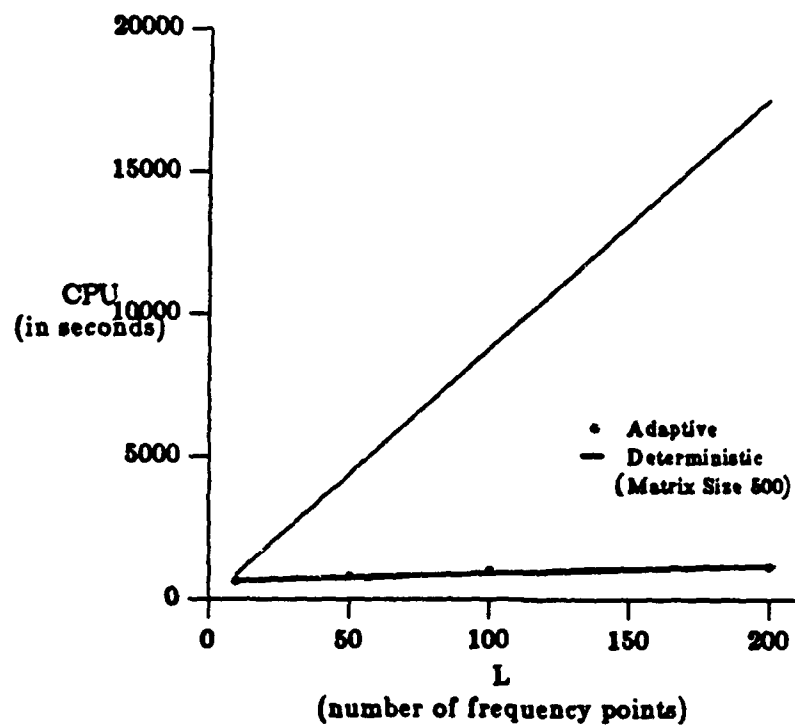


Figure 6: Comparison of the Computer Time Required to Solve a 500 by 500 System Using the Adaptive Modeling Procedure with Deterministic Approach.



MISSION of Rome Air Development Center

RADC plans and executes research, development, test and selected acquisition programs in support of Command, Control, Communications and Intelligence (C³I) activities. Technical and engineering support within areas of competence is provided to ESD Program Offices (POs) and other ESD elements to perform effective acquisition of C³I systems. The areas of technical competence include communications, command and control, battle management information processing, surveillance sensors, intelligence data collection and handling, solid state sciences, electromagnetics, and propagation, and electronic reliability/maintainability and compatibility.